Shape Statistics of Particle Clusters in a Turbulent Flow

Thesis

Shape Statistics of Particle Clusters in a Turbulent Flow

John Grant

BSc (Hons) (Edin) MSc (Open)

Supervisor: Professor Michael Wilkinson

Department of Mathematics and Statistics
The Open University

This dissertation is submitted for the degree of
Doctor of Philosophy

Milton Keynes October 2019

Abstract

The attractor of a chaotic dynamical system may have a multi-fractal measure which can be described by a spectrum of fractal dimensions. These dimensions do not characterize local geometrical structures that may exist within the attractor and in physical situations these may be important. It is therefore of interest to have a more effective means of characterizing the local structure of fractal sets and it is this problem that is addressed in this thesis. The problem is approached by considering the statistical distributions of the size and shape of very small triangular constellations of points sampling the fractal measure. The approach is illustrated, and validated, using fractal clusters of particles formed by advection and diffusion in a two-dimensional compressible random flow, which models turbulence.

Our numerical simulations show that as the compressibility parameter of the fluid passes through a critical value the distribution of the flatness of constellations undergoes a phase transition. We develop a theoretical model for this phenomenon which correctly predicts the critical value of the compressibility. Also, by representing the effects of the flow as a stochastic matrix process, we show that for a range of values of compressibility the probability density of the size of constellations is a modified power law. For a fractal cluster generated by the random flow we derive an expression for the Renyi dimension of order three, D_3, in terms of the probability density of the size of constellations and find it is in agreement with the results of other authors, obtained using other methods.

Declaration

I hereby declare that, except as stipulated in the text and Acknowledgments, the contents of this thesis are my own original work and have not been submitted, in whole or in part, for consideration for any other qualification in this or any other university.

John Grant
BSc (Hons) (Edin) MSc (Open)
October 2019

Acknowledgements

I wish to express my deepest gratitude to my supervisor Professor Michael Wilkinson, of the department of mathematics at the Open University, for his exemplary supervision of my PhD programme. The contents of chapters 3,4,5 and 6 are based on papers written in collaboration with Professor Wilkinson.

> I have come to believe that a great teacher is a great artist and that there are as few as there are any other great artists. Teaching might even be the greatest of the arts since the medium is the human mind and spirit
>
> *John Steinbeck*

To Shaun and Jill at the finest B&B in the world: thankyou.

In memory of my grandparents:

John Laurie Shearer
(14 Jan 1914 - 30 Sep 1995)

and

Rebecca Ramsay Sharp
(04 Aug 1914 - 30 Dec 1995)

Table of contents

List of figures

Chapter 1

Introduction

> There are three rules for writing a novel. Unfortunately, no one knows what they are.
>
> *W Somerset Maugham*

1.1 The subject matter

There is no single universally accepted definition of a fractal. However, roughly speaking, fractals are sets or geometrical structures which typically have a *fractional* dimension [6] and which are, precisely or approximately, *self-similar*. Under magnification any part of a fractal structure looks exactly or approximately similar to the whole. The term 'fractal' was introduced by Mandelbrot [31] in 1975 to characterize the property of having a non-integer dimension[1].

Aside from their mathematical interest and visual beauty fractals are important in many areas of science. They can arise as the result of dynamical processes and may influence phenomena as diverse as the onset of rain [7], the scattering of electromagnetic radiation from colloids and aggregates [51], the growth of coral [32] and the development of lightning paths [9, 35, 61]. Examples include clouds, snowflakes, trees, coastlines [31], the strange attractors of chaotic dynamical systems [37], distributions of particles in turbulent flows [1, 50] and, possibly, the distributions of matter resulting from gravitational collapse [39].

[1] We note, however that some fractal structures actually have integer dimension. For example the Peano curve is fractal but has dimension 2.

Figure (1.1(a)) shows the results of a simulation of diffusion limited aggregation[2]. This fractal structure starts as a single seed and, because the concentration of particles is sufficiently low, grows as particles diffuse onto the structure one at a time at random positions [72]. The resulting structure is continuous and self-similar but certainly not smooth or differentiable.

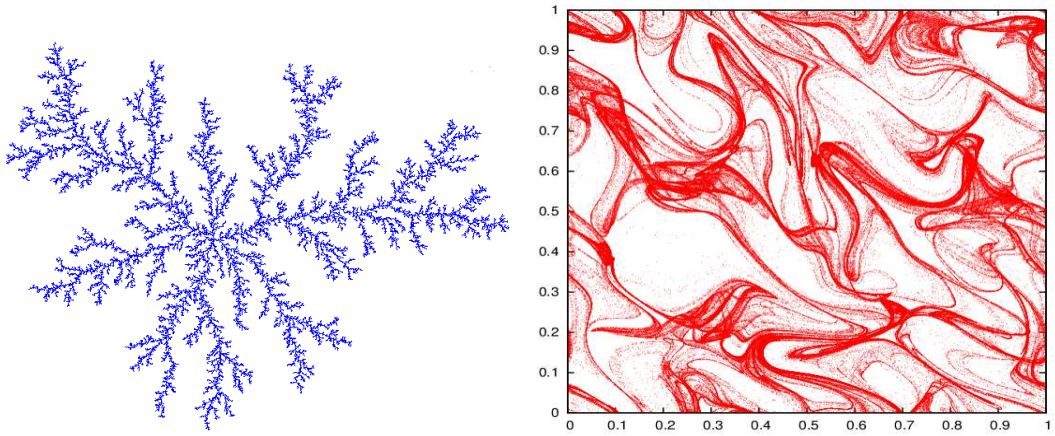

(a) A diffusion limited aggregate (b) Particles advected in a turbulent fluid flow

Fig. 1.1 The figures show fractal structures formed by two different physical processes. In plot (a) the diffusion limited aggregate starts as a single *seed* and grows as particles diffuse and coalesce to form the structure shown. In plot (b) an initially uniform distribution of particles has been advected by a turbulent two dimensional flow.

Figure (1.1(b)) shows a fractal distribution of $n = 5 \times 10^5$ particles in the unit square, produced by a stochastic model of *fully developed* turbulence in a compressible flow. Initially the particles were randomly distributed in the square and they have been *advected* by the flow. This turbulent flow model provides a generic model of chaotic dynamics which we shall use throughout the thesis; it is discussed in Chapter 2.

A multitude of *dimensions* have been defined to describe fractals. Some characterize *global* scaling properties and complexity and are typically derived from the geometry of the attractor, for example the *box-counting* dimension[3], D_{Box}, and the *correlation dimension*, D_2. Others characterize local properties, for example the *mass-dimension* describes the concentration of points, or particles, in a fractal distribution and the *spectal* dimension [68] describes the anisotropy within a distribution. For the strange attractors of chaotic dynamical

[2]The source code for this simulation has been made freely available by Dr Paul Bourke, Swinburne University of Technology, Melbourne, Australia, http://paulbourke.net/fractals/dla/.

[3]The box-counting dimension of the DLA in figure (1.1(a)) is $D_{\text{Box}} = 1.71$.

systems we also have the *Lyapunov* dimension, D_L, which is based on the dynamics of the system.

The various fractal dimensions are certainly useful, for example in the field of medicine the box-counting dimension of the human cerebellum, obtained from morphometric studies of magnetic resonance imaging scans, is being trialled for diagnostic purposes [29]. However they do have limitations, for example they are not *specific*, so that different fractals may have the same dimension. Also, they provide little information about local *structures* within the fractal which, in physical situations, may be important. For example light scattering may be strongly enhanced in some directions by specular effects if scatterers tend to align or to lie on planes [48].

In this thesis we examine the problem of analyzing and characterizing local structures in fractal sets. We address the problem by considering the distribution of size and *shape-statistics* of *constellations* of points in the set. The simplest case is treated in detail: the size and shape statistics for *triangular constellations* of points in a fractal embedded in two-dimensional Euclidean space. We illustrate and validate the approach using fractal clusters of particles generated by the turbulent flow model mentioned above. In principle our approach is generalizable to higher dimensions and to more complicated dynamical processes.

There is earlier work on the distributions of the shape statistics of triangles and tetrahedra in the fluid dynamics literature [3, 41, 73], however this is largely concerned with structures which grow larger as the particles in the constellations are transported away from each other by the action of the flow. Here we consider the opposite limit where the particles forming the structure are initially close together and where, for a period of time, they remain close together or are brought closer together by the flow.

1.2 Outline

In Chapter 2 we present some background material to help understand the main body of the thesis. We introduce dynamical systems, fractal attractors and the Renyi spectrum of fractal dimensions. We also provide a rudimentary overview of stochastic processes and introduce the synthetic turbulence model which is later used as a model of a random dynamical system.

The analysis of small triangular constellations in a fractal measure is treated in Chapter 3. We develop a parameterization of triangle shape in terms of the area and radius of gyration of the triangle and relate this to Kendall's representation of triangle shape on a sphere [23]. The results of numerical studies of a *flatness* parameter, Z, for triangles in fractals generated by the random flow model are then presented and discussed. To understand and explain these we analyze the dynamics of particles in the flow. We find that the joint probability density function (p.d.f.) of the logarithms of the size and shape parameters of constellations satisfies an advection-diffusion boundary value problem (b.v.p.), with a distributed source and reflecting and absorbing boundaries. We develop an asymptotic approximation to the solution and use it to show that the p.d.f. of the flatness parameter undergoes a *phase transition* as the compressibility parameter of the flow model passes through a critical value, which we estimate. Chapter 3 is based upon the paper *Triangular constellations in fractal measures*, published in the journal Europhysics Letters [65].

The p.d.f. of the flatness parameter obtained in Chapter 3 is specific to the dynamical system considered there, but the modelling approach is, in principle, generalizable to other geometric parameters and to other chaotic dynamical systems. We may therefore expect that the geometry of constellations in the fractal attractors of other chaotic systems will also be described by p.d.f.s which satisfy an advection diffusion problem. Consequently in Chapter 4 we study the *absorption problem* for the advection diffusion equation. We treat the absorbing boundary as a source of antiparticles and derive asymptotic expressions, valid far from the source, for the probability density along, and the flux onto, the boundary. We compare the solution to that with no boundary or, equivalently, a perfectly permeable boundary. In each case we find that, the densities and fluxes decay exponentially with distance from the source. Somewhat unexpectedly we find that the exponent is the same in both cases. Chapter 4 is based upon the paper *Advection diffusion equation with absorbing boundary*, published in the Journal of Statistical Physics [13].

The configuration of a triangular constellation of particles can be represented by a matrix. This leads us, in Chapter 5, to consider a stochastic process involving the product of a sequence of independent identically distributed (i.i.d.) random matrices. We use the singular value decomposition (s.v.d.) of the configuration matrix to represent the dynamics of a constellation as a system of stochastic differential equations (s.d.e.) for the singular values. The related boundary value problem for the joint p.d.f. of the (logarithms of the) singular values is, again, an advection-diffusion problem, with a reflecting and an absorbing boundary. From the asymptotic solution we find that the p.d.f. of $\mathcal{E}$, a measure of the size of the constellation, has the form of a modified power law which reduces to a pure power law under

certain conditions. We verify the validity of our analysis using the turbulent flow model. Chapter 5 is based on the paper *A Matrix Contraction Process*, published in the Journal of Physics A: Mathematical and Theoretical [66].

In Chapter 6 we apply a generalization of the approach taken in Chapter 5 to the fractal attractor of the turbulent flow model. We relate the distribution of the size parameter, $\mathcal{E}$, of extremely small constellations to the Renyi dimension of order three, D_3, of the attractor. Chapter 6 is based on the draft manuscript *Statistics of contracted constellations of a dynamical system*.

We conclude the thesis with a brief critical review and an outline of possible extension work, in Chapter 7.

1.3 Notation

The symbol '$\sim$' appears throughout the thesis; it is used in two ways. In most instances, the statement $f(x) \sim g(x)$ should be taken to mean that $f(x)$ is an asymptotic approximation to $g(x)$. However, to avoid writing coefficients and numerical factors which are inessential to an argument, and which would obscure the discussion, $f(x) \sim g(x)$ may also mean that $f(x) = g(x) \times h$, where h is a function of variables, other than x. In this latter use h is some function which does not affect an asymptotic limit or is a combination of constants which usually can be absorbed into a normalization factor. The specific meaning should be clear from the context.

In most cases random variables are denoted by uppercase Roman letters, or letters in a calligraphic font e.g. $X, Y, \mathcal{E}, \mathcal{Z}$, and vector-valued random variables are denoted by bold uppercase Roman letters, e.g. $\boldsymbol{X}, \boldsymbol{Z}$. However there are some exceptions, for example the lower case Greek letters λ_1, λ_2 and $\theta_1, \theta_2, \chi_0$ have been used to denote random singular values and random angles, respectively. The p.d.f. of the random variable X is denoted by P_X, or $P_X(x)$ where it is helpful to make the argument of the function explicit. The expected value of the random variable X is denoted by $\langle X \rangle$ and the variance of X is denoted by $\langle\langle X \rangle\rangle$. The notation $X \sim \mathcal{N}\left(\mu, \sigma^2\right)$ denotes that the random variable X has a Gaussian or Normal distribution with mean μ and variance σ^2.

Throughout the thesis time derivatives are denoted as follows : $\dot{\boldsymbol{x}}(t) = \dfrac{\mathrm{d}\boldsymbol{x}}{\mathrm{dt}}$ and $\ddot{\boldsymbol{x}}(t) = \dfrac{\mathrm{d}^2\boldsymbol{x}}{\mathrm{dt}^2}$.

Chapter 2

Prerequisites

> "Begin at the beginning", the King said, gravely, "and go on till you come to the end; then stop."
>
> *Lewis Carrol*, Alice in Wonderland

In this chapter we outline the background needed to understand the main body of the thesis, chapters 3-6. Since we are interested in small constellations of points in the fractal attractors of chaotic dynamical systems, we will need a few concepts from the fields of dynamical systems, fractal geometry, stochastic processes and fluid turbulence. Each of these fields has a vast literature. The main sources used for this chapter are: for dynamical systems, the texts of Ott [37], Strogatz [54] and Hirsch et. al. [18]; for fractal geometry the text of Falconer [6] and the review articles of Theiler [57] and Kinsner [25]; for stochastic processes and the Langevin and Fokker-Planck equations, the texts of Schuss [47], Coffey et. al. [4], Manhke et. al. [30], Risken [45] and vanKampen [63], and for turbulence, and particles in turbulence, the texts of Lesieur [28] and Panchev [38] and the article of Falkovich et. al. [8]. Deeper discussion of the concepts and proof of results that are outlined or merely quoted here can be found in these references, as is specified in the text. Although intended as an introduction to the thesis the reader may choose to proceed straight to Chapter 3 and refer back to this chapter as required.

2.1 Dynamical systems

2.1.1 The nature of a dynamical system

A *dynamical* system is one whose state evolves in time according to some dynamical law or equation of motion. The concept has its origins in classical mechanics [18, 37, 54]. Typically the equation of motion can be written as a system of first order differential equations, or as an iterative mapping.

If the state of a dynamical system at any time t is completely specified by $d \in \mathbb{N}$ variables then we say that the system is d-dimensional, or that it has *d degrees of freedom*. In this case the state can be represented by a *state vector*, $\boldsymbol{r}(t) = \left[x_1(t), x_2(t), \ldots, x_d(t)\right]^{\mathrm{T}}$ in an abstract space of d dimensions, the *state space* or *phase space* $\mathcal{M}$, which is $\mathbb{R}^d$ or a proper subset of $\mathbb{R}^d$. As the system evolves its state vector traces out a *trajectory* in $\mathcal{M}$. If the dynamics is defined by a system of differential equations the trajectory is an integral curve of these equations and if the dynamics is defined by an iterative map the trajectory is a discrete ordered set of points.

For most dynamical systems it is not possible to solve the equations of motion to give an explicit expression, in closed form, for the state as a function of t. Typically we then resort to numerical integration of the equations of motion to compute approximate trajectories. We may also take a more *qualitative* approach and use the governing equations to construct a *phase portrait* for the system. This may contain geometrical structures such as *fixed points*, which represent static non-evolving states, or *cycles*, which are closed trajectories representing periodic behaviour, or *strange* attractors, which are *fractal* sets arising from chaotic behaviour of the system. The analysis of the phase space structures and the stability of trajectories under small perturbations, and their sensitivity to small changes or uncertainties in the initial conditions, is an important aspect of the study of any dynamical system.

2.1.2 Strange attractors

If a dynamical system evolves toward a particular subset or region of the phase space which is *invariant*, i.e. which evolves to itself under the dynamics, then this subset is called an *attractor* and the set of points attracted to it is its *basin of attraction* [54]. Attractors can be familiar geometrical objects, for example a point or a curve, such as a limit cycle, or they

can be more complex objects including so-called *fractal sets*, in which case they are known as *strange attractors*. The best known of these is the Lorenz 'butterfly' [54, 18].

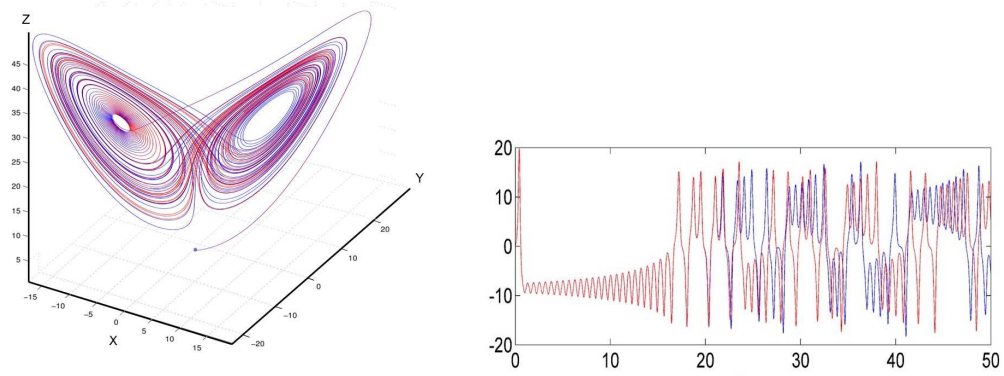

(a) Lorenz's butterfly (b) $x(t)$ for two trajectories

Fig. 2.1 Figure (a) shows two phase-space trajectories on a strange attractor, the Lorenz *butterfly*, which are initially very close together. Figure (b) shows the evolution of the x-coordinate on each of the trajectories. After an initial period during which the trajectories remain close they diverge in an erratic manner.

Figure (2.1(a)) shows two trajectories (in red and blue) in the phase space, $\mathbb{R}^3$, of the dynamical system which E. Lorenz used to model convection in the Earth's atmosphere. Each trajectory is an *integral curve* of three coupled, nonlinear differential equations[1]. On each trajectory the phase point alternates between periods where it spirals around the fixed points on each of the wings. The motion is not periodic: the trajectories never close on themselves, they are infinitely long curves contained in a finite volume of the phase space.

2.1.3 Chaos and Lyapunov exponents

The trajectories of some dynamical systems exhibit such extreme sensitivity to their initial conditions that a slight difference between two initial states may grow *exponentially fast*. Then, despite being fundamentally deterministic, the system may *appear* to behave randomly. This effect is illustrated in figure (2.1(b)) which shows the value of one of the dynamical variables, x, on two trajectories in the Lorenz model. The initial conditions are $\boldsymbol{r}_0 = (0,1,0)$ on the blue curve and $\boldsymbol{r}_0 = (0,1.01,0)$ on the red curve. Until approximately

[1] These plots were produced using the Maple® computer algebra system and code adapted from OU course MS325 Computer Algebra, Chaos and Simulations. The details of the model are unimportant for our discussion; they can be found in [54].

$t = 20$ the separation between the two trajectories is not discernible in the figure, thereafter the values of x clearly differ. The position on the attractor, and the time of jumps between the wings, differs significantly between the two trajectories. This *apparent randomness* is called *chaos*; it was first alluded to by H. Poincaré in his study of the orbits of three celestial bodies [40].

We can understand this behaviour by considering the evolution of the separation between two trajectories that are initially close, our treatment here follows that of [57]. Figure (2.2) shows two trajectories through the initial points $\boldsymbol{r}_0$ and $\boldsymbol{r}_0 + \boldsymbol{h}_0$, where $|\boldsymbol{h}_0|$ is small.

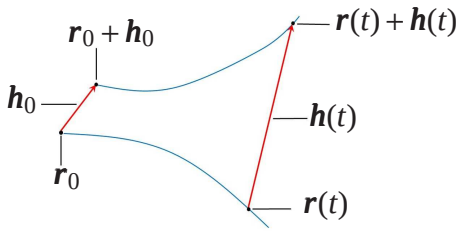

Fig. 2.2 The figure shows two trajectories in the phase space of a dynamical system. The initial separation is given by the vector $\boldsymbol{h}_0$ and the separation at time t is $\boldsymbol{h}(t)$. If $\boldsymbol{h}(t)$ grows exponentially fast in some directions but shrinks exponentially fast in others then the dynamical system exhibits chaotic behaviour.

Suppose that the dynamics is given by the first order system of o.d.e.s

$$\dot{\boldsymbol{r}} = \boldsymbol{F}(\boldsymbol{r}) \tag{2.1.1}$$

then, assuming that $\|\boldsymbol{h}(t)\|$ is small, using a Taylor expansion we find that the separation $\boldsymbol{h}(t)$ evolves as

$$\dot{\boldsymbol{h}}(r) = \boldsymbol{J}(\boldsymbol{r})\,\boldsymbol{h}(t) \tag{2.1.2}$$

where $\boldsymbol{J}(\boldsymbol{r}) \equiv \left[\partial F_i/\partial x_j\right]$ is the Jacobian matrix of $\boldsymbol{F}$, evaluated at the point $\boldsymbol{r}(t)$. The separation at time t may be thought of as a deformation of the initial separation given by

$$\boldsymbol{h}(t) \equiv \boldsymbol{M}(t)\,\boldsymbol{h}_0 \tag{2.1.3}$$

where $\boldsymbol{M}(t)$ is the *deformation or transition matrix*. From equations (2.1.2) and (2.1.3) it follows that $\boldsymbol{M}(t)$ evolves as $\dot{\boldsymbol{M}}(t) = \boldsymbol{J}(\boldsymbol{r})\,\boldsymbol{M}(t)$, with initial condition $\boldsymbol{M}(0) = \mathbb{I}_{\mathrm{d}}$. In terms of $\boldsymbol{M}(t)$ the separation at time t has magnitude

$$\|\boldsymbol{h}(t)\| = \|\boldsymbol{M}(t)\boldsymbol{h}_0\| = \left[\boldsymbol{h}_0^{\mathrm{T}}\boldsymbol{M}^{\mathrm{T}}(t)\boldsymbol{M}(t)\boldsymbol{h}_0\right]^{1/2}. \tag{2.1.4}$$

If $\boldsymbol{h}(t)$ grows exponentially fast in some directions but shrinks exponentially fast in others then the dynamical system exhibits chaotic behaviour. We can define a long-term mean *rate* of divergence, or convergence, of the two trajectories as

$$\lambda(\boldsymbol{r_0}, \boldsymbol{h}_0) = \lim_{t\to\infty} \frac{1}{t} \ln\left(\frac{||\boldsymbol{h}(t)||}{||\boldsymbol{h}_0||}\right) \tag{2.1.5}$$

provided this limit exists. The multiplicative theorem of Osedelets [36, 64] shows that, under very general conditions, this limit does exist and, further, that for almost all initial points $\boldsymbol{r}_0$ there exists an orthonormal basis $\{\boldsymbol{v}_i, i = 1\cdots d\}$ of the phase space such that the scalars

$$\lambda_i = \lim_{t\to\infty} \frac{1}{t} \ln||\boldsymbol{M}(t)\boldsymbol{v}_i|| \tag{2.1.6}$$

exists. Asymptotically, an initial displacement $\boldsymbol{h}_0$ in the direction of the vector $\boldsymbol{v}_i$ is scaled exponentially fast, at a rate given by λ_i. For an ergodic system, whose time averages equal ensemble averages, the λ_i do not depend on the initial point $\boldsymbol{r}_0$ and are therefore global properties of the dynamical system. The λ_i are called the Lyapunov exponents of the system, they are usually enumerated in descending order of magnitude: $\lambda_1 \geq \lambda_2, \geq, \ldots, \geq \lambda_d$ and the set of exponents is called the Lyapunov *spectrum* of the system [54].

The cumulative sums of Lyapunov exponents have a simple geometrical interpretation. λ_1 determines the exponential growth rate ($\lambda_1 > 0$) or contraction rate ($\lambda_1 < 0$) of the separation of two points on nearby trajectories; $\lambda_1 + \lambda_2$ determines the growth rate ($\lambda_1 + \lambda_2 > 0$) or contraction rate ($\lambda_1 + \lambda_2 < 0$) of the area of a small triangle whose vertices lie on three nearby trajectories and $\lambda_1 + \lambda_2 + \lambda_3$ determines the exponential growth or contraction rate of the volume of a small tetrahedron whose vertices lie on four nearby trajectories.

If the sum of the Lyapunov exponents $\lambda_1 + \lambda_2 +, \ldots, \lambda_d$ is negative then volumes in phase space are contracted during the evolution of the system and the system is said to be dissipative [37, 34, 64]. Strange attractors can arise only in dissipative, nonlinear dynamical systems [57] and in such a system the 'signature' of deterministic chaos is that largest Lyapunov exponent is positive, i.e. $\lambda_1 > 0$. Then, although volumes of phase space are contracted by the evolution of the system, if the initial separation of two trajectories $\boldsymbol{h}$ has a non-zero component in the direction of the eigenvector $\boldsymbol{v}_1$ of the matrix $\boldsymbol{M}(t)$, these trajectories will separate along this direction exponentially fast, and chaos will ensue. In the next section we discuss some of the characteristics of the fractal attractors of such systems.

2.2 Fractals

2.2.1 Self similarity and power laws

A geometrical or physical object which is composed of distinct, identifiable parts is said to be self similar if the parts are geometrically similar to the whole, that is if they are *scaled copies* of the whole. Self-similarity is one of the defining characteristic of fractal structure [6].

Fractal sets that are defined iteratively or recursively via deterministic rules are, typically, *exactly* self similar: the parts can be scaled to give an identical copy of the whole. In naturally occurring fractals, for example the Lorenz butterfly, the parts are only *approximately* similar to the whole. Whilst the parts do not scale to give an identical copy of the whole, their statistical properties are similar at many different length scales.

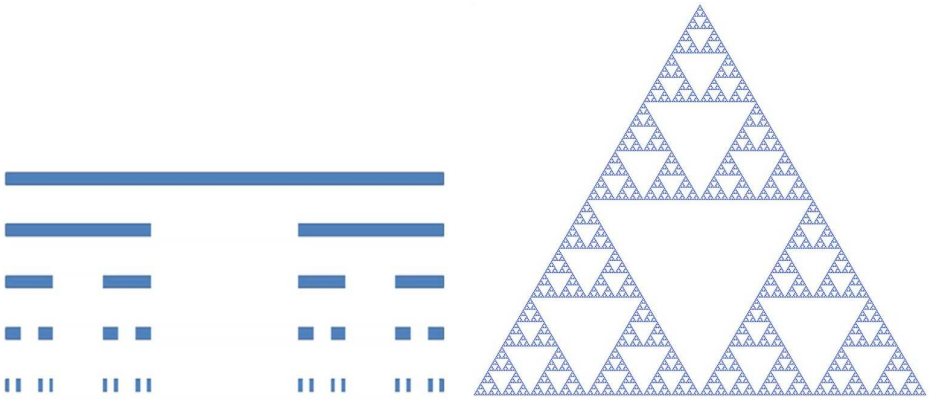

(a) A Cantor set (b) A Sierpinski triangle

Fig. 2.3 The Cantor set and Sierpinski trangle - examples of *exactly* self-similar fractals.

Figure (2.3) illustrates the concept of exact self similarity. Part (**a**) shows the first five steps in the formation of the 'missing middle third' or *ternary* Cantor set, C. The zeroth approximation is the closed unit interval, $C_0 = [0,1]$. At each subsequent iteration the open middle third of each sub-interval in the set is deleted, giving

$$C_1 = \left[0,\frac{1}{3}\right]\cup\left[\frac{2}{3},1\right],\ C_2 = \left[0,\frac{1}{9}\right]\cup\left[\frac{2}{9},\frac{1}{3}\right]\cup\left[\frac{2}{3},\frac{7}{9}\right]\cup\left[\frac{8}{9},1\right],\ \text{etc.}$$

The fractal, C, is what results when this iterative process is continued ad infinitum [20]. At the n^{th} iteration there are $N_n = 2^n$ subintervals, each of length $\varepsilon_n = (1/3)^n$ and of total length $L_n = (2/3)^n$. Hence, as $n \to \infty$, $N_n \to \infty$ and $L_n \to 0$ so that the fractal C is a set containing infinitely many elements but which has zero length.

Part (**b**) of figure (2.3) shows a Sierpinski triangle[2]. This fractal is formed from an equilateral triangle of side of unit length, by recursive subdivision into four congruent equilateral triangles and removal of the central triangle at each stage. At the zeroth iteration there is a single equilateral triangle, $\mathcal{T}_0$, of area $A_0 = \sqrt{3}/4$. At the n^{th} iteration the approximation to the fractal, $\mathcal{T}_n$, contains $N_n = 3^n$ triangles, of total area $A_n = (3/4)^n A_0$. The self similarity is evident: one can imagine a scaling transformation of the smaller triangles to produce the larger ones or, equivalently, viewing the fractal at a different level of magnification or resolution. Ever-more identical parts are seen as the resolution increases.

A second defining characteristic of fractals is that the value of a measured property depends on the resolution, or level of precision, at which the measurement is made. For example a linear fractal, such as the Cantor set, can be *covered* by a number, N say, of intervals each of some given length, ε. The quantity $L = N \times \varepsilon$ then provides an estimate of the size of the fractal, at the level of precision set by the value of ε. Changing this level of precision, for example reducing ε, will give a different value for L.

If a property of a fractal exhibits scaling behaviour then the self similarity of the fractal implies that the property must be described by a functional relationship whose *form* is invariant under a scaling transformation. Since *power law* relationships are *form-invariant* under scaling transformations, or form-invariant with respect to a change of scales, the properties of fractals are frequently described by power laws[3].

2.2.2 Fractal dimensions

In classical Cartesian geometry the Euclidean or spatial dimension of a geometrical object is defined to be the number of coordinates needed to completely specify the position of

[2] Figure courtesey of Wikimedia Commons https://commons.wikimedia.org/.

[3] Two quantities, Q and r say, are related by a power law if $Q = ar^k$, for some real constants a and k. Then, under the scaling transformation $r \to \lambda r$, where λ is some positive constant, we have $Q \to \lambda^k a r^k$, which is again a power law, with the same exponent. The original relationship can be recovered by now scaling Q, by the factor λ^{-k}. Note also that, if Q and r are related via a power law, then *relative* changes in Q and r are proportional, and the constant of proportionality is the exponent of the power law.

any point within the object. Thus, for example, a line has dimension one and cuboid has dimension three. In essence, the Euclidean dimension of an object characterizes the manner in which it fills space. At the beginning of the twentieth century this classical definition of dimension, in terms of *degrees of freedom*, was shown to be deficient when G. Peano constructed a *space filling curve*, mapping the unit interval continuously to the unit square. A formal mathematically rigorous definition of dimension was subsequently developed by F. Hausdorff in 1918, [6]. This definition is somewhat difficult to use in practice but, building on Hausdorff's approach, more practical definitions have been developed and some are used to describe fractal sets [25].

In addition to characterizing how an object fills space, the Euclidean dimension also characterizes *scaling* behaviour. For example, when the linear sizes of a cuboid are each scaled by a factor λ then the volume of the cuboid is scaled by λ^3, the exponent being the Euclidean dimension. It is this type of scaling behaviour which forms the basis of the definitions of many fractal dimensions. But fractal objects are very different from classical geometrical objects and consequently these dimensions, which describe space-filling properties, scaling characteristics and complexity, need not be integers. Indeed, it is from this characteristic, of *fractional dimensions*, that the term fractal is derived. Furthermore, whilst a strictly self-similar fractal can be characterized by a single fractional dimension, this is generally not the case for a naturally occuring fractal where the scaling behaviour may vary across the fractal, and a spectrum of dimensions may be required for an adequate description [25, 57].

For an *exactly* self similar fractal we can define a *self-similarity dimension*, D_{SIM} by *covering* the fractal with identical copies of some *covering set*, of known size[4], ε, and examining how the estimate of the size of the fractal scales with variation in the size of the covering set [25]. Typically the number, N, of sets needed to cover the fractal will increase as the size of the cover, ε, is decreased. If, in the limit that $\varepsilon \to 0$, the relationship between N and $1/\varepsilon$ is a power law, then the self-similarity dimension, D_{SIM}, is the exponent. That is, if as $\varepsilon \to 0$ we have

$$N \to a\left(\frac{1}{\varepsilon}\right)^K = a\varepsilon^{-K} \tag{2.2.1}$$

where a and K are some constants, then $D_{\mathrm{SIM}} = K$.

[4] If the covering set is a regular geometrical object, such as a line segment or a box, then we take its size to be some characteristic length.

For example, since the middle third Cantor set is exactly self similar, the n^{th} approximation C_n can be covered by $N_n = 2^n$ intervals of length $\varepsilon_n = (1/3)^n$, we have

$$D_{\text{SIM}} = \lim_{n\to\infty}\left[\frac{\ln N_n}{\ln(1/\varepsilon_n)}\right] = \lim_{n\to\infty}\left[\frac{n\ln 2}{n\ln 3}\right] = 0.631, \text{ to 3 d.p.}$$

Similarly, the n^{th} approximation, $\mathcal{T}_n$, to the Sierpinski triangle can be covered by $N_n = 3^n$ equilateral triangles with sides of length $\varepsilon_n = (1/2)^n$. Therefore the Sierpinski triangle has similarity dimension $D_{\text{SIM}} = \ln 3/\ln 2 = 1.585$, to 3 $d.p.$. Heuristically we can interpret these fractional dimensions as meaning that the Cantor set and the Seirpinski triangle fill space in a manner somewhat between a point and a line, and a line and a triangle, respectively.

The essence of the above approach, covering the fractal with miniature replicas of a known size, ε, and examining how the number of covers, N_ε, needed scales with that size, can also be applied to fractals whose self-similarity is *only approximate*. However in this case since there is no covering set which is an *exact* copy of the fractal we usually cover the fractal in ε-cells, i.e. d-dimensional boxes or 'cubes' of side ε (for a fractal in a Euclidean space of dimension d). The use of boxes is not essential and other covers, particularly ε-balls are also commonly used. This approach gives the *box-counting, morphological* or *capacity* dimension:

$$D_0 = \lim_{\epsilon\to 0}\left[\frac{\ln\ N_\varepsilon}{\ln(1/\varepsilon)}\right] \tag{2.2.2}$$

where we assume that the limit exists independently of how the cover is chosen, and its type.

In this definition each box, or ball, in the cover is treated equally; no weighting is applied to reflect any difference in the importance of particular boxes, for example the time which a trajectory spends in a ε-box. Therefore, when applied to an attractor of a dynamical system, D_0 will reflect the geometry or morphology of the attractor but less-so the dynamics.

2.2.3 The Rényi spectrum of fractal dimensions.

The Rényi or *generalized* dimensions weight the covering ε-boxes according to their 'ergodic natural measure' [57, 64]. In effect, for an attractor of a dynamical system this measure is essentially the probability that a randomly chosen point on the attractor lies in the box, so that boxes are therefore weighted according to the frequency with which they are visited, or the time that trajectories spend in them. In practice if the attractor, $\mathcal{A}$, of a dy-

namical system is just covered by a number, N_ε say , of ε-boxes $\mathcal{B}_i$, $i = 1, \cdots, N_\varepsilon$ then the probability, p_i, that the box $\mathcal{B}_i$ contains a randomly chosen point on the attractor can be estimated by counting the number of points in $\mathcal{B}_i$ and dividing by the total number of points in $\mathcal{A}$.

The dimensions in the Rényi spectrum are indexed by a continuous parameter, q, the *order* of the dimension; the Rényi dimension of order q, is defined as

$$D_q \equiv \lim_{\varepsilon \to 0} \frac{S_\varepsilon(q)}{\ln(1/\varepsilon)} \tag{2.2.3}$$

where

$$S_\varepsilon(q) \equiv \left(\frac{-1}{q-1}\right) \ln \left(\sum_{i=1}^{N_\varepsilon} p_i^q\right). \tag{2.2.4}$$

The quantity $S_\varepsilon(q)$ is called the Rényi entropy [25]. It is a generalized measure of the entropy of the probability distribution $\{p_i, i = 1, \cdots, N_\varepsilon\}$ which, in the limit as $q \to 1$ reduces to the Shannon entropy[5] [44]. From the definition of $S_\varepsilon(q)$ we see that if $q > 0$ the weighting emphasizes dense regions, corresponding to clusters of phase points. Further, as the order q increases through positive values, then the relative importance of those boxes with higher measure, the so-called 'hotspots' of the attractor, also increases. For $q < 0$ the weighting emphasizes sparse regions of the attractor. For a *mono-fractal*, characterized by unique scaling behaviour, D_q is a constant independent of q, but in general, for a *multi-fractal* D_q depends on q and is a single-valued, monotonically decreasing function of q, so that if $q_1 \geq q_2$ then $D_{q_1} \leq D_{q_2}$ and, in particular, $D_0 \geq D_1 \geq D_2$. For the fractal attractor of a chaotic dynamical system, whose points represent trajectories in phase space, the Rényi spectrum of dimensions characterizes the *clustering* of the trajectories.

The Rényi dimension of order zero is simply the box-counting dimension, D_0, discussed above. D_1 is called the *information dimension*, it is evaluated by applying L'Hôpital's rule to calculate the limiting value as $q \to 1$. In the definition of D_1 the weighting of each ε-box is proportional to the natural measure of the box. This generalized dimension therefore characterizes the natural measure, revealing any non-uniform spread of probability on the attractor.

[5] This can be seen by writing

$$\sum_{i=1}^{N_\varepsilon} p_i^q = \sum_{i=1}^{N_\varepsilon} p_i \left[p_i^{q-1}\right] = \sum_{i=1}^{N_\varepsilon} p_i \left[\exp\left((q-1)\ln p_i\right)\right] \approx \sum_{i=1}^{N_\varepsilon} p_i \left[1 + (q-1)\ln p_i\right] = 1 + (q-1)\sum_{i=1}^{N_\varepsilon} p_i \ln p_i$$

The Rényi dimension of order two, D_2, has gained particular prominence because of the ease with which it can be calculated [57, 20]. D_2 involves the sum $\sum_{i=1}^{N_\varepsilon} p_i^2$, which scales in the same way as the probability that two points are separated by a distance less than ε. Now, in a set of N *points*, located at positions $\boldsymbol{r}_i$, $i = 1, \cdots N$, the probability that points are separated by a distance less than ε is given by the *pair correlation* sum $C_2(N, \varepsilon)$:

$$C_2(N,\varepsilon) \equiv \frac{\sum_{i=1}^{N}\sum_{j=i+1}^{N} \Theta\left(\varepsilon - r_{ij}\right)}{N(N-1)/2} \tag{2.2.5}$$

where Θ is the Heaviside step function and $r_{ij} \equiv \left|\boldsymbol{r}_j - \boldsymbol{r}_i\right|$ is the separation of the particles at positions $\boldsymbol{r}_i$ and $\boldsymbol{r}_j$. Hence

$$D_2 = \lim_{\varepsilon \to 0} \frac{\ln C_2(N,\varepsilon)}{\ln \varepsilon} \tag{2.2.6}$$

and, therefore, D_2 can be estimated merely from the statistics of separations of nearby points in a (large) sample of points from the fractal. This approach to estimating a fractal dimension originates with Grassberger and Proccacia; we refer the reader to [14, 52] for the details. Because of its relation to the pair correlation sum, D_2 is called the *correlation* dimension.

For integral values of q greater than two D_q can be interpreted in terms of a q-point correlation sum, $C_q(N, \varepsilon)$. This counts q-tuples of points, in a sample of N points, for which the separation between any pair in the q-tuple is less than ε. This has scaling behavior $C_q(N, \varepsilon) \sim \varepsilon^{(q-1)D_q}$ so that

$$D_q = \frac{1}{q-1} \lim_{\varepsilon \to 0} \frac{\ln C_q(N,\varepsilon)}{\ln \varepsilon}. \tag{2.2.7}$$

In principle this result can be used to obtain D_q for all integral values of $q \geq 2$ however, implementation is not straightforward since the number of q-tuples, N^q, grows rapidly with N.

We remark that the D_q describe the scaling properties of the moments of the number, $\mathcal{N}(\varepsilon)$, of phase points in a small ε-ball[6] as $\varepsilon \to 0$. For example, the correlation sum $C_2(N, \varepsilon)$ is an estimate of the probability that two points, with positions $\boldsymbol{r}_i$ and $\boldsymbol{r}_j$, randomly selected from a set of N points are within a distance ε of each other. Therefore, if $\mathcal{B}_\varepsilon(\boldsymbol{r})$ is a ball of radius ε *centred on a particle* at point, $\boldsymbol{r}$, then $C_2(N, \varepsilon)$ measures the probability of finding a second point inside the ball, hence $\langle \mathcal{N}(\varepsilon) \rangle \sim \varepsilon^{D_2}$, as $\varepsilon \to 0$. Similarly, for $q > 1$, if $\left\langle \mathcal{N}^{(q-1)}(\varepsilon) \right\rangle$ varies

[6] Note that N_ε is the number of covers of size ε needed to cover the fractal set and $\mathcal{N}(\varepsilon)$ is the number of points in the fractal lying in an ε-ball, which is a random variable with expectation $\langle \mathcal{N}(\varepsilon) \rangle$

as some power of ε, as $\varepsilon \to 0$ then the exponent is $(q-1)D_q$, that is:

$$\langle \mathcal{N}^{(q-1)}(\varepsilon) \rangle \sim \varepsilon^{(q-1)D_q} \tag{2.2.8}$$

we use this interpretation in Chapter 6 when we consider the Rényi dimension of order 3.

2.2.4 The Lyapunov dimension

The fractal dimensions considered above are based on the geometrical scaling properties of the fractals, or on the statistics of the separations of nearby points sampling the fractal. For the strange attractor of a dynamical system Kaplan and Yorke have introduced a dimension which is calculated from the Lyapunov spectrum of the system [21] and which therefore depends on the dynamics of the system.

Suppose that the Lyapunov exponents of the system are $\lambda_1 \geq \lambda_2 \geq \lambda_3 \geq \cdots \geq \lambda_d$ and let S_m be the sum of the first m exponents, with $1 \leq m \leq d$. Since the system is dissipative we know that $S_d < 0$ and since the system is chaotic we know that $\lambda_1 > 0$, and therefore $S_1 > 0$. Therefore there exist an integer $k \geq 1$ such that $S_k > 0$ and $S_{k+1} = S_k + \lambda_{k+1} < 0$. The Lyapunov dimension, also known as the Kaplan-Yorke dimension, is defined to be that *real* number, between k and $k+1$ for which S_m would vanish, if S_m were a continuous function of m. At this hypothetical value there is neither contraction or expansion of phase-space volumes. The Lyapunov dimension, D_L, is defined by linear interpolation [20, 21]:

$$D_{\mathrm{L}} = k - \frac{S_k}{\lambda_{k+1}} = k - \frac{\sum_{i=1}^{k} \lambda_i}{\lambda_{k+1}}. \tag{2.2.9}$$

It has been conjectured that D_L is equal to the information dimension of an attractor; this conjecture remains open [10].

2.3 Stochastic processes

When we examine the shape statistics of constellations in a turbulent flow we will deal with a dynamical system whose evolution is governed by stochastic differential equations that contain random forcing or *noise* terms. The state of such a system evolves in a prob-

abilistic manner and the coordinates of the point in phase space representing the state are time-dependent random variables or *stochastic processes*. Because the state is random the system is described by a p.d.f. which determines the probability that the state lies in a small element of the phase space at any given time.

This state p.d.f. determines the properties of the system and is of primary importance in our later work. For systems with *diffusive dynamics*, from the equation of motion we can derive a partial differential equation, the so-called Fokker-Planck equation, governing the state p.d.f., which in principle allows us to determine this p.d.f.

2.3.1 The 1d random walk and its continuum limit

As a simple example of a stochastic dynamical system which illustrates some of the above concepts, consider a particle executing a random walk on the real line, see figure (2.4).

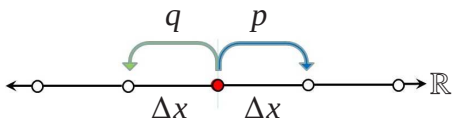

Fig. 2.4 The random walker, shown in red, starts at the origin and at times $t_k = k\Delta t$, where $k = 1,2,3,\cdots$ and Δt is a small time increment, hops to the left with probability q or to the right with probability p. After a time $n\Delta t$ the expected position of the particle is given by equation (2.3.2) and the variance of this position is given by equation (2.3.3).

Suppose that the particle is initially at the origin $x = 0$ at $t = 0$ and that at times $t_k = k\,\Delta t,\ k = 1,2,\cdots$ the particle makes a jump ΔX_i to the left or right, of magnitude Δx, with *transition probabilities* $\mathbb{P}[\Delta X_i = \Delta x] = p$ and $\mathbb{P}[\Delta X_i = -\Delta x] = q = 1-p$. Then, at any time t the position of the particle, $X(t)$, is a random variable and the probability, $\mathbb{P}_X(x_n, t_m)$, that $X(t_m) = x_n$, where $x_n \equiv n\Delta x$ and $t_m \equiv m\Delta t$ with $n, m \in \mathbb{Z}$ and $m \geq 0$, satisfies the recurrence relation

$$\mathbb{P}_X(x_n, t_{m+1}) = p\mathbb{P}_X(x_{n-1}, t_m) + q\mathbb{P}_X(x_{n+1}, t_m) \tag{2.3.1}$$

with initial condition $\mathbb{P}_X(x_n,0)=\delta_{n,0}$. The position $X(t)$ has mean and variance *functions*

$$\mu_X(t)=\langle X(t)\rangle=\sum_{i=1}^{n}\langle\Delta X_i\rangle=n(p-q)\Delta x \tag{2.3.2}$$

$$\sigma_X^2(t)=\left\langle(X(t)-\langle X(t)\rangle)^2\right\rangle=\sum_{i=1}^{n}\left\langle(\Delta X_i-\langle\Delta X_i\rangle)^2\right\rangle=4npq(\Delta x)^2 \tag{2.3.3}$$

respectively, where $n\equiv\text{Int}[t/\Delta t]$.

In the *continuum* or *diffusive* limit, where $\Delta x\to 0$, $\Delta t\to 0$ and $n\to\infty$, in such a manner that $(\Delta x)^2/\Delta t$ neither vanishes or becomes unbounded, and such that $n\Delta t=t$, we have

$$\mu_X(t)=(p-q)\left(\frac{\Delta x}{\Delta t}\right)t\equiv vt \quad \text{and} \quad \sigma_X^2(t)=4pq\frac{(\Delta x)^2}{\Delta t}t\equiv 2Dt \tag{2.3.4}$$

where $v\equiv(p-q)\Delta x/\Delta t$ is the *drift velocity* and $D\equiv 2pq(\Delta x)^2/\Delta t$ is the *diffusion coefficient*[7].

In the continuum limit the position of the particle, $X(t)$, is a continuous function of t described by a p.d.f., $P_X(x,t)$, such that at time t the probability of finding the particle in the small interval $(x,x+dx)$ is given by $\mathbb{P}(x<X\le x+dx,t)=P_X(x,t)dx$. From (2.3.1), provided that Δx and Δt are sufficiently small, it follows that

$$P_X(x,t+\Delta t)\approx pP_X(x-\Delta x,t)+qP_X(x+\Delta x,t) \tag{2.3.5}$$

then, expanding each term in a Taylor series and taking the continuum or diffusive limit, as above, it follows that $P_X(x,t)$ satisfies the *advection-diffusion* equation:

$$\frac{\partial P_X(x,t)}{\partial t}=-v\frac{\partial P_X(x,t)}{\partial x}+D\frac{\partial^2 P_X(x,t)}{\partial x^2}. \tag{2.3.6}$$

Equation (2.3.6) is also known as the F.P. equation for the p.d.f. of $X(t)$. We can deduce the solution by applying the central limit theorem (c.l.t.). Since $X(t)$ is the sum of many Δx_i, which are i.i.d. random variables, it has a Gaussian distribution and since $X(t)$ has mean $\mu_X(t)=vt$ and variance $\sigma_X^2(t)=2Dt$ it follows that

$$P_X(x,t)=\frac{1}{\sqrt{4\pi Dt}}\exp\left[\frac{-(x-vt)^2}{4Dt}\right]. \tag{2.3.7}$$

[7]The numerical coefficient, 2, is included in equation (2.3.4) to give agreement with the diffusion constant in the diffusion equation. D has physical dimensions L^2T^{-1}

This is the solution of the F.P. equation (2.3.6) with initial condition $P_X(x,0) = \delta(x)$.

Figure (2.5) shows four *trajectories, realizations* or *sample paths* of the continuum limit of the *symmetric* random walk, for which $p = q = 1/2$, $v = 0$ and $D = \Delta x^2/(2\Delta t)$.

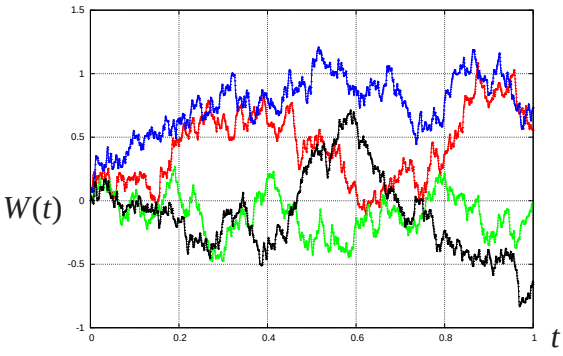

Fig. 2.5 The continuum limit of the one dimensional random walk is the Wiener process, usually denoted by $W(t)$. Each path can be thought of as the trajectory of a Brownian particle (see also figure (2.7).

The continuum limit of the symmetric random walk is called the **Wiener process** [17] and is usually denoted by $W(t)$, or $B(t)$. This process is of fundamental importance in modelling random phenomena. $W(t)$ is a mathematical model of one-dimensional *Brownian motion* - the diffusive motion, due to molecular collisions, of microscopically small particles suspended in a fluid. Each sample path shows a sequence of values of the process, $W(t)$, for $0 \leq t \leq 1$, at times $t = t_n = n\Delta t$, $n = 1, 2, \cdots$, where Δt is a small time interval, with linear interpolation between points. The paths can be thought of as the *world-lines* of particles undergoing Brownian motion, in one dimension. We shall consider the properties of $W(t)$ in section (2.3.4), after first introducing some further terminology.

2.3.2 Characterizing stochastic processes

To progress with our analysis of shape statistics it will be necessary to make some simplifying assumptions regarding the nature of the stochastic processes that we will deal with; these are outlined below. A fuller discussion of the concepts introduced below can be found in the text of vanKampern, [63].

Typically a stochastic process, $X(t)$, is characterized by specifying the p.d.f. $P_X(x,t)$ and by giving the moments and cumulants of $X(t)$. These characteristics are *ensemble* statistics,

which can be estimated from a sample of realizations of the process. However if the process is *ergodic* they can also be estimated from *temporal averages* calculated from a time series of observations on a *single realization* of the process. Further, if $X(t)$ is *stationary*, by which it is meant that the p.d.f. $P_X(x,t)$ is *invariant under the time shift* $t \to t+\tau$ for every $\tau \in \mathbb{R}$, then the parameters of the process, such as the mean and variance functions, *do not change over time*. The interpretation of this property is that the underlying mechanism causing the randomness in the process does not change with the course of time [4]. We shall assume both *ergodicity and stationarity*.

The covariance function of $X(t)$ is $K_X(t_1,t_2) \equiv \langle [X(t_1)-\mu_X(t_1)]\,[X(t_2)-\mu_X(t_2)] \rangle$ which can be written as

$$K_X(t_1,t_2) = \int_{-\infty}^{\infty}\int_{-\infty}^{\infty} [x(t_1)-\mu_X(t_1)]\,[x(t_2)-\mu_X(t_2)]\,P_{X_1,X_2}(x_1,t_1\,;\,x_2,t_2)\,\mathrm{d}x_1\mathrm{d}x_2 \quad (2.3.8)$$

where $P_{X_1,X_2}(x_1,t_1\,;\,x_2,t_2)$ is the *second order joint* p.d.f. of the process. This is defined such that the joint probability that the state lies in the interval (x_1, x_1+dx_1) at time t_1 *and* in the interval (x_2, x_2+dx_2) at time t_2 is $P_{X_1,X_2}(x_1,t_1\,;\,x_2,t_2)\,dx_1dx_2$. The covariance function $K_X(t_1,t_2)$ can be thought of as a measure of the similarity of the process at times t_1 and t_2 and $K_X(t,t)$ is the variance, $\sigma_X^2(t)$, a measure of the variability of the process at time t.

For a stationary process the covariance function $K_X(t_1,t_2)$ depends only on the magnitude of the time difference $|t_2-t_1|$. Then, if there exists a constant, τ_c, such that for any times t_1 and t_2 with $|t_2-t_1| > \tau_c$ we have $K_X(t_1,t_2) \approx 0$, the values of the process $X(t_1)$ and $X(t_2)$ are, in effect, uncorrelated. We call τ_c the correlation time of the process. If τ_c is very small then as a first approximation we may take $\tau_c = 0$, so that $X(t)$ is *delta-correlated* in time. Roughly speaking, this means that the system has no memory of its history: the future state depends only on the current state, not the past history of the system. This *memory-less* property is characteristic of *Markov* processes and we shall assume that it holds.

We note that, if for any strictly increasing sequence of *sample times* $t_0 = 0 < t_1 < t_2 < t_3, \cdots$ the process increments $\Delta X_i \equiv X(t_{i+1}) - X(t_i)$ are independent random variables, i.e. if $X(t)$ has *independent increments* on *any* non-overlapping time intervals, then it is a Markov process [63].

2.3.3 Gaussian processes

A stochastic process, $X(t)$, is Gaussian if $X_i = X(t_i)$, $i = 1, 2, \cdots, k$, are *jointly* Gaussian random variables for all $k \in \mathbb{N}$, and all choices of $t_1, t_2, \cdots, t_k$. Many naturally occurring random processes are the net result of a great many microscopic effects and are therefore Gaussian, or very nearly so. For this reason, and because of their relative mathematical simplicity, Gaussian stochastic processes are often the first choice when modelling a random physical process [63].

If $X(t)$ is a Gaussian process with mean function $\mu_X(t)$ and covariance function $K_X(t,t')$, then the k^{th} order joint p.d.f. of $X_1, X_2, \cdots, X_k$ is the Gaussian function

$$P_{X_1,X_2,\cdots,X_k}(x_1,t_1;x_2,t_2;\cdots;x_k,t_k) = \frac{\exp\left[-\frac{1}{2}(\boldsymbol{x}-\boldsymbol{\mu})^{\mathrm{T}} K (\boldsymbol{x}-\boldsymbol{\mu})\right]}{\sqrt{(2\pi)^k |\det K|}} \tag{2.3.9}$$

where $\boldsymbol{\mu} = [\mu_1, \mu_2, \cdots, \mu_k]^{\mathrm{T}}$ and $K = \left[K_{ij}\right]$ with $\mu_i \equiv \mu_X(t_i)$ and $K_{ij} \equiv K_X\left(t_i, t_j\right)$. Since the higher order cumulants vanish[8] a Gaussian process is *completely determined* by its mean function, $\mu_X(t)$, and its covariance function, $K_X(t,t')$. Estimation of these functions is a relatively simple task since it involves, at most, pairs of data points.

2.3.4 The Wiener process

In section (2.3.1) we introduced the Wiener process, $W(t)$, a model of Brownian motion in one dimension, as the continuum limit of a symmetric random walk. $W(t)$ is a Gaussian process with mean zero, i.e. $\mu_W(t) = \langle W(t) \rangle = 0$, and covariance function $K(s,t)$ given by

$$K(s,t) = \langle W(s)W(t) \rangle = \sigma^2 \mathrm{Min}(s,t) \tag{2.3.10}$$

where σ^2 is a positive constant and $\mathrm{Min}(s,t)$ is the smaller of the two variables s and t, see [17]. From (2.3.10) it follows that the variance of $W(t)$ is

$$K(t,t) = \left\langle W(t)^2 \right\rangle = \sigma^2 t \tag{2.3.11}$$

[8] See, for example, [22] section 2.4.

and, therefore, $W(t)$ is a $\mathcal{N}\left(0,\sigma^2 t\right)$ random variable. Also, from (2.3.10) it follows that for times s,t

$$\left\langle [W(t)-W(s)]^2 \right\rangle = \sigma^2 |t-s| \tag{2.3.12}$$

so that the *increment* $W(t)-W(s)$ is an $\mathcal{N}\left(0,\sigma^2|t-s|\right)$ random variable.

If $W(0)=0$ and $\sigma=1$ then $W(t)$ is called the standard Wiener process. For this process if the particle is at position $W(s)$ at time s, then at a future time $t>s$, with a probability $[2\pi(t-s)]^{-1/2}\times\exp\left[-z^2/(2(t-s))\right]$ it will have changed position by an amount z. The mean change of position is zero, and the standard deviation of the change in position grows as $\sqrt{t-s}$. The particle is therefore most likely to be found in an interval of width $\sqrt{t-s}$ centred on its initial location, $W(s)$. This growth in the width of this interval, as the square root of the elapsed time, is characteristic of a diffusion process.

Since $W(t)$ is a Gaussian process the values of the process, $W_i, i=1,2,\cdots$, at any *sample* times, $t_i, i=1,2,\cdots$, are Gaussian random variables and their joint p.d.f.s are Gaussian. Also, the increments $\Delta W_i \equiv W_{i+1}-W_i$ during the intervals $(t_i,t_{i+1}], i=1,2,\cdots$ are Gaussian and for $i\neq j$ we have $\left\langle \Delta W_i \Delta W_j \right\rangle = 0$; the increments ΔW_i are therefore independent for non-overlapping intervals and $W(t)$ is a Markov process.

When we consider stochastic differential equations we shall deal with the differential increment $\mathrm{d}W(t)\equiv W(t+\mathrm{d}t)-W(t)$ in the standard Wiener process during the infinitesimal time interval $(t,t+\mathrm{d}t]$. This increment has mean $\langle \mathrm{d}W(t)\rangle = 0$ and variance $\langle\langle \mathrm{d}W(t)\rangle\rangle = \mathrm{d}t$. We can therefore interpret $\mathrm{d}W(t)$ as a *stochastic differential* with an $\mathcal{N}(0,\mathrm{d}t)$ distribution, and this property is used when simulating stochastic processes *driven* by Wiener noise. Note that although the mean of the increment $\mathrm{d}W(t)$ is zero, the mean of the *magnitude* of the increment is $\langle|\mathrm{d}W(t)|\rangle = \sqrt{2\mathrm{d}t/\pi} \sim \sqrt{\mathrm{d}t}$. Further[9], since $\mathrm{d}W(t)\sim\mathcal{N}(0,\mathrm{d}t)$ the square of the Wiener increment, $\mathrm{d}W^2(t)$, has mean $\mathrm{d}t$ and variance $\mathrm{d}t^2$. In the continuum limit the variance vanishes and we may treat $\mathrm{d}W^2(t)$ as a *deterministic* quantity, equal to its mean value: i.e. $\mathrm{d}W^2(t) = \left\langle \mathrm{d}W^2(t)\right\rangle = \mathrm{d}t$. We use this result in subsection (5.2.2) when deriving a system of stochastic differential equations for a diffusive random matrix process driven by Wiener noise. We consider the nature of these so-called Langevin equations in the next section.

[9] Since $\mathrm{d}W\sim\mathcal{N}(0,\mathrm{d}t)$, $\left\langle \mathrm{d}W^{2k}\right\rangle = \dfrac{(2k)!}{2^k k!}\mathrm{d}t^k, k=1,2,\cdots$

2.3.5 The Langevin equation

The first appearance of a stochastic differential equation in Physics is due to Langevin who applied Newton's second law to a particle undergoing Brownian motion [27]. In the absence of any exterior force, e.g. gravity, Langevin's equation (for a particle of unit mass) can be written in the reduced form [4]

$$\frac{\mathrm{d}V}{\mathrm{d}t} = -\gamma V(t) + F_{\mathrm{L}}(t). \tag{2.3.13}$$

The $-\gamma V(t)$ term represents the *Stoke's drag* force on the 'Brownian' particle due to *viscous damping*, caused by the surrounding fluid particles.

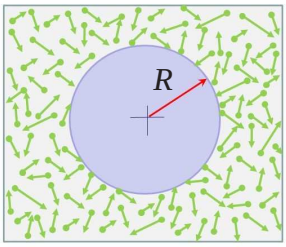

Fig. 2.6 The figure shows a sphere of radius R immersed in a fluid comprised of particles whose size is much smaller than R. The constant bombardment of the sphere by the fluid particles produces a random net impulse driving the erratic *Brownian* motion of the sphere, and viscous drag on the sphere.

For a spherical particle of radius R the constant $\gamma = 6\pi R\eta$, where η is the fluid viscosity. The 'Langevin' forcing term $F_{\mathrm{L}}(t)$, is the *randomly fluctuating* impulsive force on the particle, due to the molecular bombardment by the fluid particles, see figure (2.6) .

The Langevin force, $F_{\mathrm{L}}(t)$, can be written as $\sqrt{2D}\xi(t)$, where D is the diffusion coefficient for the motion and $\xi(t)$ is white noise[10], the formal derivative of the Wiener process. The process $\xi(t)$ is a zero-mean Gaussian process which is delta-correlated in time:

$$\langle \xi(t) \rangle = 0 \quad \text{and} \quad \langle \xi(t)\xi(t') \rangle \equiv \delta(t - t'). \tag{2.3.14}$$

In general a s.d.e. for a random process $X(t)$ driven by *Wiener noise* is a relationship between the stochastic differentials, $\mathrm{d}X(t)$ and $\mathrm{d}W(t)$. We are interested in processes which satisfy

[10] This name reflects the fact that the power spectral density of the process is constant: all frequencies are present, with equal power, as is the case for the white light. See for example [4].

Langevin equations of the form

$$\frac{\mathrm{d}X(t)}{\mathrm{dt}} = v[X(t),t] + \sigma[X(t),t]\xi(t) \tag{2.3.15}$$

or, written in differential form using $\mathrm{d}W(t) = \xi(t)\mathrm{dt}$,

$$\mathrm{d}X(t) = v[X(t),t]\mathrm{dt} + \sigma[X(t),t]\mathrm{d}W(t). \tag{2.3.16}$$

The increment $\mathrm{d}X(t)$ is therefore comprised of two terms, a *transport* or *drift* term, which is proportional to the length of the time interval, and a *diffusive* term which, being a multiple of $\mathrm{d}W(t)$, is proportional to $\sqrt{\mathrm{dt}}$ and which may, therefore, be much larger than the former. We note that if $X(t)$ satisfies (2.3.16) then, in the continuum limit, we have

$$F_1 \equiv \frac{\langle \mathrm{d}X \rangle}{\mathrm{dt}} = v \ \text{ and } \ F_2 \equiv \frac{\left\langle \mathrm{d}X^2 \right\rangle}{\mathrm{dt}} = \sigma^2. \tag{2.3.17}$$

Equation (2.3.16) can be used to model the position, $X(t)$, of a small particle which undergoes diffusive motion with drift, then the coefficient v is the *drift velocity* and $\sigma^2/2$ is the *diffusion coefficient*. A process satisfying (2.3.16) is a *diffusion* in $\mathbb{R}^1$.

The solution of a stochastic differential equation

The Langevin equation for the velocity $V(t)$ of a Brownian particle can be formally integrated to give

$$V(t) = \sqrt{2D}\int_{-\infty}^{t} e^{-\gamma(t-s)}\xi(s)\mathrm{d}s \tag{2.3.18}$$

this velocity process, $V(t)$, is called the *Ornstein-Uhlenbeck* process [62].

However, in general, very few s.d.e.s can be integrated exactly, and given a s.d.e. for a process, $X(t)$, *solving* it usually means determining the *statistical properties* of $X(t)$ using numerical methods [12]. One numerical method of solution, which we shall use in our simulations, is the stochastic analogue of the Euler method for o.d.e.s. Using this method, for the s.d.e. given in (2.3.16), an approximate realization or sample path on the time interval $[0,T]$ consists of lines joining the points (t_i, x_i), $i = 0, 1, \cdots, N$ where $t_k = k\Delta t$, $k = 0, 1, \cdots N$ with $\Delta t \equiv T/N$, and where the x_k are given by the iterative scheme

$$x_{k+1} = x_k + v(x_k, t_k)\,\Delta t + \sigma(x_k, t_k)\,\zeta_k\,\sqrt{\Delta t} \tag{2.3.19}$$

where the ζ_k, $k = 1, 2, \cdots, N$ are i.i.d. $\mathcal{N}(0,1)$ random variables.

2.3.6 The Fokker-Planck equation

In addition to using the Langevin equation, (2.3.16), to construct approximate sample paths, using (2.3.19), we can also use it to derive a partial differential equation, the Fokker-Planck (F.P.) equation, for the p.d.f. $P_X(x,t)$, [4, 30, 45, 63]. To derive this equation we note that *for a Markov process* $P_X(x,t)$ is, in fact, the *transition* p.d.f. $P(x,t \mid x_0,t_0)$, with the initial condition $(x_0,t_0) = (x_0,0)$ understood. Now, the transition p.d.f. of any Markov process satisfies the Chapman-Kolmogorov identity:

$$P(x_3,t_3 \mid x_1,t_1) = \int_{\mathbb{R}} \mathrm{d}x_2 P(x_3,t_3 \mid x_2,t_2) P(x_2,t_2 \mid x_1,t_1) \tag{2.3.20}$$

where $P\left(x_j,t_j \mid x_i,t_i\right)$ is the p.d.f. for the transition to state x_j at time t_j *given* that the process was in state x_i at time t_i. The meaning of this identity is illustrated in figure (2.7).

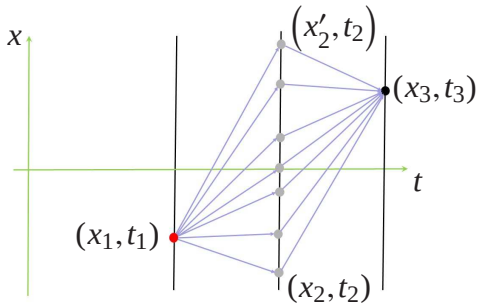

Fig. 2.7 During the evolution of the stochastic process, $X(t)$, between the times t_1 and t_3, at the intermediate time t_2 the process may have any allowable value. The transition probability from (x_1,t_1) to (x_3,t_3) is computed by calculating the probabilities of transitioning via every intermediate state and summing over the intermediate states.

To reach the state x_3 at time t_3 from the state x_1 at time t_1 we can, in principle, proceed through any intermediate state x_2 at the intermediate time t_2. The density $P(x_3,t_3 \mid x_1,t_1)$ is therefore obtained by integrating contributions from every possible intermediate state. Hence, $P(x_3,t_3 \mid x_1,t_1)$ involves the products of the transition probabilities from (x_1,t_1) to (x_2,t_2) and from (x_2,t_2) to (x_3,t_3), integrated over every possible value of x_2.

Setting $(x_3,t_3)=(x,t+\Delta t)$, $(x_2,t_2)=(x',t)$ and $(x_1,t_1)=(x_0,t_0)$ gives

$$P_X(x,t+\Delta t)=\int_{\mathbb{R}} \mathrm{d}x' P(x,t+\Delta t|x',t)\,P_X(x',t). \tag{2.3.21}$$

The F.P. equation is obtained by making a series expansion of the integrand. We have

$$\begin{aligned} P(x,t+\Delta t|x',t)\,P_X(x',t) &= P([x-\Delta x]+\Delta x,t+\Delta t,\mid [x-\Delta x],t)\,P_X([x-\Delta x],t) \\ &= \sum_{k=0}^{\infty} \frac{(-1)^k(\Delta x)^k}{k!}\frac{\partial^k}{\partial x^k}\left[P(x+\Delta x,t+\Delta t\mid x,t)\,P_X(x,t)\right] \end{aligned} \tag{2.3.22}$$

where $\Delta x \equiv x-x'$. Substituting this into equation (2.3.21) and performing the integration with respect to x' gives

$$P_X(x,t+\Delta t)=\sum_{k=0}^{\infty}\frac{(-1)^k}{k!}\frac{\partial^k}{\partial x^k}\left[M_k(x,t,\Delta t)\,P_X(x,t)\right] \tag{2.3.23}$$

where $M_k(x,t,\Delta t)$ is the k^{th} *jump moment* for the system, defined as

$$M_k(x,t,\Delta t)\equiv\int_{\mathbb{R}}\mathrm{d}z(z-x)^k P(z,t+\Delta t\mid x,t). \tag{2.3.24}$$

Now, $M_0=1$ and, since $P(z,t\mid x,t)=\delta(z-x)$ it follows from equation (2.3.24) that, for $k\geq 1$, $M_k(x,t,\Delta t)\to 0$ as $\Delta t\to 0$. Therefore, assuming that for $k\geq 1$ the jump moments are of the form

$$M_k(x,t,\Delta t)=F_k(x,t)\Delta t+\mathrm{o}(\Delta \mathrm{t}) \tag{2.3.25}$$

for some functions $F_k(x,t)$ and substituting this into equation (2.3.23) gives, in the limit as $\Delta t\to 0$

$$\frac{\partial P_X(x,t)}{\partial t}=\sum_{k=1}^{\infty}\frac{(-1)^k}{k!}\frac{\partial^k}{\partial x^k}\left[F_k(x,t)\,P_X(x,t)\right]. \tag{2.3.26}$$

Equation (2.3.26) is called the Kramers-Moyal expansion

Any change of $P_X(x,t)$ with time t is due to the difference between an increase caused by transitions to the state x at time t and a decrease due to transitions away from this state. By considering this balance we may use the Chapman Kolmogorov equation, to derive a so-called *master equation*. This is an integro-differential equation for the evolution of $P_X(x,t)$; the derivation can be found in reference [4], we simply quote the result:

$$\frac{\partial P_X(x,t)}{\partial t}=\int_{\mathbb{R}}\mathrm{d}x'\left[T(x|x',t)\,P_X(x',t)-T(x'|x,t)\,P_X(x,t)\right] \tag{2.3.27}$$

where $T(x_2|x_1,t)$ is interpreted as the *transition probability per unit time* from x_1 to x_2 at time t. The Kramers-Moyal expansion, equation (2.3.26) is, therefore, essentially a series expansion of the master equation.

For a diffusive Markov process governed by a Langevin equation it can be shown that F_1 and F_2 are the functions given in equation (2.3.17) and that the moments higher than the second vanish [45]. Therefore, for a such a process, the Kramers-Moyal series terminates after two terms giving the Fokker-Planck equation for $P_X(x,t)$:

$$\frac{\partial P_X(x,t)}{\partial t} = -\frac{\partial [F_1(x,t)P_X(x,t)]}{\partial x} + \frac{1}{2}\frac{\partial^2 [F_2(x,t)P_X(x,t)]}{\partial x^2}. \tag{2.3.28}$$

The F_1 term is called the drift or transport term and the F_2 term is the diffusion term. If F_1 and F_2 are independent of t then the process is stationary. The advection-diffusion equation (2.3.6) is a particular case of the F.P. equation.

Note that we can write the F.P. equation, (2.3.28), as a *continuity equation*:

$$\frac{\partial P_X(x,t)}{\partial t} + \frac{\partial J(x,t)}{\partial x} = 0 \tag{2.3.29}$$

where the *probability current* $J(x,t)$ is

$$J(x,t) \equiv F_1(x,t)P_X(x,t) - \frac{1}{2}\frac{\partial [F_2(x,t)P_X(x,t)]}{\partial x}. \tag{2.3.30}$$

Hence, the F.P. equation can be thought of as a continuity equation for the evolution of the probability density $P_X(x,t)$.

2.3.7 The multivariate case

The results of the previous sections generalize to the multivariate case. For a d-dimensional vector-valued stochastic process, governed by a system of Langevin equations, the joint p.d.f. of the stochastic variables satisfies a multivariate F.P. equation.

Let $X_i,\ i = 1,\cdots,d$ be stochastic processes driven by the Wiener processes[11] $W_i,\ i = 1,\cdots,d$ where the $\mathrm{d}W_i$ satisfy $\left\langle \mathrm{d}W_i \mathrm{d}W_j \right\rangle = \mathrm{dt}\ \delta_{ij}$ and let $\boldsymbol{x} = [x_1,\cdots,x_d]^{\mathrm{T}}$, $\boldsymbol{X} = [X_1,\cdots,X_d]^{\mathrm{T}}$ and

[11] We assume here that there are d independent Wiener noise processes, but this is not strictly necessary.

$\boldsymbol{W} = [W_1, \cdots, W_d]^{\mathrm{T}}$. Then, if the X_i satisfy the d-dimensional system of Langevin equations

$$\mathrm{d}X_i = v_i(\boldsymbol{X}, t)\mathrm{d}t + \sum_{j=1}^{d} \sigma_{ij}(\boldsymbol{X}, t)\,\mathrm{d}W_j, \quad i = 1, \cdots, d, \tag{2.3.31}$$

where the transport and drift coefficients $v_i(\boldsymbol{X}, t)$ and $\sigma_{ij}(\boldsymbol{X}, t)$ are known functions of position and time, the joint p.d.f. of $X_1, \cdots, X_d$, $P_{\boldsymbol{X}}(\boldsymbol{x}, t)$, satisfies the multivariate F.P. equation

$$\frac{\partial P_{\boldsymbol{X}}}{\partial t} = -\sum_{i=1}^{d} \frac{\partial}{\partial x_i}(v_i P_{\boldsymbol{X}}) + \sum_{i=1}^{d}\sum_{j=1}^{d} \frac{\partial^2}{\partial x_i \partial x_j}\left(D_{ij} P_{\boldsymbol{X}}\right) \tag{2.3.32}$$

where the v_i, D_{ij} and $P_{\boldsymbol{X}}$ and their derivatives are evaluated at $(\boldsymbol{X}, t)$ and the D_{ij} are the elements of the *covariance matrix* matrix of the X_i, given, in the limit as $\mathrm{d}t \to 0$, by

$$D_{ij} \equiv \frac{\left\langle \mathrm{d}X_i \mathrm{d}X_j \right\rangle}{2\mathrm{d}t} = \frac{1}{2\mathrm{d}t} \sum_{r=1}^{d}\sum_{s=1}^{d} \sigma_{ir}\sigma_{js} \langle \mathrm{d}W_r \mathrm{d}W_s \rangle = \frac{1}{2}\left[\boldsymbol{\sigma}\boldsymbol{\sigma}^T\right]_{ij}. \tag{2.3.33}$$

The system of s.d.e.s (2.3.31) can be written in vector form

$$\mathrm{d}\boldsymbol{X} = \boldsymbol{v}(\boldsymbol{X}, t)\mathrm{d}t + \boldsymbol{\sigma}(\boldsymbol{X}, t)\,\mathrm{d}\boldsymbol{W} \tag{2.3.34}$$

with $\boldsymbol{v} \equiv [v_1, \cdots, v_d]^{\mathrm{T}}$ and $\boldsymbol{\sigma} \equiv \left[\sigma_{ij}\right]$ and the F.P. equation (2.3.32) can be written as the continuity equation

$$\frac{\partial P_{\boldsymbol{X}}}{\partial t} + \boldsymbol{\nabla} \cdot \boldsymbol{J} = 0 \tag{2.3.35}$$

where $\boldsymbol{J} \equiv [J_1, \cdots, J_d]^{\mathrm{T}}$ and each component, J_i, is given by

$$J_i = v_i P_{\boldsymbol{X}} - \sum_{j=1}^{d} \frac{\partial}{\partial x_j}\left(D_{ij} P_{\boldsymbol{X}}\right). \tag{2.3.36}$$

$\boldsymbol{J}$ is referred to as the probability current. If $\boldsymbol{D}$ is independent of $\boldsymbol{x}$, we say that the diffusion is homogeneous; in this case $\boldsymbol{J}$ simplifies to $\boldsymbol{J} \equiv (\boldsymbol{v}P_{\boldsymbol{X}}) - \boldsymbol{D}\boldsymbol{\nabla}P_{\boldsymbol{X}}$.

We shall encounter equations of the form (2.3.32) and (2.3.34) in chapters 3,4 and 5.

2.4 Synthetic turbulence

2.4.1 The nature of turbulence

Turbulence, the most common state of fluid motion, is characterized by chaotic behavior [28]. At any point in a turbulent flow the fluid velocity appears to fluctuate randomly and unpredictably, about some mean value. Figure (2.8)[12] shows an example of a turbulent flow, caused by a jet of fluid being injected into a surrounding bath. The jet is injected from the left and the colours indicates the age of the vortices and eddys, with the youngest on the left in green and the oldest, towards the right in blue. Note that, on the right of the figure, although the velocity field is very irregular it is so in a somewhat homogeneous and isotropic manner.

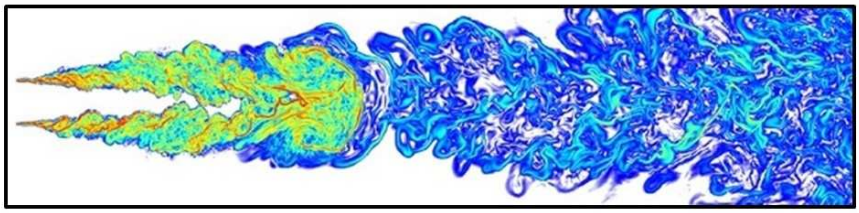

Fig. 2.8 The figure shows a jet of fluid injected, from the left, into a bath of fluid. The jet creates a turbulent wake in which the flow is highly irregular. On the right of the figure the turbulence is fully developed: the vortices and eddys of the flow appear to be distributed in an isotropic and homogeneous manner.

In principle, a turbulent flow is described by the Navier Stokes equations but, because the ensemble of particles comprising the fluid has a great many degrees of freedom, and because of the randomness in the flow, it is necessary to take a statistical approach when modelling turbulence. In a *fully developed* turbulent flow the velocity field is *homogeneous and isotropic*, so that the statistical properties of the flow are the same at any point and in any direction.

Particle-laden turbulent flows, such as volcanic plumes, are particularly interesting [46, 53]. A remarkable feature of some particle-laden turbulent flows is the tendency of the particles in suspension to form *fractal clusters* [1, 2, 50, 73] and it is these structures that are of primary interest to us. For further detail on turbulence we refer the reader to [11, 28, 59, 60].

[12] Courtesey Dr. Dong-Hyuk Shin, School of Engineering, The University of Edinburgh.

2.4.2 A stochastic model of fully developed turbulence in 2D

We shall consider fractal structures formed by particles suspended in a fully developed turbulent flow in two-dimensions. To simulate the flow we shall adopt a simple stochastic model, due to Kraichnan [26], which reproduces the statistical characteristics of fully developed turbulence sufficiently well for our purposes.

For a two dimensional flow in the x_1x_2 plane, the fluid velocity $\boldsymbol{u}(\boldsymbol{r},t)$ can be written as the sum of irrotational and solenoidal components:

$$\boldsymbol{u} = \beta\,\nabla\phi + \nabla\wedge\boldsymbol{\Psi} = \left(\beta\frac{\partial\phi}{\partial x_1} + \frac{\partial\psi}{\partial x_2},\, \beta\frac{\partial\phi}{\partial x_2} - \frac{\partial\psi}{\partial x_1}\right)^{\mathrm{T}} \tag{2.4.1}$$

where $\phi(\boldsymbol{r},t)$ is the *scalar potential* and $\boldsymbol{\Psi}(\boldsymbol{r},t) = \psi(\boldsymbol{r},t)\boldsymbol{e}_3$, is the *vector potential* and $\nabla\wedge\boldsymbol{\Psi}$ is the curl of $\boldsymbol{\Psi}$. The function ψ is the *stream function* and $\boldsymbol{e}_3$ is the unit normal to the x_1x_2 plane. The potentials ϕ and ψ are *independent of each other*. The parameter β is a measure of the *compressibility* of the flow: when $\beta = 0$ then $\mathrm{div}(\boldsymbol{u}) = 0$, corresponding to an incompressible flow.

For a turbulent flow the potential functions are *random fields*, in both time and space [38]. At any given fixed point the potentials $\phi(\boldsymbol{r},t)$ and $\psi(\boldsymbol{r},t)$ are stochastic process which fluctuate randomly in time. Also, since we are interested in fully developed turbulence, at any instant the *spatial* fields have isotropic and homogeneous spatial statistics.

In two dimensions an isotropic and homogeneous random field, $\phi(\boldsymbol{r})$, satisfies the following isotropy relation [71], which we proceed to show,

$$\left\langle(\phi_{x_1x_1})^2\right\rangle = \left\langle(\phi_{x_2x_2})^2\right\rangle = 3\left\langle(\phi_{x_1x_2})^2\right\rangle = 3\left\langle(\phi_{x_1x_1})(\phi_{x_2x_2})\right\rangle \tag{2.4.2}$$

where subscripts denote partial differentiation. This relation can be derived from the Fourier representation of $\phi(\boldsymbol{r})$:

$$\phi(\boldsymbol{r}) = \int_{\mathbb{R}^2} \mathrm{d}\boldsymbol{k}\;\hat{\phi}(\boldsymbol{k})\;\exp\left[i\boldsymbol{k}\cdot\boldsymbol{r}\right]. \tag{2.4.3}$$

The Fourier transform, $\hat{\phi}(\boldsymbol{k})$, has the following statistics

$$\left\langle\hat{\phi}(\boldsymbol{k})\right\rangle = 0 \;\text{ and }\; \left\langle\hat{\phi}(\boldsymbol{k})\overline{\hat{\phi}(\boldsymbol{k}')}\right\rangle = S(k)\delta(\boldsymbol{k}-\boldsymbol{k}') \tag{2.4.4}$$

where $S(k) = S(|\boldsymbol{k}|)$ is the *spectral intensity*. From (2.4.3) differentiating with respect to x_1 we have

$$\phi_{x_1x_1} = \int_{\mathbb{R}^2} \mathrm{d}\boldsymbol{k}\left(-k_x^2\right) \exp\left[i\boldsymbol{k}\cdot\boldsymbol{r}\right]\hat{\phi}(\boldsymbol{k})$$

and therefore

$$\left\langle(\phi_{x_1x_1})^2\right\rangle = \int_{\mathbb{R}^2} \mathrm{d}\boldsymbol{k}\left(-k_x^2\right)\int_{\mathbb{R}^2} \mathrm{d}\boldsymbol{k}'\left(-k_x'^{\,2}\right)\left\langle\hat{\phi}(\boldsymbol{k})\hat{\phi}(\boldsymbol{k}')\right\rangle. \tag{2.4.5}$$

Writing the integrals in polar coordinates in $\boldsymbol{k}$-space, with $\boldsymbol{k} = (k_x, k_y) = (k\cos\theta, k\sin\theta)$, and using (2.4.4) gives

$$\left\langle(\phi_{x_1x_1})^2\right\rangle = \int_0^{2\pi} \mathrm{d}\theta\cos^4\theta \int_0^\infty \mathrm{d}k\, k^5\, S(k) = \frac{3\pi}{4}\int_0^\infty \mathrm{d}k\, k^5\, S(k). \tag{2.4.6}$$

Similarly, we find that

$$\left\langle(\phi_{x_1x_2})^2\right\rangle = \left\langle(\phi_{x_1x_1})(\phi_{x_2x_2})\right\rangle = \frac{\pi}{4}\int_0^\infty \mathrm{d}k\, k^5\, S(k). \tag{2.4.7}$$

Comparing (2.4.6) and (2.4.7) gives the isotropy relation (2.4.2).

To model a fully developed two-dimensional turbulent flow we expand the potential fields $\phi(\boldsymbol{r},t)$ and $\psi(\boldsymbol{r},t)$ as Fourier series with time-dependent coefficients that are random variables. The statistics of the coefficients are chosen so that at each instant in time the series produces a smooth, translationally invariant, isotropic spatial field. Therefore at any time $\phi(\boldsymbol{r},t)$ and $\psi(\boldsymbol{r},t)$ satisfy equation (2.4.2). Also, since we are interested in diffusive effects, the Fourier coefficients are chosen so that the fields values are delta correlated in time.

Taking the coordinate space to be the square $[0,L]\times[0,L]$ of the x_1x_2 plane, with *periodic boundary conditions*, then at time t the Fourier series expansion of ϕ is of the form

$$\phi \equiv \phi(\boldsymbol{r},t) = \sum_{\boldsymbol{k}} a_{\boldsymbol{k}}(t)\sin(\boldsymbol{k}\cdot\boldsymbol{r}) + b_{\boldsymbol{k}}(t)\cos(\boldsymbol{k}\cdot\boldsymbol{r}) \tag{2.4.8}$$

and similarly for ψ. The Fourier coefficients, $a_{\boldsymbol{k}}$, are i.i.d. random variables with the following statistics:

$$\langle a_{\boldsymbol{k}}(t)\rangle = 0 \quad \text{and} \quad \langle a_{\boldsymbol{k}}(t)\, a_{\boldsymbol{k}'}(t')\rangle = C_0\,\delta_{t,t'}\,\delta_{\boldsymbol{k},\boldsymbol{k}'}\exp\left[-\frac{1}{2}\boldsymbol{k}^2\xi^2\right] \tag{2.4.9}$$

and similarly for $b_{\boldsymbol{k}}$. The parameter ξ is the *correlation length* of the flow. Field values at points separated by a distance greater than ξ are, in effect, uncorrelated but field values at

closer points are correlated and the Gaussian nature of the correlation function assures the smoothness of the spatial field. The wave vectors, $\boldsymbol{k}$, are given by

$$\boldsymbol{k} = \frac{2\pi}{L}(n,m) \ , \quad n,m = 0,1,2,\ldots. \tag{2.4.10}$$

In practice the Fourier series is finite, so that $0 \le m,n \le N$ for some integer N. We find that if $N < 6$ the truncated series approximations of the potential fields are not very smooth and if $N > 20$ the computation of the field values is time-consuming. In our simulations we have $N = 12$.

Note that, since the potential fields ϕ and ψ are independent of each other, the expectation value of their product and of any product of their derivatives of vanishes. The statistics of the fields can be calculated from the Fourier expansions of the potentials, by replacing the sum over the discrete states in k-space by integrals, using the *density of states* rule:

$$\sum_{\boldsymbol{k}}[\cdots] \to \frac{L^2}{(4\pi)^2}\int_0^\infty \mathrm{d}k_x \int_0^\infty \mathrm{d}k_y\,[\cdots] = \frac{L^2}{16\pi^2}\int_{\mathbb{R}^2} \mathrm{d}\boldsymbol{k}\,[\cdots] \tag{2.4.11}$$

where the last integral is over all of $\boldsymbol{k}$ space, and it is assumed that the integrand is an even function of k_x and k_y. For example, using the Fourier expansion of ϕ and the orthogonality and correlation properties of the coefficients we have

$$\begin{aligned}
\left\langle (\phi_{x_1 x_1})^2 \right\rangle &= \sum_{\boldsymbol{k}} C_0\, k_x^4\ exp\left[-\boldsymbol{k}^2\xi^2/2\right] \\
&= \frac{C_0 L^2}{16\pi^2}\int_{\mathbb{R}^2} \mathrm{d}\,\boldsymbol{k}\, k_x^4\, exp\left[-\boldsymbol{k}^2\xi^2/2\right] \\
&= \frac{C_0 L^2}{16\pi^2}\int_0^{2\pi} \mathrm{d}\theta\, \cos^4\theta \int_{-\infty}^{\infty} \mathrm{d}k\, k^5\, exp\left[-k^2\xi^2/2\right] \\
&= \frac{3C_0 L^2}{8\pi\xi^6}
\end{aligned}$$

and with normalization $\left\langle (\phi_{x_1 x_1})^2 \right\rangle = 3$, it follows that the coefficient $C_0 = \dfrac{8\pi\xi^6}{L^2}$.

In the simulations $L = 1$, so that the coordinate space is the unit square with the edges identified to make a torus, and the correlation length of the flow is set to $\xi = 0.25$. The flow model therefore has a single parameter, β, the compressibility of the flow.

2.4.3 Advection of particles in a turbulent flow

Particles advected in a two dimensional turbulent flow can sample a fractal measure [50]. We may think of the two dimensional flow as being on the surface of a fluid, and the particles as identical spheres sitting on the surface. Suppose that the particles have radius R and mass m and that the fluid has density ρ_f, kinematic viscosity ν and is moving with a velocity field $\boldsymbol{u}(\boldsymbol{r},t)$. Then, provided that the motion of a particle does not affect the velocity field and that it is dominated by viscous, Stoke's, drag, the equation of motion of a particle at point $\boldsymbol{r}$ at time t is [33]:

$$\ddot{\boldsymbol{r}} = \gamma\,(\boldsymbol{u}(\boldsymbol{r},t) - \dot{\boldsymbol{r}}\,) \tag{2.4.12}$$

where $\gamma = 6\pi R\rho_f \nu/m$. In advective motion, the particles are carried along with the flow, so that $\ddot{\boldsymbol{r}} = \boldsymbol{0}$ and the particle velocity is

$$\dot{\boldsymbol{r}} = \boldsymbol{u}(\boldsymbol{r},t). \tag{2.4.13}$$

Particles advected in this way are called *tracer particles*; their trajectories are the *pathlines* of the flow and their dynamics is important in the study of so-called passive scalar problems, for example the dispersion of pollutants.

2.4.4 The flow mapping used in the numerical investigations

In our numerical investigations we start with an ensemble of particles randomly distributed in the unit square and compute the positions of the points at discrete times $t_n = n\delta t, n = 1,2,\cdots$. After many timesteps the positions of the particles sample a fractal measure, as shown in figure (1.1(b)). We then select a number of triples of points which form the vertices of triangular constellations, whose size and shape parameters we then analyze. To simulate the effects of advection *and diffusion* on the particle positions we use the *map*

$$\boldsymbol{r}_{n+1} = \boldsymbol{r}_n + \boldsymbol{u}_n(\boldsymbol{r}_n,\ t_n)\ \sqrt{\delta t}, \quad n = 0,1,\cdots \tag{2.4.14}$$

where $\boldsymbol{r}_n \equiv \boldsymbol{r}\,(t_n),\ n = 0,1,\cdots$

The velocity field is given by (2.4.1) evaluated at time t_n:

$$\boldsymbol{u}_n = \left(\beta\frac{\partial\phi_n}{\partial x} + \frac{\partial\psi_n}{\partial y},\ \beta\frac{\partial\phi_n}{\partial y} - \frac{\partial\psi_n}{\partial x}\right) \tag{2.4.15}$$

where $\partial\phi_n/\partial x \equiv \partial\phi/\partial x(x_n, y_n, t_n)$, etc., with the derivatives of the fields ϕ and ψ being determined from Fourier expansions of the form (2.4.8). The timestep δt is set sufficiently small to allow the use of a *diffusive approximation*, which is equivalent to using a velocity field which is *delta-correlated* in time [8].

Chapter 3

Triangular constellations in fractal measures

> The laws of Nature are written in the language of mathematics...the symbols are triangles, circles and other geometrical figures, without whose help it is impossible to comprehend a single word.
>
> *Galileo Galilei*

In subsection (2.2.3) we saw that the correlation dimension of a fractal set, D_2, can be interpreted as the exponent in a power law giving the expected number of points in a small ball, centred on a reference point, as a function of the radius of the ball [69, 70]. Essentially, D_2 depends on the distribution of the separation of pairs of points sampling the fractal or, in other words, on the distribution of the *size* of binary constellations. Given this relationship, between a fractal dimension and the distribution of the size of binary constellations, it is natural to consider the distribution of the geometrical properties of constellations containing more than two points.

In this chapter we consider *triangular constellations* formed by triples of points in a fractal measure in two spatial dimensions. Here, in addition to a measure of size, we can also define measures of *shape*. These *shape parameters* are based on the intrinsic geometrical properties of constellations, they are independent of their size, location and orientation. It is reasonable to expect that the statistics of these parameters will reflect, and provide insight into, the local structure of the fractal measure.

We introduce a measure of the *flatness* of a triangle, Z, and we analyze its statistics. Using the random compressible flow model, introduced in section (2.4.2), as a generic model of chaotic dynamics we consider the p.d.f., P_Z, for a one-parameter family of point fractals in the plane. We find that P_Z is associated with power-laws and undergoes a *phase transition* as the compressibility parameter, β, (see equation (2.4.1)), is reduced through a critical value. In the concluding section of the chapter we provide an interpretation of these findings.

This chapter is based on [65], *Triangular constellations in fractal measures*, published in the journal European Physics Letters.

3.1 Characterising fractals via constellations

3.1.1 A statistical approach to the problem

Constellations in a fractal are sets of points sampling the fractal which form the vertices of a simplex. Roughly speaking they are the simplest geometrical structures that can be formed in the space in which the fractal is embedded. For a fractal embedded in $\mathbb{R}^2$ we may consider binary and triangular constellations. These consist of two and three distinct points respectively and they form one and two dimensional simplexes, i.e. line segments and triangles, respectively. For a fractal embedded in $\mathbb{R}^3$ we may also consider three dimensional tetrahedral constellations, comprised of four distinct non-coplanar vertices. See figure (3.1).

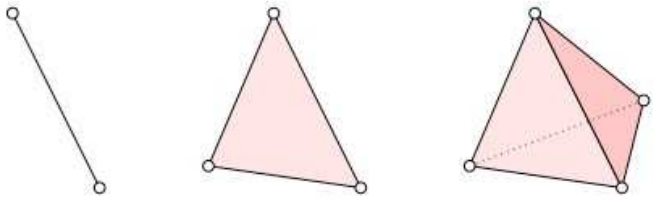

Fig. 3.1 Binary, triangular and tetrahedral constellations correspond to simplices, the simplest sets which *span* a volume element, in $d = 1, 2$ and 3 dimensions, respectively.

To characterize the local structure of a fractal using the properties of constellations we will construct numerically determined probability distributions of the size and shape parameters of a large *sample* of constellations whose vertices are points in the fractal. We describe the

sampling procedure below, taking the simplices to be triangles in $d = 2$ and tetrahedra in $d = 3$ spatial dimensions, respectively.

We first select, at random, a large number of *reference* points in the fractal, these are the *reference vertices*. Then in a ball of radius ε centred on each reference vertex we select a number of sets of points; for a fractal embedded in $\mathbb{R}^d$ each set contains d points. Each set of points together with the reference vertex defines the $d+1$ vertices of a constellation which lies inside the ball. We then compute the values of the size and shape parameters for each such constellation and from this data we construct the numerically determined p.d.f.s. By taking a smaller value of the radius, ε, and selecting new sets of vertices lying in the smaller ε-ball we can examine how the distributions of size and shape parameters behaves as $\varepsilon \to 0$.

The approach is illustrated schematically, for $d = 2$, in figure (3.2). This figure shows three epsilon-disks each centred on a reference vertex, which is a point in the fractal. Within each disk there are four triangular constellations with the reference point as one of the vertices.

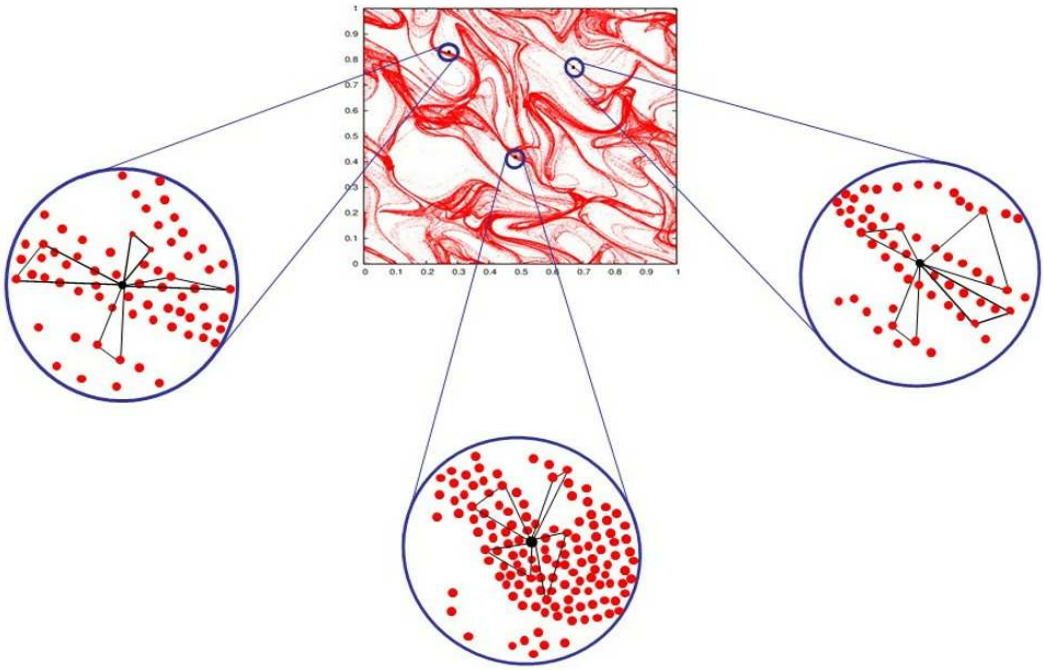

Fig. 3.2 At each timestep in the evolution of the system a large number of reference particles are selected at random (only three references particles are shown here). Within a small disk centred on each reference particle a number of triangular constellations are then obtained by selecting pairs of particles. The size and shape parameters are calculated for each of these triangular constellations and the results are tallied to give numerical probability density functions. The asymptotic behaviour of the p.d.f.s is be obtained by taking a sequence of diminishing disk sizes.

3.1.2 Describing the size and shape of a triangular constellation

Figure (3.3) shows a triangular constellation in a fractal in $\mathbb{R}^2$, formed by a reference point P_0 and two points, P_1 and P_2, lying in some ε disk centred on P_0. Q is the foot of the perpendicular to P_0P_1 through P_2 and G is the centroid of the triangle. Using the nomenclature of elementary geometry, we may think of P_0P_1 as the *base* and QP_2 as the *altitude* of the triangle.

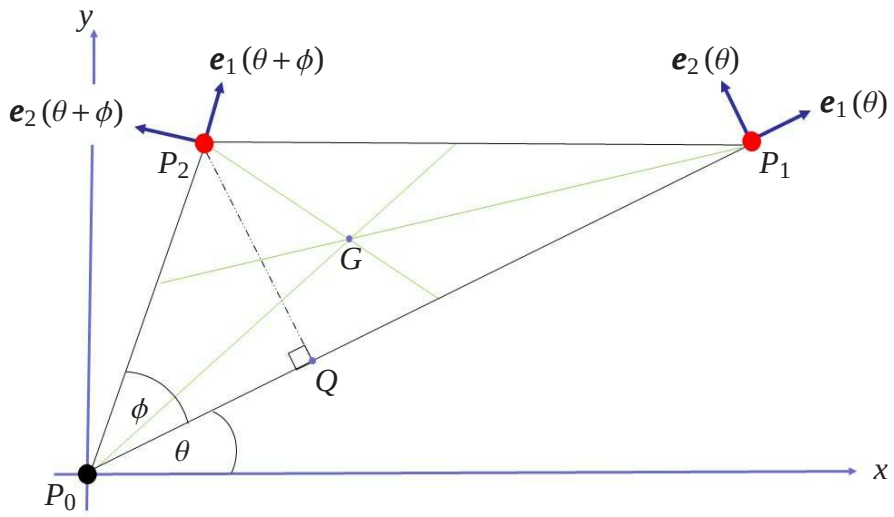

Fig. 3.3 P_0 is the reference particle, P_0P_1 is the base of the triangle, QP_2 is the altitude and G is the centroid. The angle θ defines the orientation of the triangle and ϕ determines the *flatness*.

We are interested in the statistics of the *s*ize and shape of triangles, irrespective of their location and orientation, for the case where ε is very small. We therefore introduce a *local* Cartesian coordinate system with origin at the reference point P_0 and axes P_0x and P_0y, as shown. Further, at the point P_1 we introduce a *local right-handed basis* $\{\boldsymbol{e}_1(\theta),\boldsymbol{e}_2(\theta),\boldsymbol{e}_3\}$ where $\boldsymbol{e}_1(\theta)$ is a unit vector parallel to $\overrightarrow{P_0P_1}$, $\boldsymbol{e}_2(\theta)$ is a unit vector perpendicular to $\boldsymbol{e}_1(\theta)$ lying in the plane and $\boldsymbol{e}_3$ is the unit vector perpendicular to the plane. Similarly, at P_2 we introduce the basis $\{\boldsymbol{e}_1(\theta+\phi),\boldsymbol{e}_2(\theta+\phi),\boldsymbol{e}_3\}$. These basis vectors will play an important role later, when we consider the time-evolution of triangular constellations in fractals arising in a dynamical system.

The constellation is completely specified by the six coordinates of the three vertices, relative to some origin O (which, for clarity is not shown in the figure). Its position relative to O may be taken to be the position vector, $\boldsymbol{r}_0$, of the vertex P_0, or the position vector, $\bar{\boldsymbol{r}}$, of the centroid G; each is specified by two coordinates. Its orientation, with respect to the Ox axis, is given by the rotation angle $x\widehat{P_0P_1} \equiv \theta$. There are then three remaining parameters available to define the intrinsic geometry of the triangle and this can be done using a number of different sets of three variables. For example, by giving the lengths of the three sides $|P_0P_1| \equiv R_1$, $|P_0P_2| \equiv R_2$ and $|P_1P_2| \equiv R_3$, or the lengths of the base $|P_0P_1|$, the altitude $|QP_2| \equiv h$ and $|P_0Q| \equiv \ell$, or we may specify the lengths of any pair of sides and their included angle, for example R_1, R_2 and ϕ.

As a measure of size we might be tempted to adopt the *signed* area, $\mathcal{A}$, of the triangle, given by[1]

$$\mathcal{A}\boldsymbol{e}_3 \equiv \frac{1}{2}\delta\boldsymbol{r}_1 \wedge \delta\boldsymbol{r}_2 = \frac{1}{2}R_1R_2\sin(\phi)\boldsymbol{e}_3 \tag{3.1.1}$$

where $\delta\boldsymbol{r}_1$ and $\delta\boldsymbol{r}_2$ are the displacements of P_1 and P_2 relative to P_0:

$$\delta\boldsymbol{r}_1 \equiv \overrightarrow{P_0P_1} = R_1\boldsymbol{e}_1(\theta) = \begin{pmatrix} \delta x_1 \\ \delta y_1 \end{pmatrix}, \quad \delta\boldsymbol{r}_2 \equiv \overrightarrow{P_0P_2} = R_2\boldsymbol{e}_1(\theta+\phi) = \begin{pmatrix} \delta x_2 \\ \delta y_2 \end{pmatrix}. \tag{3.1.2}$$

However we note that, even when R_1 and R_2 are large, if $\phi \approx 0$ or π then the area may be small, and it will vanish if the triangle is degenerate. To avoid this problem we adopt an alternative measure, the (scaled) radius of gyration of the triangle about its centroid, R, defined by

$$R^2 \equiv \sum_{i=0}^{2}(\boldsymbol{r}_i - \bar{\boldsymbol{r}})^2 = \frac{R_1^2 + R_2^2 + R_3^2}{3}. \tag{3.1.3}$$

Given that the vertices are assumed to be distinct, this measure of size is positive definite and is small *only* when the three vertices are close together.

Having decided on the measure of size, there remain two independent variables which we can use to define two distinct measures of shape. Since the shape of a triangle is unaltered by a similarity transformation, i.e. a linear scaling, then scaling all linear dimensions by $\frac{1}{R_1}$, we see that the shape of the triangle can be specified by, for example, the ratio of lengths, $\rho \equiv \frac{R_2}{R_1}$, and the included angle ϕ.

[1] Note that $\mathcal{A}$ becomes negative as the angle, ϕ, at the vertex P_0, passes through the value π in which case it becomes a *reflex* or exterior angle to the triangle and the cyclic order of the vertices, reading anticlockwise, changes from $P_0P_1P_2$ to $P_2P_1P_0$. Henceforth in the text we shall simply refer to $\mathcal{A}$ as the area of the triangle, understanding that, when it is negative there has been an inversion in the order of the vertices.

Figure (3.4) shows some triangles for $\rho \ll 1$ and $\rho \approx 1$, for several values of ϕ (for $\rho \gg 1$ the triangles are similar to those for $\rho \ll 1$ and are not shown).

In figures (b), (c) and (d) $\rho \ll 1$ and, for all values of ϕ, the triangles are *flat.* Also, they resemble a binary constellation with a third, satellite, vertex. Borrowing a term from astronomy, we say that they have high *binarity*. In figures (e), (f) and (g) $\rho \approx 1$ and the triangle is flat when ϕ is very small or when $\phi \approx \pi$. Figure (f) shows the least binary and least flat case, an equilateral triangle. In all cases, as $\phi \to 0$ or π the triangle degenerates onto a completely flat line.

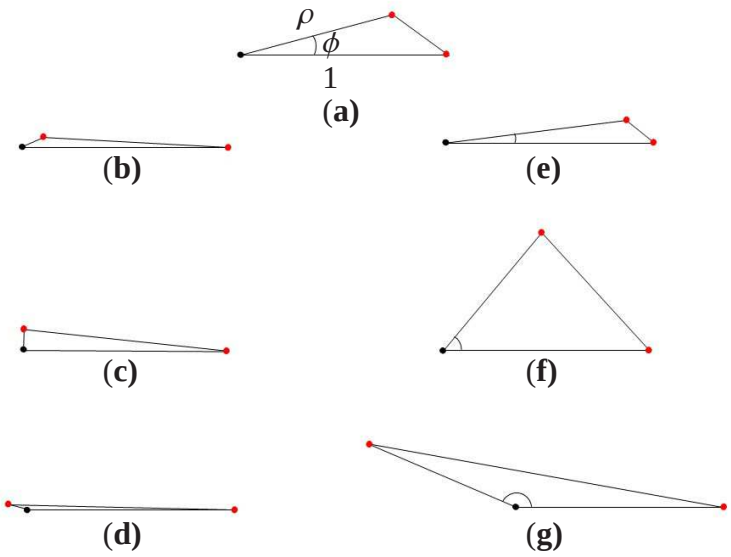

Fig. 3.4 The constellations in the figure illustrate different degrees of *flatness* and *binarity*. Triangles are flat when the smallest included angle, ϕ, is very small and are least flat when the smallest included angle is $\frac{\pi}{3}$. If a pair of vertices lies very close together and the third vertex is an outlier we say that the triangle has high binarity.

The area of the triangle, $\mathcal{A}$, is also a poor choice as a measure of *flatness.* For example, if the vertices of the triangle are close together (so that its size, R, is small), then the area is small *regardless* of whether or not the triangle is flat. A good measure of flatness must avoid this defect and we consider, instead, the *dimensionless ratio* of the area relative to the square of the radius of gyration, which can be written as:

$$\frac{\mathcal{A}}{R^2} = \frac{3}{4}\left(\frac{\sin\phi}{\rho + \frac{1}{\rho} - \cos\phi}\right). \tag{3.1.4}$$

This ratio is small if $\phi \approx 0$ or π, or if $\rho \ll 1$ or if $\rho \gg 1$, that is, when the triangle is flat or highly binary. Further, for $\rho = 1$ the ratio has a maximum value of $\frac{\sqrt{3}}{4}$ when $\phi = \frac{\pi}{3}$ and a minimum value of $-\frac{\sqrt{3}}{4}$ when $\phi = \frac{5\pi}{3}$; in both cases the triangle is equilateral. This ratio therefore has the characteristics of a good measure of flatness and we define our flatness parameter, Z, to be a multiple of it:

$$Z = \frac{4}{\sqrt{3}}\left(\frac{\mathcal{A}}{R^2}\right). \tag{3.1.5}$$

Small values of $|Z|$ correspond to flat triangles and, with this choice of numerical coefficient, $-1 \leq Z \leq 1$ for all values of ϕ and for equilateral triangles $Z = \pm 1$.

3.1.3 The Kendall sphere, a shape space for triangles

Since the shape of a triangle depends on only two variables it may be represented by a point in a two dimensional *shape* space. One choice of this space is due to D G Kendall [23]. Whilst examining the statistics of shapes drawn from a *random scatter* of points, Kendall showed that the shape of a triangle can be represented uniquely by a point on a compact manifold, the surface of a sphere [24]. In contrast to the treatment in section (3.1.2) where P_0 is singled out as a reference point, which is convenient in the context of dynamical systems where we consider the separation of phase space trajectories relative to a test trajectory, this elegant representation of triangle shape has the advantage that it does not distinguish any one vertex: all vertices are placed on an equal footing. The Kendall sphere[2], showing the corresponding shapes of triangles at some points on it, is shown in figure (3.5).

The position of a point on the sphere is given by two angles[3]: the co-latitude, θ, with $0 \leq \theta \leq \pi$, and the azimuth, ϕ, with $0 \leq \phi \leq 2\pi$. For $\theta \leq \frac{\pi}{2}$, the triangle at point $(\pi - \theta, \phi)$ in the southern hemisphere has the same shape as that at (θ, ϕ) in the northern hemisphere, but the cyclic order of its vertices is inverted. Therefore, the southern hemisphere is essentially an *inverted* copy of the northern hemisphere.

[2]Kendall used a sphere of radius $\frac{1}{2}$; we shall use a unit sphere. He also considered the order of the vertices as important, so that the 6 ways of labelling a triangle give rise to 6 different shapes. For our purposes this distinction is unimportant.

[3]Note that these angles are *not* the angles shown in figure (3.3).

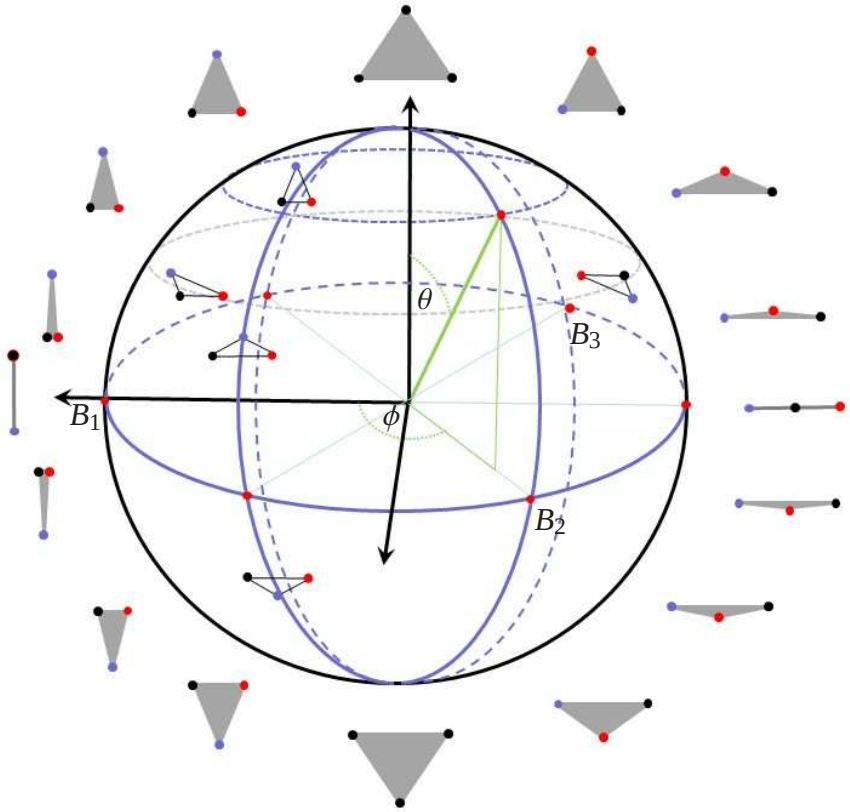

Fig. 3.5 The Kendall sphere: the shape of a triangle can be represented by a point on the surface of a sphere. This representation of shape is due to D G Kendall. Flat triangles correspond to points near the equator and the least flat, equilateral, triangles are represented by the poles. The triangles placed around the outside of the sphere show the shapes of isosceles triangles corresponding to different latitudes on the meridians at $\phi = 0$ and $\phi = \pi$.

At the poles, ($\theta = 0$ and $\theta = \pi$), there are equilateral triangles of opposite orientation. As the co-latitude, increases from 0 to $\frac{\pi}{2}$ the triangles flatten until, on the equator, they degenerate into sets of collinear points. The three points $B_1 = \left(\frac{\pi}{2}, 0\right), B_2 = \left(\frac{\pi}{2}, \frac{2\pi}{3}\right)$ and $B_3 = \left(\frac{\pi}{2}, \frac{4\pi}{3}\right)$ represent *binary coincidences* at which two vertices of the degenerate triangle coincide[4]. Isosceles triangles lie along the meridians $\phi = \frac{n\pi}{3}$, $n = 0, 1, \cdots, 5$, which together with the equator, $\theta = \frac{\pi}{2}$, partition the sphere into 12 equal half-lunes. A family of isosceles triangles, lying on the great circle formed by the meridians $\phi = 0$ and $\phi = \pi$, is shown around the outside of the sphere. On a given line of latitude increasing the azimuth, ϕ, by $\frac{2\pi}{3}$ corresponds to a cyclic permutation of the vertices. Therefore, neglecting inversions (i.e. reflections) and

[4]With the vertices labelled as in figure (3.3), then at B_1, vertices P_0 and P_1 coincide, at B_2, vertices P_1 and P_2 coincide, and at B_3, vertices P_0 and P_2 coincide.

cyclic permutations of the order of the vertices, the shape of any triangle can be represented by a point in a half lune.

For our purposes, the most important point to note is that *a point on the sphere with co-latitude θ represents a triangle with flatness $Z = \cos\theta$.* The interpretation of the azimuth, ϕ, is more complicated and is discussed in the next subsection.

Kendall considered the behaviour of the representative point on the sphere as the three vertices of the triangle undergo independent Brownian motions in plane [23]. He observed that the point undergoes Brownian motion on the surface of the sphere[5] and he showed that the equilibrium distribution of diffusion on a spherical surface is a uniform probability density. This important result implies that *for a random scatter of points the probability density of the flatness variable, Z, is uniform on* $[-1,1]$:

$$P_Z(z) = \frac{1}{2}, \quad -1 \le z \le 1 \ . \tag{3.1.6}$$

One of the motivations for Kendall's work was to determine whether or not the many apparent alignments among standing stones near Land's End in Cornwall could occur by chance, and to test claims that certain sites of geographical and archeological interest are aligned on *ley lines.* He argued that these apparent alignments are no more prevalent than those observed in random scatters of points. One possible criticism of his reasoning is that settlements and geographical features may not be randomly scattered, and that fractal measures might be a better model. We return to this point in our conclusion.

3.1.4 The Euler matrix of a triangle

The position, size, shape and orientation of a triangle are fully determined by the position vectors, $\boldsymbol{r}_0, \boldsymbol{r}_1, \boldsymbol{r}_2$, of the three vertices, P_0, P_1, P_2 with respect to some origin O. However, it only requires a single vector to specify the position of the triangle, for example $\boldsymbol{r_0}$, or $\bar{\boldsymbol{r}}$, the position vector of the centroid G. It therefore follows that the size, shape and orientation, which are independent of position, are fully determined by only *two vectors.* The representation of the geometry of a triangle via a pair of vectors has its origins in the work of Euler and, in essence, Kendall utilised a pair of *Euler* vectors in his treatment of triangle shape; in

[5] He did not give an explicit demonstration of this result; one is given in [42].

our notation these are:

$$\boldsymbol{u}_1 \equiv \frac{1}{\sqrt{2}}(\boldsymbol{r}_1 - \boldsymbol{r}_0) = \frac{1}{\sqrt{2}}\delta\boldsymbol{r}_1\,, \quad \boldsymbol{u}_2 \equiv \frac{1}{\sqrt{6}}(2\boldsymbol{r}_2 - \boldsymbol{r}_0 - \boldsymbol{r}_1) = \frac{1}{\sqrt{6}}(2\delta\boldsymbol{r}_2 - \delta\boldsymbol{r}_1)\,. \tag{3.1.7}$$

Figure (3.6) illustrates these vectors, with $\boldsymbol{u}_1, \boldsymbol{u}_2$ located at the centroid G; note that $\boldsymbol{u}_2$ passes through vertex P_2

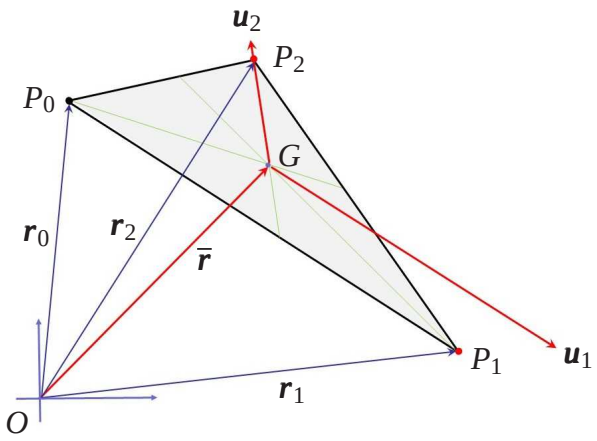

Fig. 3.6 The Euler vectors of a triangle. Any triangle can be specified completely by the position vectors of its vertices or, equivalently, by the position vector of its centroid, G, and the two Euler vectors, $\boldsymbol{u}_1$ and $\boldsymbol{u}_2$ introduced in this section. $\boldsymbol{u}_1$ is parallel to the base of the triangle and when originating from the centroid $\boldsymbol{u}_2$ passes through the vertex opposite the base. $\boldsymbol{u}_1$ and $\boldsymbol{u}_2$ therefore characterize the orientation, size and flatness of the triangle.

We can use the vectors $\boldsymbol{u}_1$ and $\boldsymbol{u}_2$ to construct a 2×2 matrix, $\boldsymbol{E}$, which we shall refer to as the *Euler matrix* of the triangle:

$$\boldsymbol{E} = \begin{pmatrix} u_{1,x} & u_{2,x} \\ u_{1,y} & u_{2,y} \end{pmatrix} \tag{3.1.8}$$

where $u_{1,x}$ and $u_{1,y}$ are the Cartesian components of $\boldsymbol{u}_1$, and similarly for $\boldsymbol{u}_2$.

The singular-value decomposition (s.v.d.) of $\boldsymbol{E}$ can be written as

$$\boldsymbol{E} = \boldsymbol{R}(\theta_1)\,\boldsymbol{\Lambda}\boldsymbol{R}(\theta_2) \tag{3.1.9}$$

where the $\boldsymbol{R}$s are rotation matrices and $\boldsymbol{\Lambda} = \mathrm{diag}(\lambda_1, \lambda_2)$.

The angle θ_1 in (3.1.9) describes an overall rotation of the triangle and therefore contains no information about its size or shape. Hence the singular values λ_1 and λ_2 and the angle θ_2, alone, completely determine the size and shape of the triangle[6].

The *Frobenius norm*, $\|\boldsymbol{E}\|$, of the Euler matrix is equal to the radius of gyration of the triangle:

$$\|\boldsymbol{E}\|^2 \equiv \mathrm{tr}\left(\boldsymbol{E}^{\mathrm{T}}\boldsymbol{E}\right) = \boldsymbol{u}_1^2 + \boldsymbol{u}_2^2 = R^2 \tag{3.1.10}$$

and the determinant, $\det(\boldsymbol{E})$, is a multiple of the signed area, $\mathcal{A}$:

$$\mathcal{A} = \frac{\sqrt{3}}{2}\det(\boldsymbol{E}). \tag{3.1.11}$$

Hence, the flatness of the triangle can be written entirely in terms of the *rotational invariants* of its Euler matrix:

$$Z = \frac{2\det(\boldsymbol{E})}{\mathrm{tr}(\boldsymbol{E}^{\mathrm{T}}\boldsymbol{E})}. \tag{3.1.12}$$

In terms of the singular values, from equation (3.1.9) it follows that $\det(\boldsymbol{E}) = \lambda_1\lambda_2$ and $\|\boldsymbol{E}\|^2 = \mathrm{tr}\left(\boldsymbol{E}^{\mathrm{T}}\boldsymbol{E}\right) = \lambda_1^2 + \lambda_2^2$, giving

$$Z = \frac{2\lambda_1\lambda_2}{\lambda_1^2 + \lambda_2^2} = \frac{2}{\left(\nu + \frac{1}{\nu}\right)} \tag{3.1.13}$$

where $\nu \equiv \frac{\lambda_2}{\lambda_1}$, so that the flatness parameter depends only on the *ratio of the singular values* of the Euler matrix. Also, in terms of the singular values and the angle θ_2, we have

$$\boldsymbol{E}^{\mathrm{T}}\boldsymbol{E} = \lambda_1^2 \begin{pmatrix} \left(\frac{1+\nu^2}{2}\right) + \left(\frac{1-\nu^2}{2}\right)\cos 2\theta_2 & -\left(\frac{1-\nu^2}{2}\right)\sin 2\theta_2 \\ -\left(\frac{1-\nu^2}{2}\right)\sin 2\theta_2 & \left(\frac{1+\nu^2}{2}\right) - \left(\frac{1-\nu^2}{2}\right)\cos 2\theta_2 \end{pmatrix}. \tag{3.1.14}$$

Since this is invariant under an increase of π in θ_2 we identify the double angle $2\theta_2$ with the azimuthal coordinate ϕ on the Kendall sphere. Then, within the subset of triangles defined by a given pair of singular values, an increment of $\frac{\pi}{3}$ in θ_2 corresponds to an increment of $\frac{2\pi}{3}$ in ϕ, which corresponds to a cyclic permutation of the vertices of the triangle on the sphere.

In summary, a triangle can be represented by its Euler matrix, $\boldsymbol{E}$, which has a singular value decomposition $\boldsymbol{E} = \boldsymbol{R}(\theta_1)\boldsymbol{\Lambda}\boldsymbol{R}(\theta_2)$, with singular values λ_1 and λ_2. In terms of these the size of the triangle is $R = \lambda_1^2 + \lambda_2^2$ and its flatness is $Z = (2\lambda_1\lambda_2)/\left(\lambda_1^2 + \lambda_2^2\right)$. Also, the shape of

[6]The s.v.d. is discussed in [49, 19]. We note here that although the s.v.d. of $\boldsymbol{E}$ is not unique the singular values λ_1, λ_2 are uniquely determined .

the triangle can be represented by a point (θ, ϕ) on the Kendall sphere. The co-latitude θ, is given by $Z = \cos\theta$ and depends only on the ratio of singular values $\nu = \frac{\lambda_2}{\lambda_1}$. All triangles corresponding to a given pair of singular values have the same size and flatness and lie on the same line of latitude and the azimuth ϕ is double the rotation angle θ_2 in the s.v.d. of $\boldsymbol{E}$.

3.2 Numerical investigation of the flatness p.d.f. P_Z

3.2.1 The numerical model

As a concrete example of a dynamical process which generates a fractal measure, we consider the distribution of an ensemble of (5×10^5) particles produced by the mapping discussed in subsection (2.4.4). The initial distribution of the particles is uniform in the unit square and after many iterations the positions of the particles sample a fractal measure, as shown in figure (1.1(b)) in Chapter 1. The equation of motion of each particle is given by the map (2.4.14), where the velocity field $\boldsymbol{u}_n$ is given by equation (2.4.1) with the potentials normalized as in equation (2.4.2).

3.2.2 Results

Figure (3.7) shows the numerically determined p.d.f., $P_Z(z)$, of the flatness parameter, Z, for small triangular constellations formed by triplets of randomly chosen points inside a disc of radius $\varepsilon \ll \xi$, where ξ is the correlation length of the flow. Each plot shows eight p.d.f.s for the same value of β, corresponding to eight values of ε. The scales are logarithmic on both axes. We are particularly interested in the distribution of flat triangles, i.e. those in the equatorial region of the Kendall sphere[7], and therefore in the behaviour of $P_Z(z)$ in the limit as $z \to 0$.

In the first three plots, where the compressibility β is small, the p.d.f.s for Z are approximately independent of the value of ε and uniform[8]. With respect to the distribution of the flatness of triangular constellations, fractals formed in flows with these values of β are similar to random scatters of points.

[7] Kendall termed very flat (and very tall) triangles *splinters*.

[8] apart from a cusp at $z = 1$, which arises because our sampling criterion is different from Kendall's, in that we require that the three points lie inside a disc of radius ε.

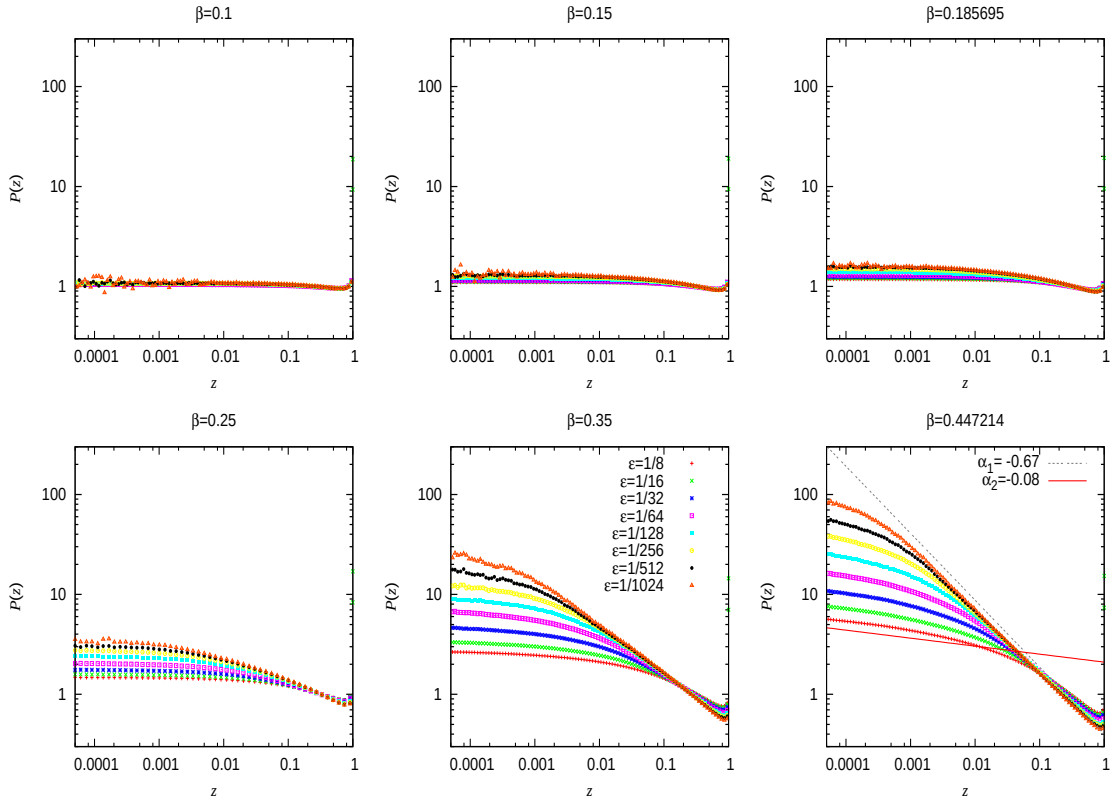

Fig. 3.7 The p.d.f. of the flatness parameter $P_Z(z)$ for sampling disc radii $\varepsilon = \frac{1}{8}, \frac{1}{16}, \cdots, \frac{1}{1024}$, for various values of the compressibility parameter β. The p.d.f. of the flatness parameter undergoes a phase transition: for β less than a critical value $\beta_c \approx 0.185$ the distribution of flatness is uniform, above this critical value, in the limit as $\varepsilon \to 0$, the p.d.f. is asymptotic to two different power laws.

In the second row of plots $P_Z(z)$ is dependent upon ε and in the limit as $\varepsilon \to 0$, $P_Z(z)$ appears to be asymptotic to two power laws. For z small, but exceeding some value $z_c(\varepsilon)$, we have $P_Z(z) \sim z^{\alpha_1}$. For $z \ll z_c$, $P_Z(z) \sim z^{\alpha_2}$. The value $z_c(\varepsilon)$ decreases as $\varepsilon \to 0$.

The straight lines on the last plot in figure (3.7) indicate estimates for the exponents α_1 and α_2 for a compressibility value of $\beta_1 = \frac{1}{\sqrt{5}} \approx 0.447$. We note that even at this value of β, the p.d.f. $P_Z(z)$ is normalisable (i.e. $\alpha_1 > -1$).

The interpretation of these findings is that the p.d.f. of the flatness parameter, $P_Z(z)$, appears to undergo a *phase transition* as the compressibility parameter in the flow model, β, passes through a critical value, which we estimate in section (3.5) to be $\beta_c = \frac{1}{\sqrt{29}} \approx 0.185$. For $\beta \leq \beta_c$ then $P_Z(z)$ is independent of ε, and approximately uniform, but above the critical compressibility $P_Z(z)$ is dependent on ε and very flat triangles predominate. For fractal

measures generated by this compressible flow the correlation dimension is [2, 70]

$$D_2 = \frac{2(1-\beta^2)}{1+3\beta^2}. \tag{3.2.1}$$

The plots in figure (3.7) therefore show the p.d.f.s, $P_Z(z)$, for values of of D_2 lying between 2 and 1, corresponding to values of β between $\beta = 0$ and $\beta = 1/\sqrt{5}$ respectively. Note that for $\beta = \beta_c = \frac{1}{\sqrt{29}}$ we have $D_2 = \frac{7}{4}$. So, in terms of the correlation dimension the prevalence of very flat triangles remains constant until the critical value $D_2 = \frac{7}{4}$ is reached. Below this value the distribution of triangle shapes has a strong dependence upon D_2 and very flat triangles become predominant.

In the remainder of this chapter we develop a theoretical explanation for these observations, showing why there is a critical compressibility and estimating its value, and we provide a qualitative explanation of why the distribution $P_Z(z)$ has two exponents for $\beta > \beta_c$.

3.3 Shape parameters and advective diffusion

3.3.1 Dynamics of constellations

To understand the results of the numerical simulation shown in section (3.2.2) we must consider how the geometry of a small flat constellation behaves in the flow. In this section we shall show that, for the fractal measure produced by the mapping (2.4.14), with the flow (2.4.1), the logarithms of the size and flatness parameters of triangular constellations evolve according to an advection-diffusion process.

Figure (3.8) shows a constellation, at two times t and $t' = t + \delta t$. In the short time interval the vertices P_0, P_1 and P_2 move from positions $\boldsymbol{r}_0, \boldsymbol{r}_1$ and $\boldsymbol{r}_2$ to the points P'_0, P'_1 and P'_2 with position vectors $\boldsymbol{r}'_0, \boldsymbol{r}'_1$ and $\boldsymbol{r}'_2$, respectively. And, in the notation of subsection (3.1.2), the lengths R_1, R_2, the angle ϕ and the area $\mathcal{A}$ become, respectively, R'_1, R'_2, ϕ' and $\mathcal{A}'$.

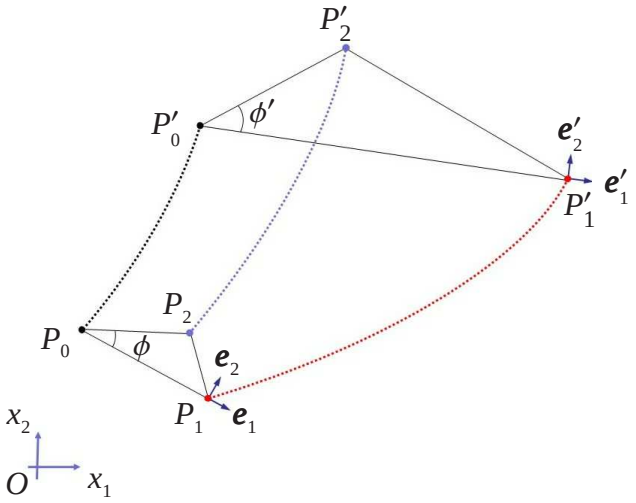

Fig. 3.8 The figure shows the configuration of a triangular constellation at times t and $t' = t + \delta t$. As the flow transports the particles the lengths and angles defining the size and shape of the constellation evolve. The basis vectors at P'_1 are obtained from those at P_1 via a random rotation.

From equation (2.4.14) we have

$$\boldsymbol{r}'_i = \boldsymbol{r}_i + \boldsymbol{u}(\boldsymbol{r}_i, t)\ \sqrt{\delta t},\ i = 0, 1, 2 \tag{3.3.1}$$

so that

$$\delta \boldsymbol{r}'_i \equiv \boldsymbol{r}'_i - \boldsymbol{r}'_0 = \boldsymbol{r}_i - \boldsymbol{r}_0 + \sqrt{\delta t}\,[\boldsymbol{u}(\boldsymbol{r}_i, t) - \boldsymbol{u}(\boldsymbol{r}_0, t)],\ i = 1, 2. \tag{3.3.2}$$

Hence, provided that the particle separations $R_1 = |P_0P_1|$ and $R_2 = |P_0P_2|$ are sufficiently small, we have to first order in $\delta \boldsymbol{r}_i$,

$$\delta \boldsymbol{r}'_i = \delta \boldsymbol{r}_i + \sqrt{\delta t}\,(\delta \boldsymbol{r}_i \cdot \boldsymbol{\nabla})\boldsymbol{u} = \left[\boldsymbol{I} + \sqrt{\delta t}\boldsymbol{A}\right]\delta \boldsymbol{r}_i,\ i = 1, 2 \tag{3.3.3}$$

where

$$\boldsymbol{A} = \left[A_{ij}\right] = \left[\frac{\partial u_i}{\partial x_j}\right]$$

and the field derivatives are evaluated at the reference point, P_0, at time t.

Introducing local bases $\{\boldsymbol{e}_1, \boldsymbol{e}_2\}$ and $\left\{\boldsymbol{e}'_1, \boldsymbol{e}'_2\right\}$ at P_1 and P'_1 respectively, we can write

$$\delta \boldsymbol{r}'_1 = R'_1 \boldsymbol{e}'_1 = R_1 \boldsymbol{e}_1 + \sqrt{\delta t}\boldsymbol{A}(R_1 \boldsymbol{e}_1) \tag{3.3.4}$$

and, defining $F_{ij}(t)$ for $i, j = 1, 2$, to be the projection of $\boldsymbol{A}\boldsymbol{e}_j$ onto the basis vector $\boldsymbol{e}_i$:

$$F_{ij}(t) \equiv \boldsymbol{e}_i \cdot \boldsymbol{A}\boldsymbol{e}_j \tag{3.3.5}$$

so that

$$\boldsymbol{A}\boldsymbol{e}_1 = F_{11}(t)\boldsymbol{e}_1 + F_{21}(t)\boldsymbol{e}_2 \quad \text{and} \quad \boldsymbol{A}\boldsymbol{e}_2 = F_{12}(t)\boldsymbol{e}_1 + F_{22}(t)\boldsymbol{e}_2$$

we have , dropping the argument t for clarity,

$$\delta\boldsymbol{r}_1' = R_1'\boldsymbol{e}_1' = R_1\left\{\left(1+\sqrt{\delta t}F_{11}\right)\boldsymbol{e}_1 + \sqrt{\delta t}F_{21}\boldsymbol{e}_2\right\}. \tag{3.3.6}$$

Comparing the magnitudes of each expression for $\delta\boldsymbol{r}_1'$ we have

$$\frac{R_1'}{R_1} = \left[1 + 2\sqrt{\delta t}F_{11} + \delta t\left(F_{11}^2 + F_{21}^2\right)\right]^{\frac{1}{2}}. \tag{3.3.7}$$

This equation expresses the ratio of the lengths of the base of the triangle at times t and $t+\delta t$ in terms of the randomly fluctuating quantities F_{11} and F_{21}. Introducing the random variable $X_1 \equiv -\ln\frac{R_1}{\xi}$, where ξ is the correlation length of the flow[9], then the increment in X_1 between times t and $t+\delta t$ is

$$\delta X_1 \equiv X_1' - X_1 = -\ln\left(\frac{R_1'}{R_1}\right) \tag{3.3.8}$$

note that, since $X_1 = -\ln\left(\frac{R_1}{\xi}\right)$ we have $\delta X_1 \approx \frac{-\delta R_1}{R_1}$. Using (3.3.7) and expanding the right hand side of equation (3.3.8) in a series of powers of $\sqrt{\delta t}$, retaining only terms upto order δt, we have

$$\delta X_1 \approx -\frac{1}{2}\ln\left[1 + 2\sqrt{\delta t}F_{11} + \delta t\left(F_{11}^2 + F_{21}^2\right)\right] \approx -\sqrt{\delta t}F_{11} + \delta t\left(\frac{F_{11}^2 - F_{21}^2}{2}\right). \tag{3.3.9}$$

Equation (3.3.9) is essentially a stochastic differential equation, in differential rather than derivative form, for the increment δX_1 in the random variable X_1 during the time interval $(t, t+\delta t)$.

Now, the local basis $\{\boldsymbol{e}_1, \boldsymbol{e}_2\}$ at P_1 is a *random rotation* of the coordinate basis $\{\boldsymbol{i}, \boldsymbol{j}\}$. Therefore, since $F_{ij} = \boldsymbol{e}_i \cdot \boldsymbol{A}\boldsymbol{e}_j$ and since the fields ϕ and ψ are random functions which have isotropic statistical properties, it follows that the statistics of the F_{ij} must be the same as those of $\boldsymbol{A}$:

$$\left\langle F_{ij}\right\rangle = \left\langle A_{ij}\right\rangle = 0 \quad \text{and} \quad \left\langle F_{ij}F_{kl}\right\rangle = \left\langle A_{ij}A_{kl}\right\rangle \equiv 2\mathcal{D}_{ijkl}. \tag{3.3.10}$$

[9]We are interested in the case where $R_1 \ll \xi$ so that the minus sign ensures that X_1 is positive.

Hence, X_1 has drift velocity v_1 where

$$v_1 \equiv \frac{\langle \delta X_1 \rangle}{\delta t} = \frac{\left\langle A_{11}^2 \right\rangle - \left\langle A_{21}^2 \right\rangle}{2} = \mathcal{D}_{1111} - \mathcal{D}_{2121} \tag{3.3.11}$$

and the diffusion coefficient D_{11} is

$$D_{11} \equiv \frac{\langle \delta X_1 \delta X_1 \rangle}{2\delta t} = \frac{\left\langle A_{11}^2 \right\rangle}{2} = \mathcal{D}_{1111}. \tag{3.3.12}$$

A near identical argument shows that R_2 has the same equation of motion. Since the triangle is very flat $\cos\phi \approx 1$ and $\sin\phi \approx \phi$ so that $\delta \boldsymbol{r}_2 \approx R_2(\boldsymbol{e}_1 + \phi \boldsymbol{e}_2)$ and equation (3.3.3) gives

$$\delta \boldsymbol{r}_2' = R_2 \boldsymbol{e}_2' = R_2 \left\{ \left(1 + \sqrt{\delta t}(F_{11} + \phi F_{12})\right) \boldsymbol{e}_1 + \left(\phi + \sqrt{\delta t}(F_{21} + \phi F_{22})\right) \boldsymbol{e}_2 \right\} \tag{3.3.13}$$

and we find that

$$\begin{aligned} \frac{R_2'}{R_2} = \Big[1 + 2\sqrt{\delta t}\Big(F_{11} + \phi(F_{12} + F_{21}) + \phi^2 F_{22}\Big) \\ + \delta t\Big(F_{11}^2 + F_{21}^2 + 2\phi(F_{11}F_{12} + F_{21}F_{22}) + \phi^2\left(F_{12}^2 + F_{22}^2\right)\Big) + \phi^2 \Big]^{\frac{1}{2}}. \end{aligned} \tag{3.3.14}$$

Introducing the random variable $-\ln\left(\frac{R_2}{\xi}\right)$ and performing a Taylor expansion in powers of $\sqrt{\delta t}$ the results follows. Note that it also then follows that the random variable $X_3 \equiv \ln\left(\frac{R_1}{R_2}\right) = -\ln\rho$ is degenerate, in the sense that it is *frozen* on some deterministic value.

To yield an equation of motion for the angle ϕ we note that since ϕ is small[10] we have

$$\phi \approx \sin\phi = \frac{2\mathcal{A}}{R_1 R_2}$$

so that

$$\ln\left(\frac{\phi'}{\phi}\right) = \ln\left(\frac{\mathcal{A}'}{\mathcal{A}}\right) - \ln\left(\frac{R_1'}{R_1}\right) - \ln\left(\frac{R_2'}{R_2}\right) = \ln\left(\frac{\mathcal{A}'}{\mathcal{A}}\right) - 2\delta X_1. \tag{3.3.15}$$

We therefore consider the ratio of the areas of the triangle at times t and $t' = t + \delta t$.

At time t' the area is $\mathcal{A}'$, given by $\mathcal{A}' \boldsymbol{e}_3 = \delta \boldsymbol{r}_1' \wedge \delta \boldsymbol{r}_2'$. Using equations (3.3.6) and (3.3.13) we find that

$$\frac{\mathcal{A}'}{\mathcal{A}} = 1 + \sqrt{\delta t}\,\mathrm{Tr}(\boldsymbol{F}) + \delta t\,\det(\boldsymbol{F}) \tag{3.3.16}$$

[10] Without loss of generality we may assume that ϕ is the *smallest* angle in the triangle, if necessary relabelling the vertices to assure this. In this case ϕ cannot exceed $\frac{\pi}{3}$ and when $\phi = \frac{\pi}{3}$ the triangle *must* be equilateral.

giving

$$\ln\left(\frac{\mathcal{A}'}{\mathcal{A}}\right) \approx 1 + \sqrt{\delta t}\,\mathrm{Tr}(\boldsymbol{F}) + \delta t\left[\det(\boldsymbol{F}) - \frac{1}{2}(\mathrm{tr}(\boldsymbol{F}))^2\right]. \tag{3.3.17}$$

Now, introducing the random variable $X_2 = -\ln\left(\frac{\phi}{\pi/3}\right)$, we have

$$\delta X_2 \equiv \left(X_2' - X_2\right) = -\ln\left(\frac{\phi'}{\phi}\right)$$

and, using equations (3.3.9) and (3.3.17), equation (3.3.15) gives

$$\delta X_2 = -\sqrt{\delta t}(F_{22} - F_{11}) - \delta t\left(\det(\boldsymbol{F}) + \frac{F_{11}^2 - F_{22}^2}{2} - \left(F_{11}F_{22} + F_{21}^2\right)\right). \tag{3.3.18}$$

Hence X_2 has drift velocity v_2 where

$$v_2 = \frac{1}{2}\left\{\left\langle A_{22}^2\right\rangle - \left\langle A_{11}^2\right\rangle\right\} + \left\langle A_{21}^2\right\rangle - \langle A_{21}A_{12}\rangle = \mathcal{D}_{2222} - \mathcal{D}_{1111} + 2(\mathcal{D}_{2121} - \mathcal{D}_{2112})$$

and the remaining diffusion coefficients are

$$D_{22} = \frac{\langle \delta X_2 \delta X_2\rangle}{2\delta t} = \frac{1}{2}\left\{\left\langle A_{11}^2\right\rangle - 2\langle A_{11}A_{22}\rangle + \left\langle A_{22}^2\right\rangle\right\} = \mathcal{D}_{1111} - 2\mathcal{D}_{1122} + \mathcal{D}_{2222} \tag{3.3.19}$$

and

$$D_{12} = D_{21} = \frac{\langle \delta X_1 \delta X_2\rangle}{2\delta t} = \frac{1}{2}\left\{\langle A_{11}A_{22}\rangle - \left\langle A_{11}^2\right\rangle\right\} = \mathcal{D}_{1122} - \mathcal{D}_{1111}. \tag{3.3.20}$$

Equations (3.3.9) and (3.3.18) express the increments in the *logarithms* of the lengths R_1 and the angle ϕ, during time δt, in terms of the randomly fluctuating quantities $F_{ij}(t)$. By mapping the three variables R_1, R_2 and ϕ to the point (X_1, X_2, X_3), where

$$X_1 \equiv -\ln\left(\frac{R_1}{\xi}\right), \quad X_2 \equiv -\ln\left(\frac{\phi}{\pi/3}\right), \quad X_3 \equiv \ln\left(\frac{R_1}{R_2}\right) = -\ln\rho \tag{3.3.21}$$

and ξ is the correlation length of the velocity field and $\rho = \frac{R_2}{R_1}$, we have expressed the dynamics of small flat constellations, and therefore the evolution of the shape parameter $Z \sim \phi$, in terms of the motion of a point in the abstract $X_1X_2X_3$ space.

In the region corresponding to very small flat triangles, i.e. where $X_1 \gg 0$ and $X_2 \gg 0$, the picture is actually relatively simple: X_1 and X_2 have diffusive dynamics, and X_3 is *frozen*.

Further, in this case ρ is then constant and since ϕ is very small, equations (3.1.4) and (3.1.5) imply that the flatness parameter $Z \sim \phi$.

Note that $X_2 = 0$ when $\phi = \frac{\pi}{3}$. In this case, if ϕ is the smallest angle in the triangle, the triangle is equilateral, so that $\rho = 1$. From equations (3.1.4) and (3.1.5) it then follows that $Z = 1$. Hence $X_2 = 0$ corresponds to the North pole of the Kendall sphere.

We emphasize here that the modelling carried out above is approximate, in two senses. The *derivation* of the stochastic equations of motion (3.3.9) and (3.3.18) clearly involves simplifying assumptions and approximations. However it is important to note that the assumption that the dynamics is diffusive, with advection, and can be described by a Fokker-Planck equation is also an approximation. Consequently, any deductions we make will also be approximations.

3.3.2 The boundary value problem for the p.d.f. $P_{\boldsymbol{X}}$

Since X_3 is frozen we will assume that the joint p.d.f. for the steady-state distribution of X_1, X_2 and X_3 is separable, of the form $P_{\boldsymbol{X}}(x_1, x_2)P_{X_3}(x_3)$, with $P_{X_3}(x_3)$ some normalized p.d.f., (which we need not specify). Then, assuming that the standard techniques and results from Fokker-Planck dynamics are applicable (2.3.6) it follows that, for $x_1 \gg 0$ and $x_2 \gg 0$, the p.d.f. for the joint distribution of X_1 and X_2, $P_{\boldsymbol{X}}(x_1, x_2)$, obeys a steady-state advection-diffusion equation[11]:

$$-v_i\left(\frac{\partial P_{\boldsymbol{X}}}{\partial x_i}\right) + D_{ij}\left(\frac{\partial^2 P_{\boldsymbol{X}}}{\partial x_i \partial x_j}\right) = 0. \tag{3.3.22}$$

In terms of the velocity gradients, A_{ij}, the drift coefficients are

$$v_1 = \frac{1}{2}\left(\left\langle A_{11}^2\right\rangle - \left\langle A_{21}^2\right\rangle\right) \tag{3.3.23a}$$

$$v_2 = 2\left(\left\langle A_{22}^2\right\rangle - \left\langle A_{11}^2\right\rangle\right) + \left\langle A_{21}^2\right\rangle - \langle A_{21}A_{12}\rangle \tag{3.3.23b}$$

[11] with $i, j = 1, 2$ and summation over repeated indices.

and the diffusion coefficients are

$$D_{11} = \frac{1}{2}\left\langle A_{11}^2 \right\rangle \tag{3.3.24a}$$

$$D_{12} = \frac{1}{2}\left(\langle A_{11}A_{22}\rangle - \left\langle A_{11}^2 \right\rangle\right) = D_{21} \tag{3.3.24b}$$

$$D_{22} = \frac{1}{2}\left(\left\langle A_{11}^2 \right\rangle - \langle A_{11}A_{22}\rangle + \left\langle A_{22}^2 \right\rangle\right). \tag{3.3.24c}$$

For the fluid velocity defined by (2.4.1) since the potentials ϕ and ψ have spatially homogeneous statistical properties the various expected values are *independent of position* and the drift and diffusion coefficients are therefore functions of the compressibility parameter, β, alone.

At this point we can already make some observations about the nature of solutions of equation (3.3.22). First, since the equation of motion for $\boldsymbol{X} = (X_1, X_2)$ in the region $x_1 \gg 0$, $x_2 \gg 0$ is invariant under translation in x_1 and x_2, any steady-state solution for $P_{\boldsymbol{X}}$ must be translationally invariant, up to a change of normalisation. Therefore, because the exponential function is translationally invariant up to a change of normalisation, solutions exist in the form[12]

$$P_{\boldsymbol{X}}(x_1, x_2) \sim \exp\left[\gamma_1 x_1 + \gamma_2 x_2\right]. \tag{3.3.25}$$

For these solutions the corresponding distributions of R_1 and the angle ϕ will have probability densities proportional to $r_1^{\gamma_1 - 1}$ and $\phi^{\gamma_2 - 1}$ respectively. It is then apparent why Z *may* have a power-law distribution: since $Z \sim \phi$, then if ϕ has a power-law distribution Z will also have a power-law distribution, with the same exponent. So for such solutions $P_Z(z) \sim z^{\alpha}$ with $\alpha = \gamma_2 - 1$.

Second, if we identify R_1 with the radius of the sampling disk, ε, then a solution of the from (3.3.25) implies that the probability density for both vertices P_1 and P_2 to lie within a ball of radius ε centred on the reference point P_0 varies as ε^{γ_1}. We may therefore infer that $\gamma_1 = 2D_3$, where D_3 is the third Renyi dimension [16]. Note, however, that since our approximations fail near $x_2 = 0$ it is impractical to evaluate γ_1 (and therefore D_3) using our approach[13].

The above translational invariance argument indicates why $P_Z(z)$ may have a power-law distribution but it does not identify the value of the exponent. To do this we must consider the effect of the boundary conditions on the lines $x_1 = 0$ and $x_2 = 0$. The line $x_1 = 0$ corresponds

[12] Normalisation requires that the constants γ_1, γ_2 are negative.

[13] Formulae for D_3 which are applicable to our model are given in [2].

to constellations of points where the separation R_1 is equal to the correlation length ξ. Some of these are *squeezed* by the linearised flow and enter the region $x_1 > 0$. The line $x_1 = 0$ is therefore a *distributed source*. 'Phase' points, $\boldsymbol{X}$, representing these constellations are created on the line $x_1 = 0$ at some rate, $J(x_2)$, which, from inspection of figure (3.7) corresponds to φ having a uniform probability density in the limit as $\phi \to 0$. Noting Kendall's random scatter result [23] this implies that the source flux density on the boundary $x_1 = 0$ is

$$J(x_2) = \begin{cases} J_0 \exp[-x_2] & x_2 > 0 \\ 0 & x_2 \leq 0 \end{cases} \tag{3.3.26}$$

where J_0 is a constant, which determines the normalisation of the joint probability density, $P_{\boldsymbol{X}}(x_1, x_2)$. On the line $x_2 = 0$ the situation is more complicated: $x_2 = 0$ is a non-absorbing boundary, so that $\frac{\partial P_{\boldsymbol{X}}}{\partial x_2}(x_1, 0) = 0$, but the approximations that X_3 is frozen and that X_1 and X_2 obey a simple advection-diffusion equation fail close to $x_2 = 0$.

Two instances of the advection-diffusion process for $\boldsymbol{X} = (X_1, X_2)$ are shown schematically in figure (3.9).

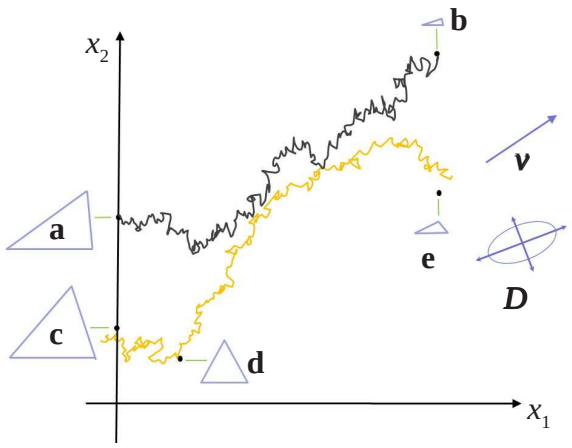

Fig. 3.9 The figure shows two realizations of the advection-diffusion process for $\boldsymbol{X} = (X_1, X_2)$. The phase points diffuse and drift, as shown, and the size and shape of the triangular constellations evolve correspondingly. As the phase points diffuse towards the x_1 axis triangles become less flat, as they drift to the right and up they are squeezed and flattened.

The phase point initially at **a** represents a triangle with $R_1 = \xi$ which is squeezed by the flow, so that the point enters the region $x_1 > 0$. Then, as the phase point drifts broadly in the direction of $\boldsymbol{\nu}$ as shown in the figure, the triangle is squeezed and flattened. Similarly, the phase point initially at **c** represents a triangle with $R_1 = \xi$, but which is not as flat as the

triangle originally at **a**. At first this point enters the region $x_1 > 0$ and approaches $x_2 = 0$, so that R_1 shrinks and φ, or equivalently Z, grows. Therefore at first the triangle becomes smaller and less flat until, at point **d**, it is nearly equilateral. Since the axis $x_2 = 0$ is a non-absorbing boundary the phase point eventually drifts towards point **e**. Note that, graphically, we represent the diffusion tensor by the ellipse $\boldsymbol{x}^{\mathrm{T}} \cdot \boldsymbol{D}\boldsymbol{x} = 1$, whose principal axes are parallel to the eigenvectors of $\boldsymbol{D}$.

3.4 A model for the shape distribution

It is not possible to determine the solution to the steady-state advection-diffusion equation (3.3.22) exactly. However, since the probability density $P_{\boldsymbol{X}}$ can be expected to vary over a wide range of values, we appeal to the large deviation principle [58] and assume that it can be expressed in exponential form:

$$P_{\boldsymbol{X}}(\boldsymbol{x}) \sim \exp[-\Psi(\boldsymbol{x})] \tag{3.4.1}$$

where the exponent, $\Psi(\boldsymbol{x})$, is some *large deviation function*. Then by constructing an approximate expression for the large deviation function we can develop a quantitative theory for the critical compressibility, β_{c}.

To construct the approximate expression for $\Psi(\boldsymbol{x})$ we will take account of the distributed source on the boundary $x_1 = 0$ but will ignore the effect of the non-absorbing boundary. This approach can be expected to produce a reasonable approximation to the exact solution in the region of interest, far from the non-absorbing boundary. To construct the approximation to $\Psi(\boldsymbol{x})$ we will treat the distributed source as a continuum of point sources of different strengths, spread along the line $x_1 = 0$, and will sum the contributions from each point source on the line.

For advection and diffusion, with drift velocity $\boldsymbol{v}$ and diffusion tensor $\boldsymbol{D}$ and a *point source* located at the origin at time $t = 0$, the joint probability density of $\boldsymbol{X}$ is a Gaussian propagator centred at $\boldsymbol{x} = \boldsymbol{v}t$. The steady-state probability density, $P^{(0)}_{\boldsymbol{X}}$, due to a *constant source of unit intensity* located at the origin can then be obtained by integrating this propagator over t, so that

$$P^{(0)}_{\boldsymbol{X}}(\boldsymbol{x}) \sim \int_0^\infty \frac{\mathrm{d}t\ \exp[-S(\boldsymbol{x},t)]}{4\pi t\sqrt{\det(\boldsymbol{D})}} \tag{3.4.2}$$

where

$$S(\boldsymbol{x},t) = \frac{(\boldsymbol{x}-\boldsymbol{v}t)\cdot\boldsymbol{D}^{-1}(\boldsymbol{x}-\boldsymbol{v}t)}{4t}. \tag{3.4.3}$$

We can estimate the value of the integral in equation (3.4.2) by transforming it into a form to which Laplace's method can be applied, as follows. We introduce a *scaled* time τ, defined by $\tau = t/t^*$, where t^* is the time at which $S(\boldsymbol{x},t)$ has a minimum with respect to t. Since t^* satisfies $\partial S/\partial t(\boldsymbol{x},t^*) = 0$ we have

$$t^* = \sqrt{\frac{\boldsymbol{x}\cdot\boldsymbol{D}^{-1}\boldsymbol{x}}{\boldsymbol{v}\cdot\boldsymbol{D}^{-1}\boldsymbol{v}}}. \tag{3.4.4}$$

Then

$$S(\boldsymbol{x},t) = \frac{1}{2}\left(\boldsymbol{x}\cdot\boldsymbol{D}^{-1}\boldsymbol{v}\right) + \lambda g(\tau) \tag{3.4.5}$$

where

$$\lambda \equiv \frac{1}{4}\left(\sqrt{\boldsymbol{v}\cdot\boldsymbol{D}^{-1}\boldsymbol{v}}\,\sqrt{\boldsymbol{x}\cdot\boldsymbol{D}^{-1}\boldsymbol{x}}\right) \quad \text{and} \quad \mathrm{g}(\tau) = \tau + \frac{1}{\tau} \tag{3.4.6}$$

so that equation (3.4.2) becomes

$$P_{\boldsymbol{X}}^{(0)}(\boldsymbol{x}) \sim \frac{\exp\left[\frac{1}{2}\boldsymbol{x}\cdot\boldsymbol{D}^{-1}\boldsymbol{v}\right]}{4\pi\sqrt{\det(\boldsymbol{D})}} \int_0^\infty \mathrm{d}\tau\left(\frac{1}{\tau}\right)\exp\left[-\lambda g(\tau)\right]. \tag{3.4.7}$$

Laplace's method is applicable, directly[14], to the integral in equation (3.4.7) and gives

$$\int_0^\infty \mathrm{d}\tau\left(\frac{1}{\tau}\right)\exp\left[-\lambda g(\tau)\right] \approx \left(\frac{1}{\tau^*}\right)\sqrt{\frac{2\pi}{\lambda g''(\tau^*)}}\exp\left[-\lambda g(\tau^*)\right] \tag{3.4.8}$$

where τ^* is defined by $g'(\tau^*) = 0$. Since $g(\tau) = \tau - \frac{1}{\tau}$ we have $\tau^* = 1$ and $g(\tau^*) = g''(\tau^*) = 2$, giving

$$\int_0^\infty \mathrm{d}\tau\left(\frac{1}{\tau}\right)\exp\left[-\lambda g(\tau)\right] = \sqrt{\frac{\pi}{\lambda}}\exp\left[-2\lambda\right].$$

Hence

$$P_{\boldsymbol{X}}^{(0)}(\boldsymbol{x}) \sim \frac{\exp\left[-\Psi_0(\boldsymbol{x})\right]}{\sqrt{4\pi\,\det(\boldsymbol{D})}\left(\boldsymbol{v}\cdot\boldsymbol{D}^{-1}\boldsymbol{v}\right)^{1/4}\left(\boldsymbol{x}\cdot\boldsymbol{D}^{-1}\boldsymbol{x}\right)^{1/4}} \tag{3.4.9}$$

[14]This method provides an estimate for integrals of the form $I(\lambda) = \int_a^b \mathrm{d}\tau f(\tau)\exp[-\lambda g(\tau)]$ in the limit as $\lambda \to \infty$, when $g(\tau)$ has a minimum in the interval $[a,b]$. Here $\lambda \sim \sqrt{\boldsymbol{x}\cdot\mathbf{D}^{-1}\boldsymbol{x}}\,\sqrt{\boldsymbol{v}\cdot\mathbf{D}^{-1}\boldsymbol{v}} \sim |\boldsymbol{x}|$, so that we expect the asymptotic approximation to be good when $|\boldsymbol{x}|$ is large.

where $\Psi_0(\boldsymbol{x})$ given by

$$\Psi_0(\boldsymbol{x}) = \frac{1}{2}\left[\sqrt{\boldsymbol{x}\cdot\boldsymbol{D}^{-1}\boldsymbol{x}}\sqrt{\boldsymbol{v}\cdot\boldsymbol{D}^{-1}\boldsymbol{v}} - \boldsymbol{x}\cdot\boldsymbol{D}^{-1}\boldsymbol{v}\right]. \tag{3.4.10}$$

Note that, apart from the prefactor $\left(\boldsymbol{x}\cdot\boldsymbol{D}^{-1}\boldsymbol{x}\right)^{-1/4}$, the approximation given in (3.4.9) is of the expected form (3.4.1), and the exponent, $\Psi_0(\boldsymbol{x}) = S(\boldsymbol{x}, t^*)$.

The approximation to the p.d.f., $P_{\boldsymbol{X}}$, for the distributed source may now be obtained from a weighted integral of $P_{\boldsymbol{X}}^{(0)}$. The weight function is equal to the intensity of the distributed source along the half-line $\left\{(x,y)\in\mathbb{R}^2 : x = 0, y \geq 0\right\}$, i.e. $J(y) = \exp(-y)$. Therefore, neglecting the prefactors,

$$P_{\boldsymbol{X}}(x_1,x_2) \sim \int_0^\infty \mathrm{d}y\ \exp(-y)\exp(-\Psi_0(x_1,x_2-y)) = \int_0^\infty \mathrm{d}y\ \exp\{-[y+\Psi_0(x_1,x_2-y)]\}. \tag{3.4.11}$$

We apply the method of Laplace again, assuming that for any given (x_1,x_2) the integral is dominated by contributions from the neighbourhood of some critical value, y^*, at which the exponent in the integrand has a minimum with respect to y. This gives

$$P_{\boldsymbol{X}}(x_1,x_2) \sim \exp[-\Psi(x_1,x_2)] \tag{3.4.12}$$

where

$$\Psi(x_1,x_2) = \Psi_0(x_1,x_2-y^*) + y^* \tag{3.4.13}$$

with y^* defined by the condition

$$\frac{\partial\Psi_0}{\partial x_2}(x_1,x_2-y^*) = 1\,. \tag{3.4.14}$$

Clearly, the value of y^* depends on x_1 and x_2 and, since $\boldsymbol{D}$ and $\boldsymbol{v}$ depend on the compressibility parameter β, it also depends on β. We now consider this dependence.

From equation (3.4.10), writing $\boldsymbol{x} = x\,\hat{\boldsymbol{x}}$, where $\hat{\boldsymbol{x}}$ is a unit vector, we can see that the value of $\Psi_0(\boldsymbol{x})$ is proportional to the magnitude of $\boldsymbol{x}$, with the constant of proportionality depending on the direction of $\hat{\boldsymbol{x}}$. In particular, on the line $\boldsymbol{x} = \lambda\boldsymbol{v},\ \lambda\in\mathbb{R}$,

$$\Psi_0(\boldsymbol{x}) = \frac{1}{2}(|\lambda|-\lambda)\left(\boldsymbol{v}\boldsymbol{D}^{-1}\boldsymbol{v}\right) = \begin{cases} 0 & \lambda \geq 0 \\ -\lambda\left(\boldsymbol{v}\boldsymbol{D}^{-1}\boldsymbol{v}\right) & \lambda < 0. \end{cases} \tag{3.4.15}$$

Therefore, $\Psi_0(\boldsymbol{x})$ vanishes directly 'downwind' of the source, i.e. for $\lambda \geq 0$, but 'upwind' of the source, i.e. for $\lambda \leq 0$, and on any other ray emerging from the source the value of $\Psi_0(\boldsymbol{x})$ increases linearly with distance from it, and, correspondingly, there is an exponential reduction of $P^{(0)}_{\boldsymbol{X}}$ along any such ray (asymptotically).

$\Psi_0(x_1, x_2)$ therefore has a simple geometrical interpretation, shown in figure (3.10), it is the height of a *tilted cone* above the x_1x_2 plane, where the vertex of the cone lies at the source point and a generator of the cone lies along the direction of the drift velocity vector $\boldsymbol{v}$.

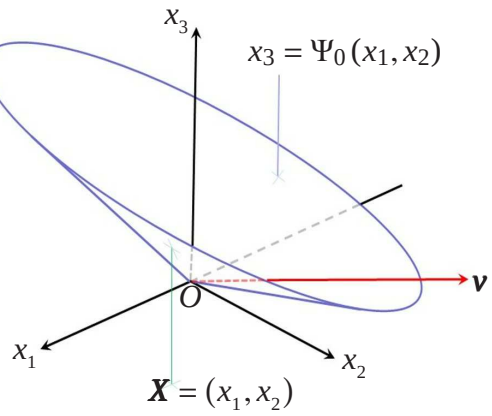

Fig. 3.10 The large deviation rate function, $\Psi_0(x_1, x_2)$ can be interpreted as the height of a tilted cone above the x_1x_2 plane. The vertex of the cone lies at the source of the phase points and one generator lies along the drift vector $\boldsymbol{v}$.

Given this geometrical interpretation of $\Psi_0(\boldsymbol{x})$ it immediately follows that the gradient of $\Psi_0(\boldsymbol{x})$ is constant on any ray from the critical source point $(0, y^*)$. Therefore, for any given value of β and any given field point (x_1, x_2), the condition in equation (3.4.14) is satisfied on some ray through the source point which has a slope $m(\beta)$, say. Hence

$$y^* = x_2 - m(\beta)x_1 \tag{3.4.16}$$

and equation (3.4.13) then gives

$$\Psi(x_1, x_2) = \Psi_0(x_1, m(\beta)x_1) + x_2 - m(\beta)x_1 \ . \tag{3.4.17}$$

The preceding analysis is correct only if there is a *valid* stationary point, i.e. when equation (3.4.14) predicts $y^* \geq 0$. Figure (3.11) illustrates the position of the critical source point $(0, y^*)$ corresponding to an arbitrary 'field' point (x_1, x_2) in three different cases:

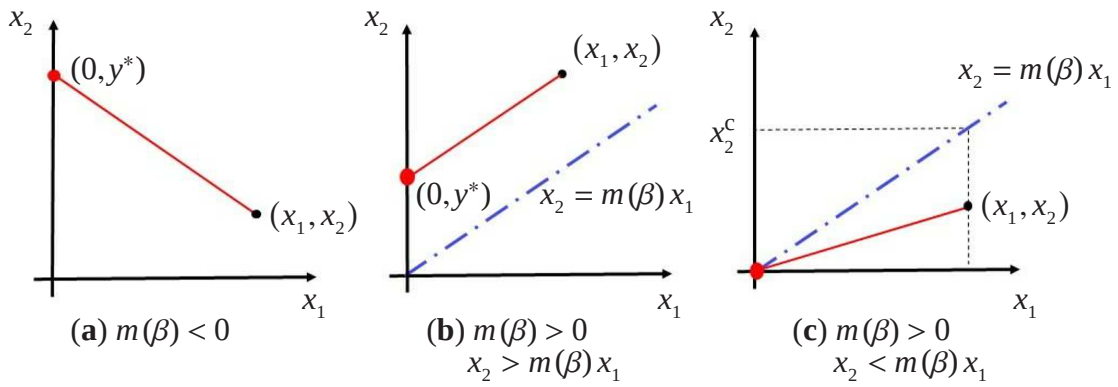

Fig. 3.11 For a given field point (x_1, x_2) the ordinate, y^*, of the critical point $(0, y^*)$ depends on the ordinate, x_2, of the field point and on $m(\beta)$ and whether $m(\beta)$ is positive or negative. For $m(\beta) < 0$ then $y^* > 0$ for all values of x_2. However for $m(\beta) > 0$ then $y^* > 0$ only if $x_2 > m(\beta)\,x_1$, but if $x_2 \leq m(\beta)\,x_1$ we must take $y^* = 0$.

From inspection of plot (**a**) in figure (3.11), or equivalently from equation (3.4.16), we can see that, if $m(\beta) < 0$ then corresponding to every field point (x_1, x_2) there is always a positive solution to equation (3.4.14). However, if $m(\beta) > 0$, as in plots (**b**) and (**c**), then valid stationary points only exist if $x_2 \geq x_2^c \equiv m(\beta)x_1$, as in plot (**b**). If $x_2 < x_2^c$, as in plot (**c**), then the integral (3.4.11) is dominated by the contribution from the origin, i.e. $y^* = 0$, and in this case $\Psi(x_1, x_2) \sim \Psi_0(x_1, x_2)$.

Identifying R_1 with ε we can see that the condition $x_2 \geq x_2^c$ is equivalent to a condition $z \leq z_c$, where z_c depends on β and ε. Hence, when $m(\beta) \geq 0$ we expect $P_Z(z)$ to be characterized by different exponents, depending upon whether z is greater or less than some value z_c, which depends on β and ε.

These conclusions are wholly consistent with the results shown in figure (3.7). The critical compressibility for the phase transition is determined by the condition $m(\beta_c) = 0$ and, for $\beta > \beta_c$, the discussion of cases (**b**) and (**c**) in figure (3.11) explains, qualitatively, why $P_Z(z)$ is characterized by a power law with different exponents, α_1 and α_2 depending upon whether z is greater or less than some value z_c (see the last plot of figure (3.7)). Our analysis also gives an insight onto the origin of small, non-flat triangles, for which $X_1 \gg 0$ and $X_2 \approx 0$. When $\beta < \beta_c$, there is a solution of (3.4.14) and these triangles are predominantly formed by squeezing of flat triangles from $(0, y^*)$ along their axis. When $\beta > \beta_c$, small triangles are formed by approximately isotropic squeezing of triangles that, initially, are not flat.

3.5 Estimate of critical compressibility

For the map defined by equations (2.4.14) and (2.4.1) we have

$$\mathbf{A} \equiv \left[A_{ij}\right] = \left[\frac{\partial u_i}{\partial x_j}\right] = \begin{pmatrix} \beta\phi_{x_1x_1} + \psi_{x_1x_2}, & \beta\phi_{x_1x_2} + \psi_{x_2x_2} \\ \beta\phi_{x_2x_1} - \psi_{x_1x_1}, & \beta\phi_{x_2x_2} - \psi_{x_1x_2} \end{pmatrix}. \tag{3.5.1}$$

Therefore, with the normalisation as given in equation (2.4.2), we have $\mathcal{D}_{1111} = \mathcal{D}_{2222} = \frac{1}{2}\left(1+3\beta^2\right)$, $\mathcal{D}_{1212} = \mathcal{D}_{2121} = \frac{1}{2}\left(3+\beta^2\right)$ and $\mathcal{D}_{1122} = \mathcal{D}_{1221} = \frac{1}{2}\left(\beta^2-1\right)$. Hence, from equations (3.3.23) it follows that the drift velocity is

$$\boldsymbol{v} = \begin{pmatrix} \beta^2 - 1 \\ 2\left(1+\beta^2\right) \end{pmatrix} \tag{3.5.2}$$

and from equations (3.3.24) the diffusion tensor $\boldsymbol{D}$ is

$$\boldsymbol{D} = \begin{pmatrix} \frac{1}{2}\left(1+3\beta^2\right), & -\left(1+\beta^2\right) \\ -\left(1+\beta^2\right), & 2\left(1+\beta^2\right) \end{pmatrix}. \tag{3.5.3}$$

This gives

$$\boldsymbol{D}^{-1}\boldsymbol{v} = \begin{pmatrix} 2 \\ 2 \end{pmatrix}, \quad \boldsymbol{x}\boldsymbol{D}^{-1}\boldsymbol{v} = 2\left(x_1+x_2\right), \quad \boldsymbol{v}\boldsymbol{D}^{-1}\boldsymbol{v} = 2\left(1+3\beta^2\right)$$

and

$$\Psi_0(\boldsymbol{x}) = \kappa\sqrt{x_2^2 + \Lambda\left(x_1x_2 + x_1^2\right)} - (x_1+x_2) \tag{3.5.4}$$

where

$$\kappa = \frac{1+3\beta^2}{2\beta\sqrt{2(1+\beta^2)}}, \quad \Lambda = \frac{4(1+\beta^2)}{1+3\beta^2}. \tag{3.5.5}$$

Figure (3.12) shows contours of $\Psi_0(x_1,x_2)$, for $\beta = \frac{1}{3}$, on the domain $\left[-\frac{1}{2},1\right]\times\left[-\frac{1}{2},1\right]$, with $\Psi_0(x_1,x_2)$ increasing from a value of zero at the origin. The asymmetry of the contours shows that the tilted cone is *skew*. The uniformity of the distribution of the contours in the first quadrant in figure (3.12) shows that, in this quadrant, the surface $x_3 = \Psi_0(x_1,x_2)$ is approximately planar. Hence the exponent $\Psi_0(x_1,x_2) \approx \gamma_1x_1 + \gamma_2x_2$, for some constants γ_1,γ_2. Equation (3.4.12) then shows that $P_{\boldsymbol{X}}(x_1,x_2)$ is of the form given in equation (3.3.25). We can therefore see that it is the near-planar structure of $\Psi_0(x_1,x_2)$ which results in the existence of the power law behaviour in the p.d.f., $P_{\boldsymbol{X}}$.

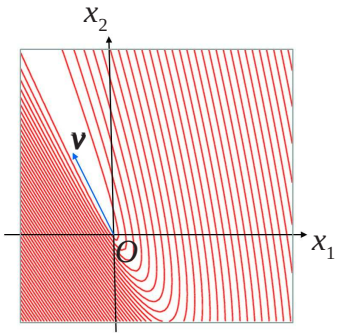

Fig. 3.12 The plot shows the contours of $\Psi_0(x_1, x_2)$ on the domain $\left[-\frac{1}{2}, 1\right] \times \left[-\frac{1}{2}, 1\right]$, for $\beta = \frac{1}{3}$. Along the direction of the drift vector through the source, O, $\Psi_0(x_1, x_2) = 0$. The asymmetry of the contours shows that the conical surface $z = \Psi_0(x_1, x_2)$ is skew, whilst the uniformity of the contours in the first quadrant shows that the surface is nearly planar in this quadrant.

Figure (3.13) shows the advection-diffusion process for the phase point $\boldsymbol{X} = (X_1, X_2)$ for $\beta = \frac{1}{3}$. Although the diffusion can take the phase point into the region $x_1 > 0$ the effect of the drift is to transport the phase point upwards and onto the x_2 axis, i.e. back onto the distributed source. This is a general feature of the motion for all non-zero values of β.

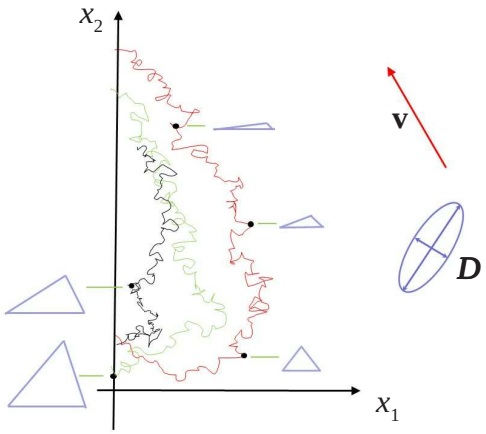

Fig. 3.13 The advection-diffusion process for $\boldsymbol{X} = (X_1, X_2)$ for $\beta = \frac{1}{3}$, c.f. figure (3.9).

With $\Psi_0(\boldsymbol{x})$ given by equations (3.5.4) and (3.5.5) the stationary point condition (3.4.14) is

$$\frac{\kappa(2\zeta + \Lambda x_1)}{\sqrt{\zeta^2 + \Lambda(x_1\zeta + \zeta^2)}} = 2 \tag{3.5.6}$$

where $\zeta = x_2 - y^*$. This gives a quadratic equation for ζ:

$$\zeta^2 + (\Lambda x_1)\zeta + \frac{1}{4} r(\beta)(\Lambda x_1)^2 = 0 \tag{3.5.7}$$

where

$$r(\beta) = \frac{1 - 26\beta^2 - 87\beta^4}{1 - 26\beta^2 - 23\beta^4}.$$

The solution is

$$\zeta = x_2 - y^* = \frac{\Lambda}{2}\left\{-1 \pm \frac{8\beta^2}{\sqrt{1 - 26\beta^2 - 23\beta^4}}\right\} x_1$$

giving $y^* = x_2 - m(\beta)\, x_1$ with

$$m(\beta) = \frac{2\left(1+\beta^2\right)}{(1+3\beta^2)}\left[\pm\frac{8\beta^2}{\sqrt{1 - 26\beta^2 - 23\beta^4}} - 1\right]. \tag{3.5.8}$$

We seek the critical value of compressibility, β_c, for which $m(\beta_c) = 0$. A solution can only exist for the positive root in equation (3.5.8) and in this case $\beta_c = 1/\sqrt{29}$.

Hence for $\beta \le \beta_c$ we expect $P(z) \sim z^0$, independent of β, and for $\beta > \beta_c$, we expect two different exponents for $P_Z(z)$, as discussed in section (3.4), because the dominant contribution to the propagator depends upon the position in the (x_1, x_2) plane. These predictions are in good agreement with our numerical results, illustrated in figure (3.7).

3.6 Discussion of results

We have characterized the shape of a triangular constellation using a flatness parameter $Z = \frac{4}{\sqrt{3}}\mathcal{A}/R^2$, where $\mathcal{A}$ is the area of the triangle and $\mathcal{R}$ is its radius of gyration. Using numerical simulations we have examined the p.d.f. of Z, $P_Z(z)$, for triangular constellations in fractal sets arising from a compressible chaotic flow. We found that below a critical value of compressibility, β_c, the p.d.f. is approximately independent of the compressibility and above the critical value $P_Z(z) \sim z^\alpha$, with an exponent which takes one of two different values , α_1 or α_2, depending upon how small z is.

By relating the triangle size and flatness to an advection-diffusion process we were able to determine β_c analytically for our simple model flow, and we gave a qualitative explanation

of the existence of the two values of the exponent α. We remark, however, that a quantitative treatment of the exponents α_1, α_2 when $\beta > \beta_c$ will require a more sophisticated model for the propagator of the advection diffusion process, which takes account of the behaviour near and on the non-absorbing boundary $x_2 = 0$.

Our analysis has dealt with the simplest case of advective motion in two dimensions and the distribution of $P_Z(z)$ reported in figure (3.7) is specific to this case, but the techniques used here are, in principle, readily generalised to three dimensional systems, and to more complex equations of motion, e.g. those describing inertial particles. We therefore expect that other variables characterising the shape of constellations of nearby points in a random flow, and in particular the logarithms of the angles and lengths defining a small simplex, will satisfy simple stochastic equations of motion. The corresponding joint probability density will then satisfy an advection-diffusion equation, with boundary condition similar to those encountered here.

We conclude with a remark about Kendall's discussions of *ley lines*. Kendall's analysis of triangle shapes in a random scatter of points appears to confirm that the suspected alignments may occur purely by chance. However, one possible criticism of his argument is that human settlements are not randomly scattered. Indeed they could well be described by a fractal measure, and then the distribution of acute triangles described by P_Z would be different from that of a random scatter. However, our results show that, even if the pattern of human settlement were, for some reason, fractal in nature the distribution P_Z would remain almost unchanged until the fractal dimension passes below some threshold value ($D_c = 7/4$ for our model). This is an unexpected vindication of Kendall's arguments.

Chapter 4

Advection and diffusion with an absorbing boundary

> Lord Ronald said nothing; he flung himself from the room, flung himself upon his horse and rode madly off in all directions.
>
> *Stephen Leacock, in Gertrude and the Governess*

In Chapter 3 we saw that the so-called *absorption problem*, the solution of the advection diffusion equation with an absorbing boundary, arises in the study of the structure of the fractal measure generated by a random flow. The p.d.f. of the flatness parameter obtained in Chapter 3 is specific to the dynamical system considered there but the modelling approach is, in principle, generalizable to other geometric parameters, and to other random dynamical systems. We therefore expect that the absorption problem will be a general feature of studies of the structure of fractal measures generated by random dynamical systems that serve as models for particles in turbulent flows [2, 8, 41]. Consequently, in this chapter, we consider the solution of the spatially homogeneous advection-diffusion equation, where the drift velocity $\boldsymbol{v}$ and the diffusion tensor $\mathbf{D}$ are independent of position and time and where there is an absorbing boundary.

For the two dimensional case (see figure (4.1)) we investigate the flux of particles onto the x_2 axis due to a steady point source at $(x_0, 0)$ under two circumstances. First when the x_2 axis has no effect on the particles, i.e. when it is a completely *transparent* or *permeable* boundary, and second when it is an *absorbing* boundary. To model the absorption we treat

the boundary as a source of 'antiparticles'. We show that, in each case, far from the source the flux onto the boundary has the form

$$J(x_2) \sim A(x_2)e^{-\Psi(x_2)}$$

where $\Psi(x_2)$ and $A(x_2)$ depend upon the source position x_0. We find that as $x_2 \to \infty$ the coefficient $A(x_2) \sim x_2^{-p}$, with $p = \frac{1}{2}$ for the transparent boundary and $p = \frac{3}{2}$ for the absorbing boundary. However, somewhat surprisingly, we find that the exponent $\Psi(x_2)$ is the same in each case and grows linearly as $x_2 \to \infty$.

We conclude the chapter with some numerical illustrations of the quality of the approximations and some comments on the structure of our asymptotic results. This chapter is based upon the paper *Advection diffusion equation with absorbing boundary*, published in the Journal of Statistical Physics [13].

4.1 The advection diffusion equation

In Chapter 3 we considered triangular constellations formed by triplets of points lying inside a disk of radius ε, sampling a fractal measure generated by a random flow. We characterized the size and shape of a constellation using the variables X_1 and X_2, defined by equation (3.3.21), and showed that in the region $x_1 \gg 0$ and $x_2 \gg 0$ these evolve according to a spatially homogeneous advection-diffusion process for which the x_2 axis is both a distributed source and an absorbing boundary. We are thus led to consider the situation illustrated in figure (4.1):

Particles are created by a steady unit source at $(x_0, 0)$ and undergo advection and diffusion, with drift velocity $\boldsymbol{v}$ and diffusion tensor $\mathbf{D}$, where both $\boldsymbol{v}$ and $\mathbf{D}$ are independent of position and time[1] .

The displacement of a particle from the source is denoted by $\boldsymbol{\zeta}$ and the diffusion tensor is represented by the ellipse $\boldsymbol{x}^{\mathrm{T}}\boldsymbol{D}\boldsymbol{x} = 1$. During a time interval of length t, in the absence of advection a droplet containing many particles initially concentrated at a point will expand to occupy an ellipse centred on the point. The axes of this ellipse are parallel to the eigenvectors of $\mathbf{D}$ and their half-lengths are $\sqrt{\mathcal{D}_1 t}$ and $\sqrt{\mathcal{D}_1 t}$, where $\mathcal{D}_1$ and $\mathcal{D}_2$ are the eigenvalues of $\boldsymbol{D}$.

[1] We will later consider the limit as $x_0 \to 0$.

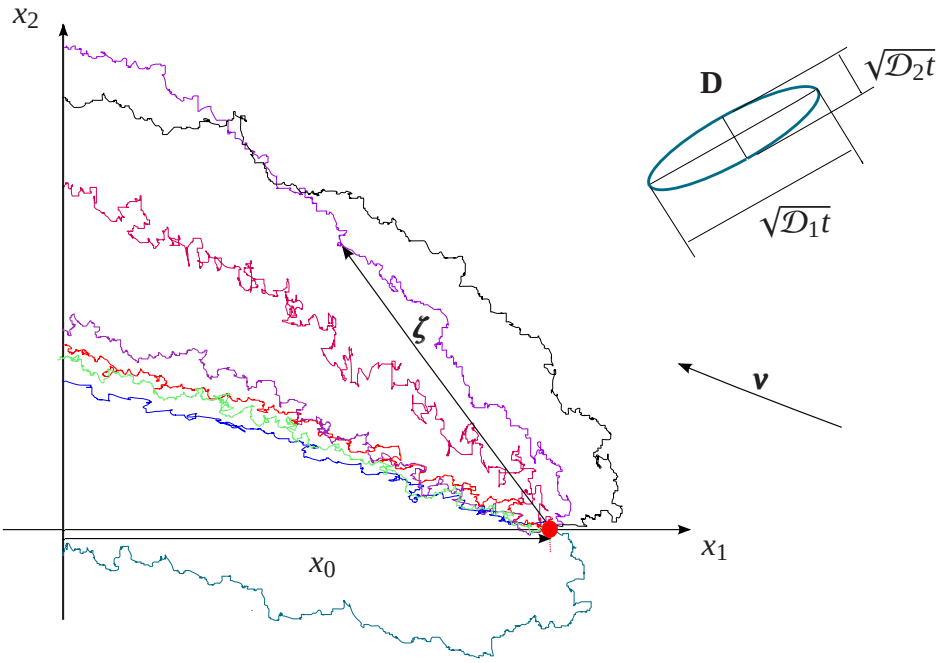

Fig. 4.1 The figure illustrates a source of particles located at $(x_0, 0)$ and the paths of a number of particles undergoing advection and diffusion, with drift velocity $\boldsymbol{v}$ and diffusion tensor $\mathbf{D}$, and being absorbed on contact with the x_2 axis.

In d spatial dimensions with a point source of intensity $\sigma(t)$ located at $\boldsymbol{x}_0$ the particle density $\rho(\boldsymbol{x}, \boldsymbol{x}_0, t)$ at position $\boldsymbol{x}$ at time t satisfies the advection-diffusion equation:

$$\frac{\partial \rho}{\partial t} = -\sum_{i=1}^{d} v_i \frac{\partial \rho}{\partial x_i} + \sum_{i=1}^{d}\sum_{j=1}^{d} D_{ij} \frac{\partial^2 \rho}{\partial x_i \partial x_j} + \sigma(t)\delta(\boldsymbol{x} - \boldsymbol{x}_0) \tag{4.1.1}$$

where the v_i are components of the drift velocity $\boldsymbol{v}$ and the D_{ij} are elements of the diffusion tensor $\mathbf{D}$.

Our objective is, for the two-dimensional case, to determine the particle flux $J_a(x_2)$ onto the boundary $x_1 = 0$ when there is a *steady* source and when the particles are absorbed on contact with this boundary. Dealing with an absorbing boundary is difficult when there is both advection and diffusion because there is no simple local boundary condition which $\rho(\boldsymbol{x}, \boldsymbol{x}_0, t)$ must satisfy. For this reason, in the next section, we first consider a reference problem where the boundary is completely permeable.

4.2 Particle density and flux for a permeable boundary

By definition, when the x_2 axis is a completely permeable or 'transparent' boundary it has no effect on the particles so, for example, they may cross the boundary many times at different locations. We can therefore use the free-space propagator, or Green's function, for the advection-diffusion equation to calculate the steady state particle density and the corresponding boundary flux arising from a steady point source.

4.2.1 Particle flux for a non-singular diffusion tensor

The free space propagator for (4.1.1) for a particle released at $\boldsymbol{x}_0$ at time zero, is the probability density for the particle to reach $\boldsymbol{x}$ at time t. This is given by

$$K_0(\boldsymbol{x},\boldsymbol{x}_0,t) = G_0(\boldsymbol{x},\boldsymbol{x}_0,t)\,\Theta(t) = \left[\frac{\exp\left[-S(\boldsymbol{\zeta},t)\right]}{\sqrt{\det(\mathbf{D})\,(4\pi t)^d}}\right]\Theta(t) \tag{4.2.1}$$

where $\Theta(t)$ is the Heaviside step function, $\boldsymbol{\zeta} = \boldsymbol{x} - \boldsymbol{x}_0$ is the displacement vector and

$$S(\boldsymbol{\zeta},t) = \frac{(\boldsymbol{\zeta} - \boldsymbol{v}t)\cdot\mathbf{D}^{-1}(\boldsymbol{\zeta} - \boldsymbol{v}t)}{4t}\ . \tag{4.2.2}$$

The particle density at point $\boldsymbol{x}$ at time t is therefore

$$\rho_0(\boldsymbol{x},\boldsymbol{x}_0,t) = \int_{-\infty}^{t} \mathrm{d}t'\ \sigma(t')G_0(\boldsymbol{x},\boldsymbol{x}_0,t-t')\ . \tag{4.2.3}$$

If the source is steady and active from $t = 0$ then $\sigma(t) = \sigma_0\Theta(t)$ where σ_0 is some constant, and equation (4.2.3) gives (after a change of dummy integration variable),

$$\rho_0(\boldsymbol{x},\boldsymbol{x}_0,t) = \sigma_0 \int_0^t \mathrm{d}t'\ G_0(\boldsymbol{x},\boldsymbol{x}_0,t')\ . \tag{4.2.4}$$

As $t \to \infty$ the density $\rho_0(\boldsymbol{x},\boldsymbol{x}_0,t)$ reaches a *steady state* value, given by

$$\rho_0(\boldsymbol{x},\boldsymbol{x}_0) = \sigma_0 \int_0^\infty \mathrm{d}t'\ G_0(\boldsymbol{x},\boldsymbol{x}_0,t')\ . \tag{4.2.5}$$

Since $\boldsymbol{v}$ and $\mathbf{D}$ are independent of $\boldsymbol{x}$ we can write equation (4.1.1) in the form

$$\frac{\partial \rho}{\partial t} + \boldsymbol{\nabla} \cdot \boldsymbol{J}_0 = \sigma(t)\delta(\boldsymbol{x} - \boldsymbol{x}_0) \tag{4.2.6}$$

where the *flux vector* $\boldsymbol{J}_0(\boldsymbol{x}, \boldsymbol{x}_0, t)$ is

$$\boldsymbol{J}_0(\boldsymbol{x}, \boldsymbol{x}_0, t) = \rho_0(\boldsymbol{x}, \boldsymbol{x}_0, t)\, \boldsymbol{v} - \boldsymbol{D}\, \boldsymbol{\nabla}\rho_0(\boldsymbol{x}, \boldsymbol{x}_0, t) \tag{4.2.7}$$

with the gradient being taken with respect to $\boldsymbol{x}$. From equation (4.2.4) it follows that

$$\boldsymbol{\nabla}\rho_0(\boldsymbol{x}, \boldsymbol{x}_0, t) = \sigma_0 \int_0^t \mathrm{d}t\, \boldsymbol{\nabla} G_0(\boldsymbol{x}, \boldsymbol{x}_0, t) \tag{4.2.8}$$

then, noting that

$$\boldsymbol{\nabla} G_0(\boldsymbol{x}, \boldsymbol{x}_0, t) = -G_0(\boldsymbol{x}, \boldsymbol{x}_0, t)\boldsymbol{\nabla} S(\boldsymbol{x}, \boldsymbol{x}_0, t) \quad \text{and} \quad \nabla \mathrm{S}(\boldsymbol{x}, \boldsymbol{x}_0, \mathrm{t}) = \frac{1}{2\mathrm{t}}\left[\boldsymbol{D}^{-1}(\boldsymbol{\zeta} - \boldsymbol{v}\mathrm{t})\right]$$

we have

$$\boldsymbol{D}\boldsymbol{\nabla}\rho_0(\boldsymbol{x}, \boldsymbol{x}_0, t) = -\sigma_0 \int_0^t \mathrm{d}t'\, G_0(\boldsymbol{x}, \boldsymbol{x}_0, t')\left[\frac{\boldsymbol{\zeta} - \boldsymbol{v}t'}{2t'}\right]$$

Hence

$$\boldsymbol{J}_0(\boldsymbol{x}, \boldsymbol{x}_0, t) = \sigma_0 \int_0^t \mathrm{d}t'\, G_0(\boldsymbol{x}, \boldsymbol{x}_0, t')\, \boldsymbol{v}_{\mathrm{eff}}(\boldsymbol{x}, \boldsymbol{x}_0, t') \tag{4.2.9}$$

where the *effective velocity* is

$$\boldsymbol{v}_{\mathrm{eff}}(\boldsymbol{x}, \boldsymbol{x}_0, t) \equiv \frac{1}{2}\left(\frac{\boldsymbol{x} - \boldsymbol{x}_0}{t} + \boldsymbol{v}\right). \tag{4.2.10}$$

As $t \to \infty$ this tends to the steady state value:

$$\boldsymbol{J}_0(\boldsymbol{x}, \boldsymbol{x}_0) = \sigma_0 \int_0^\infty \mathrm{d}t'\, G_0(\boldsymbol{x}, \boldsymbol{x}_0, t')\boldsymbol{v}_{\mathrm{eff}}(\boldsymbol{x}, \boldsymbol{x}_0, t') \tag{4.2.11}$$

4.2.2 Asymptotic values of particle density and flux

The integrals in equations (4.2.5) and (4.2.11) cannot be expressed exactly in a closed form. However for large $|\boldsymbol{\zeta}| = |\boldsymbol{x} - \boldsymbol{x}_0|$, they are dominated by contributions from a neighbourhood of the critical point t^* at which $S(\boldsymbol{\zeta}, t)$ has a minimum. The method of Laplace can therefore be applied to provide asymptotic estimates of the integrals and gives the following expres-

sions for the steady-state density and flux:

$$\rho_0(\boldsymbol{x},\boldsymbol{x}_0) \sim \gamma\sigma_0 G_0(\boldsymbol{x},\boldsymbol{x}_0,t^*) \quad \text{and} \quad \boldsymbol{J}_0(\boldsymbol{x},\boldsymbol{x}_0) \sim \rho_0(\boldsymbol{x},\boldsymbol{x}_0)\boldsymbol{v}_{\text{eff}}(\boldsymbol{x},\boldsymbol{x}_0,\mathrm{t}^*) \tag{4.2.12}$$

where γ is the Gaussian integral

$$\gamma = \int_{-\infty}^{\infty} \mathrm{d}u\ \exp\left[-\frac{1}{2}\frac{\partial^2 S(\boldsymbol{\zeta},t^*)}{\partial t^2}u^2\right]. \tag{4.2.13}$$

The condition that S is stationary with respect to t is

$$\frac{\partial S}{\partial t}(\boldsymbol{\zeta},t^*) = \frac{1}{4}\left(\boldsymbol{v}\cdot\mathbf{D}^{-1}\boldsymbol{v} - \frac{\boldsymbol{\zeta}\cdot\mathbf{D}^{-1}\boldsymbol{\zeta}}{(t^*)^2}\right) = 0$$

giving

$$t^* = \sqrt{\frac{\boldsymbol{\zeta}\cdot\mathbf{D}^{-1}\boldsymbol{\zeta}}{\boldsymbol{v}\cdot\mathbf{D}^{-1}\boldsymbol{v}}}\,. \tag{4.2.14}$$

Now, since **D** is symmetric,

$$S(\boldsymbol{\zeta},t^*) = \frac{1}{2}\left(\sqrt{\boldsymbol{\zeta}\cdot\mathbf{D}^{-1}\boldsymbol{\zeta}}\sqrt{\boldsymbol{v}\cdot\mathbf{D}^{-1}\boldsymbol{v}} - \boldsymbol{\zeta}\cdot\mathbf{D}^{-1}\boldsymbol{v}\right) \equiv \Psi_0(\boldsymbol{x},\boldsymbol{x}_0) \tag{4.2.15}$$

also, the second derivative and the Gaussian integral (4.2.13) are

$$\frac{\partial^2 S}{\partial t^2}(\boldsymbol{\zeta},t^*) = \frac{1}{2}\boldsymbol{v}\cdot\mathbf{D}^{-1}\boldsymbol{v}\sqrt{\frac{\boldsymbol{v}\cdot\mathbf{D}^{-1}\boldsymbol{v}}{\boldsymbol{\zeta}\cdot\mathbf{D}^{-1}\boldsymbol{\zeta}}}\,, \quad \gamma = \frac{2\sqrt{\pi}\left(\boldsymbol{\zeta}\cdot\mathbf{D}^{-1}\boldsymbol{\zeta}\right)^{\frac{1}{4}}}{\left(\boldsymbol{v}\cdot\mathbf{D}^{-1}\boldsymbol{v}\right)^{\frac{3}{4}}}\,. \tag{4.2.16}$$

Substituting these results into (4.2.12) gives

$$\rho_0(\boldsymbol{x},\boldsymbol{x}_0) \sim \sigma_0 A_0(\boldsymbol{x},\boldsymbol{x}_0)\exp\left[-\Psi_0(\boldsymbol{x},\boldsymbol{x}_0)\right] \tag{4.2.17}$$

and

$$\boldsymbol{J}_0(\boldsymbol{x},\boldsymbol{x}_0) \sim \frac{\sigma_0}{2}A_0(\boldsymbol{x},\boldsymbol{x}_0)\left[\boldsymbol{v} + \left(\sqrt{\frac{\boldsymbol{v}\cdot\mathbf{D}^{-1}\boldsymbol{v}}{\boldsymbol{\zeta}\cdot\mathbf{D}^{-1}\boldsymbol{\zeta}}}\right)\boldsymbol{\zeta}\right]\exp\left[-\Psi_0(\boldsymbol{x},\boldsymbol{x}_0)\right] \tag{4.2.18}$$

where

$$\Psi_0(\boldsymbol{x},\boldsymbol{x}_0) = S(\boldsymbol{\zeta},t^*) \quad \text{and} \quad \mathrm{A}_0(\boldsymbol{x},\boldsymbol{x}_0) = \frac{\left(\boldsymbol{\zeta}\cdot\mathbf{D}^{-1}\boldsymbol{\zeta}\right)^{\left(\frac{1-\mathrm{d}}{4}\right)}\left(\boldsymbol{v}\cdot\mathbf{D}^{-1}\boldsymbol{v}\right)^{\left(\frac{\mathrm{d}-3}{4}\right)}}{\sqrt{\det(\mathbf{D})\,(4\pi)^{(d-1)}}}. \tag{4.2.19}$$

Directly *downwind* of the source the displacement vector is $\boldsymbol{\zeta} = \boldsymbol{x} - \boldsymbol{x}_0 = \lambda \boldsymbol{v}$ for some $\lambda > 0$ so that $\Psi_0(\boldsymbol{x}, \boldsymbol{x}_0) = 0$, $\rho_0(\boldsymbol{x}, \boldsymbol{x}_0) \sim \sigma_0 A_0(\boldsymbol{x}, \boldsymbol{x}_0)$ and $\boldsymbol{J}_0(\boldsymbol{x}, \boldsymbol{x}_0) \sim \sigma_0 A_0(\boldsymbol{x}, \boldsymbol{x}_0)\boldsymbol{v}$. Therefore, directly downwind of the source point, there is no exponential reduction of the steady state particle density or the particle flux and the flux is directed along the drift vector. However, there is an algebraic reduction in both as the distance $|\boldsymbol{\zeta}|$ from the source increases. On any other ray starting from $\boldsymbol{x}_0$ then as $|\boldsymbol{\zeta}|$ increases Ψ_0 increases and the particle density and flux undergo the same exponential reduction along the ray. The algebraic coefficients in the particle density and the flux are asymptotic to the same power law: $|\boldsymbol{\zeta}|^{\frac{1-d}{2}}$.

In the two-dimensional case the magnitude of the flux onto the boundary $x_1 = 0$ is the magnitude of first component of $\boldsymbol{J}_0$. At position x_2, this is

$$J_0(x_2) \equiv |[\boldsymbol{J}_0(x_2)]_1| = A_0(x_2)\exp[-\Psi_0(x_2)] \tag{4.2.20}$$

where $\Psi_0(x_2) \equiv \Psi_0((0, x_2), (x_0, 0))$, and where $A_0(x_2) \sim \dfrac{1}{\sqrt{|x_2|}}$.

4.2.3 Rank-one diffusion tensor

The above expressions for the density and flux contain $\mathbf{D}^{-1}$, the inverse of the diffusion tensor. We might therefore expect the preceeding analysis to be valid only when $\mathbf{D}$ is non-singular. However we now show that the results continue to hold for the case where $\mathbf{D}$ is a rank one matrix.

In general, since $\mathbf{D}$ is symmetric it may be diagonalized by a suitable rotation of the axes. Therefore, since we are dealing with the case of a completely permeable boundary we can, without any loss of generality, apply a rotation to diagonalize $\mathbf{D}$. We will therefore consider the case where $\mathbf{D}$ is diagonal, of the form

$$\mathbf{D} = \begin{bmatrix} D_{11} & 0 \\ 0 & \varepsilon \end{bmatrix} \tag{4.2.21}$$

and take the limit as $\varepsilon \to 0$. This limiting case corresponds to diffusive motion with drift in the x_1 direction, with a diffusion constant D_{11} and drift velocity v_1, together with drift with velocity v_2 and almost no diffusion in the x_2 direction.

With $\mathbf{D}$ given by (4.2.21) and ε small but non-zero, then using equation (4.2.17) to calculate the particle density far from the source we find that the terms in $1/\varepsilon$ cancel. Neglecting

terms of order ε^2 we find that the result is independent of ε. At $(0, x_2)$ the density is

$$\rho_0(x_2) \sim \frac{\sigma_0}{2\sqrt{\pi D_{11} x_2 v_2}} \exp\left[-\frac{x_2 v_1^2}{4 D_{11} v_2}\right] . \tag{4.2.22}$$

Now this is in fact equal to the probability density for the case where $\varepsilon = 0$, because if $\varepsilon = 0$ the displacement from x_0 in the x_1 direction is due to *one-dimensional diffusion with drift*, with diffusion coefficient D_{11} and drift velocity v_1. The propagator for the x_1 component of the motion is therefore

$$G_0(x_1, x_0, t) = \frac{1}{\sqrt{4\pi D_{11} t}} \exp\left[-\frac{(x_1 - x_0 - v_1 t)^2}{4 D_{11} t}\right] \Theta(t) . \tag{4.2.23}$$

Further, when $\varepsilon = 0$ there is no diffusion in the x_2 direction and, at time t, the x_2 coordinate of the particle is therefore given by $x_2 = v_2\, t$. The propagator for the two dimensional motion when $\varepsilon = 0$ is therefore

$$G((x_1, x_2), (x_0, 0), t) = G_0(x_1, x_0, t)\, \delta(x_2 - v_2 t) . \tag{4.2.24}$$

Hence, from (4.2.3), for a steady source of intensity $\sigma(t) = \sigma_0 \Theta(t)$ at $\boldsymbol{x}_0$ we have

$$\rho_0(\boldsymbol{x}, \boldsymbol{x}_0) = \frac{\sigma_0}{\sqrt{4\pi D_{11}}} \int_0^\infty \frac{\mathrm{d}t'}{\sqrt{t'}} \exp\left[-\frac{(x_1 - x_0 - v_1 t')^2}{4 D_{11} t'}\right] \delta(x_2 - v_2 t') .$$

This gives

$$\rho_0(\boldsymbol{x}, \boldsymbol{x}_0) = \frac{\sigma_0}{\sqrt{4\pi D_{11} x_2 v_2}} \exp\left[-\frac{v_2 (x_1 - x_0 - v_1 x_2 / v_2)^2}{4 D_{11} x_2}\right] \tag{4.2.25}$$

and on the boundary far from the source, since $x_1 = 0$ and $x_2 \gg x_0$, this reduces to (4.2.22).

4.3 Antiparticle method for an absorbing boundary

4.3.1 Integral equation for the absorption flux

It is straightforward to perform a Monte Carlo simulation of the advection diffusion process with an absorbing boundary: the particles are simply removed from the simulation whenever they cross the boundary. In contrast when solving a Fokker-Planck equation which contains

an advective term[2] for a particle density it is not possible to write down a local boundary condition which implies that particles colliding with a boundary are absorbed [45, 56]. However, we can add an additional source term to the equation which, in principle, allows us to describe an absorbing boundary by adding a suitable source of *holes* (i.e. *negative mass* particles, or *antiparticles*), at the boundary. Since this approach does not rely on any geometrical symmetries of the system[3] it is potentially more general than approaches which use the method of images.

We consider the two dimensional case, which is illustrated in figure (4.2):

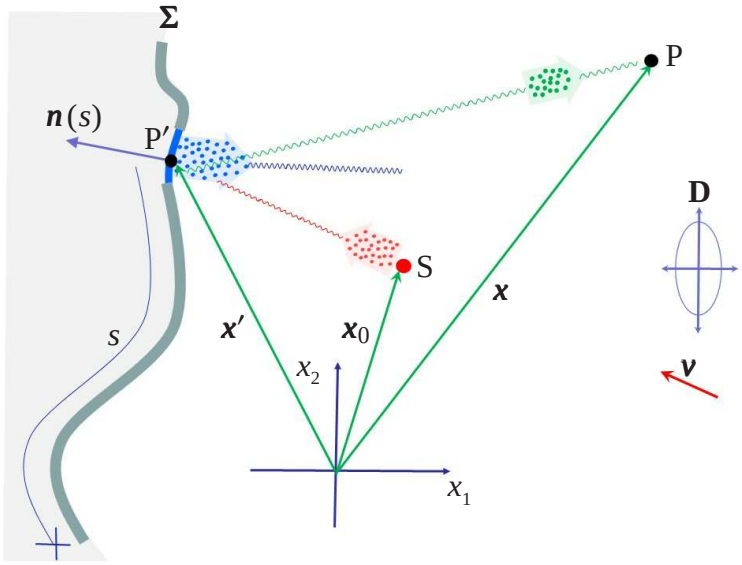

Fig. 4.2 Particle and antiparticle fluxes at a boundary. Particles emitted from the source at S drift and diffuse towards the boundary **Σ**. On first arrival at the boundary each particle generates a *hole* or *antiparticle*. The resultant particle density and flux at any field point, P, is the difference between-contributions from the source and the boundary.

Particles are emitted from the source S, which is located at $\boldsymbol{x}_0$, and undergo advection with diffusion until they reach the boundary **Σ** at some point P' located at $\boldsymbol{x}'$. An antiparticle is created corresponding to the *first arrival* of each particle at the boundary. After emission at the boundary the antiparticles propagate in the same way as particles do, but, to model absorption, the antiparticle density is *subtracted* from the particle density. The resulting particle density and flux at any *field point* P is therefore the difference between contributions from the particle source at S and the source of antiparticles distributed along **Σ**.

[2] such as equation (4.1.1)

[3] The boundary considered in this work does, however, have reflection symmetry.

Suppose that position on the boundary $\mathbf{\Sigma}$ can be parameterised by the arc length s, so that $\boldsymbol{x}' = \boldsymbol{x}'(s)$ and let $j(\boldsymbol{x}'(s), t')$ be the rate of antiparticle creation *per unit length* at point $\boldsymbol{x}'(s)$ and time t'. Then the element, ds of the boundary at point $\boldsymbol{x}'(s)$ is a source of antiparticles with intensity $j(\boldsymbol{x}'(s), t')ds$ and the antiparticles created at the boundary contribute an amount

$$-\int_{\mathbf{\Sigma}} \mathrm{d}s \int_{-\infty}^{t} \mathrm{d}t' \; j(\boldsymbol{x}'(s), t') G_0(\boldsymbol{x}, \boldsymbol{x}'(s), t - t') \tag{4.3.1}$$

to the overall density at point $\boldsymbol{x}$ at time t.

Since each antiparticle is created in response to the first arrival of a particle at the boundary the intensity of the antiparticle source is, dropping the argument s for clarity,

$$j(\boldsymbol{x}', t') = \boldsymbol{n}(\boldsymbol{x}') \cdot \boldsymbol{J}_{\mathrm{a}}(\boldsymbol{x}', \boldsymbol{x}_0, t') \tag{4.3.2}$$

where $\boldsymbol{J}_{\mathrm{a}}(\boldsymbol{x}', \boldsymbol{x}_0, t')$ is the *absorption flux* at $\boldsymbol{x}'$ and t' arising form the particle source at S and $\mathbf{n}(\boldsymbol{x}')$ is the unit normal on the boundary at $\boldsymbol{x}'$, *pointing out of the region* of diffusion-advection. The particle density in the presence of an absorbing boundary $\rho_a(\boldsymbol{x}, \boldsymbol{x}_0, t)$ is therefore

$$\rho_{\mathrm{a}}(\boldsymbol{x}, \boldsymbol{x}_0, t) = \rho_0(\boldsymbol{x}, \boldsymbol{x}_0, t) - \int_{\mathbf{\Sigma}} \mathrm{d}s \int_{-\infty}^{t} \mathrm{d}t' \; \mathbf{n}(\boldsymbol{x}') \cdot \boldsymbol{J}_a(\boldsymbol{x}', \boldsymbol{x}_0, t') \; G_0(\boldsymbol{x}, \boldsymbol{x}', t - t') \; . \tag{4.3.3}$$

Equation (4.3.3) is an integral equation for the absorption flux.

4.3.2 Exact absorption flux in one dimension

We illustrate the solution of the integral equation (4.3.3) in one dimension and derive an exact expression for the flux density $\boldsymbol{J}_{\mathrm{a}}(0, x_0, t)$ of particles absorbed at the origin, $x = 0$, arising from a source of unit strength, so that $\sigma_0 = 1$, localised at x_0, with $x_0 > 0$.

Let D be the diffusion coefficient and $\boldsymbol{v} = -v\boldsymbol{i}$ the drift velocity, so that the particles drift towards the left, then the free propagator representing propagation without absorption is

$$K_0(x, x_0, t) = G_0(x, x_0, t)\Theta(t) = \frac{1}{\sqrt{4\pi D t}} \exp\left[-\frac{(x - x_0 + vt)^2}{4Dt}\right]\Theta(t). \tag{4.3.4}$$

The corresponding free flux density is $\boldsymbol{J}_0(x,x_0,t) \equiv -J_0(x,x_0,t)\boldsymbol{i}$ where the flux *onto* the boundary (i.e. to the left) is

$$\begin{aligned} J_0(x,x_0,t) &= vG_0(x,x_0,t) + D\frac{\partial G_0}{\partial x}(x,x_0,t) \\ &= \frac{1}{\sqrt{4\pi Dt}}\left(\frac{x_0-x+vt}{2t}\right)\exp\left[-\frac{(x-x_0+vt)^2}{4Dt}\right] . \end{aligned} \tag{4.3.5}$$

The one-dimensional form of (4.3.3), giving the particle density at point x at time t for a system with an absorbing boundary at $x = 0$, is

$$\rho_{\mathrm{a}}(x,x_0,t) = \rho_0(x,x_0,t) - \int_0^t \mathrm{d}t'\; J_{\mathrm{a}}(0,x_0,t')G_0(x,0,t-t') . \tag{4.3.6}$$

The corresponding flux is

$$J_{\mathrm{a}}(x,x_0,t) = v\rho_{\mathrm{a}}(x,x_0,t) + D\frac{\partial \rho_{\mathrm{a}}}{\partial x}(x,x_0,t) \tag{4.3.7}$$

and using (4.3.6) in (4.3.7) gives

$$J_{\mathrm{a}}(x,x_0,t) = J_0(x,x_0,t) - \int_0^t \mathrm{d}t'\; J_{\mathrm{a}}(0,x_0,t')\,J_0(x,0,t-t') . \tag{4.3.8}$$

This equation expresses the absorption flux at time t from an ejection of particles at $t = 0$ as the sum of a direct flux from the source and a term resulting from the creation of 'antiparticles' due to the flux which reached the boundary at the earlier time t'. Since $J_0(x,x_0,t)$ is known from (4.3.5), equation (4.3.8) is a Volterra integral equation of the second kind for $J_{\mathrm{a}}(x,x_0,t)$, with kernel $J_0(x,0,t)$. It may be solved for J_a using the method of Laplace transforms. Noting that the integral in the equation is a convolution, the Laplace transform of (4.3.8), in the time variable, is

$$\bar{J}_{\mathrm{a}}(x,x_0,s) = \bar{J}_0(x,x_0,s) - \bar{J}_{\mathrm{a}}(0,x_0,s)\bar{J}_0(x,0,s) \tag{4.3.9}$$

where $\bar{J}_{\mathrm{a}}$ and $\bar{J}_0$ are the Laplace transforms of J_{a} and J_0, respectively.

Since $x = 0$ is an absorbing boundary we must have $J_a(x, x_0, t) = 0$ for $x < 0$, therefore, to determine $J_a(0, x_0, t)$, we consider

$$\bar{J}_a(\varepsilon, x_0, s) = \bar{J}_0(\varepsilon, x_0, s) - \bar{J}_a(0, x_0, s)\bar{J}_0(\varepsilon, 0, s) \tag{4.3.10}$$

in the limit as $\varepsilon \to 0^+$. The Laplace transform of $J_0(x, x_0, t)$ is[4]

$$\bar{J}_0(x, x_0, s) = \left(\frac{1 \mp \alpha}{2\alpha}\right)\exp\left[-\left(\frac{\zeta v}{2D}\right)(1 \pm \alpha)\right] \tag{4.3.11}$$

according as $\zeta = x - x_0$ is $\pm$ve and where

$$\alpha \equiv \sqrt{1 + \frac{4Ds}{v^2}}\,. \tag{4.3.12}$$

So equation (4.3.9) becomes

$$\bar{J}_a(\varepsilon, x_0, s) + \bar{J}_a(0, x_0, s)\left(\frac{1-\alpha}{2\alpha}\right)\exp\left[-\frac{\varepsilon v}{2D}(1+\alpha)\right] = \left(\frac{1+\alpha}{2\alpha}\right)\exp\left[\frac{(\varepsilon - x_0)v}{2D}(\alpha - 1)\right] \tag{4.3.13}$$

and in the limit as $\varepsilon \to 0^+$ this gives

$$\bar{J}_a(0, x_0, s) = \exp\left[-\frac{x_0 v}{2D}(\alpha - 1)\right] = \exp\left[-\frac{x_0 v}{2D}\left(\sqrt{1 + \frac{4Ds}{v^2}} - 1\right)\right]. \tag{4.3.14}$$

Note that, alternatively, we can consider the limit as $\varepsilon \to 0^-$. In this case there is no absorption flux at $x = 0^-$, because particles reaching $x = 0$ have been absorbed, and (4.3.9) is replaced by

$$0 = \bar{J}_0(\varepsilon, x_0, s) - \bar{J}_a(0, x_0, s)\bar{J}_0(\varepsilon, 0, s)\,. \tag{4.3.15}$$

It is readily verified that using (4.3.15) instead of (4.3.10) leads to the same result.

Inverting the Laplace transform gives the exact expression for the rate of absorption onto the boundary:

$$J_a(0, x_0, t) = \frac{1}{\sqrt{4\pi D}}\frac{x_0}{t^{3/2}}\exp\left[-\frac{(x_0 - vt)^2}{4Dt}\right]. \tag{4.3.16}$$

Distributions of this form are in a class which are sometimes referred inverse Gaussian or Wald distributions.

[4]The Laplace transforms and inverse transforms appearing in this section were obtained using the Maple® computer algebra system.

4.4 Flux onto an absorbing boundary in two dimensions

4.4.1 The method of calculation

We now apply the results derived in sections (4.2) and (4.3) to the case of absorption on a line in two dimensions. Absorption at the point $(0, x_2)$ requires that the particle *first* arrives at the boundary $x_1 = 0$ at ordinate x_2. We will consider the problem in terms of the first arrival time at the boundary and the distribution of the absorption ordinate *conditional* on that arrival time.

The first arrival time is determined by the x_1 component of the motion alone. This is a one-dimensional advection-diffusion process, with diffusion constant D_{11}, drift velocity $v_1 = -v$ and starting from initial point x_0. The p.d.f. for the first arrival time, T is the flux obtained above. In this context equation (4.3.16) becomes

$$P_T(t) = \frac{x_0}{\sqrt{4\pi D_{11} t^3}} \exp\left[-\frac{(x_0 - v_1 t)^2}{4D_{11} t}\right]. \tag{4.4.1}$$

The absorption ordinate is a random variable, X_2, whose p.d.f. may be obtained from $P_{X_2|T}(x_2, t)$, the probability density for X_2 conditional upon the first arrival time T:

$$P_{X_2}(x_2) = \int_0^\infty \mathrm{d}t \; P_{X_2|T}(x_2, t)\, P_T(t) \; . \tag{4.4.2}$$

The conditional p.d.f. in this expression can be obtained from the propagator $G_0(\boldsymbol{x}, \boldsymbol{x}_0, t)$, which is a joint probability density for X_1 and X_2 conditional upon T, by dividing by the appropriate marginal density of X_1:

$$P_{X_2|T}(x_2, t) = \frac{G_0((0, x_2), (x_0, 0), t))}{\int_{-\infty}^{\infty} \mathrm{d}x_2 \; G_0((0, x_2), (x_0, 0), t))} \; . \tag{4.4.3}$$

Using equation (4.2.1), since $t \geq 0$, we can write this as

$$P_{X_2|T}(x_2, t) = \frac{\exp[-S(\boldsymbol{\zeta}, t)]}{I(x_0, t)} \tag{4.4.4}$$

where $\boldsymbol{\zeta} = (-x_0, x_2)$ and

$$I(x_0, t) \equiv \int_{-\infty}^{\infty} \mathrm{d}x_2 \; \exp[-S(\boldsymbol{\zeta}, t)] \; . \tag{4.4.5}$$

Then equation (4.4.2) becomes

$$P_{X_2}(x_2) \sim \frac{x_0}{\sqrt{4\pi D_{11}}} \int_0^\infty \frac{\mathrm{d}t}{t^{3/2}} \left[\frac{1}{I(\zeta_1, t)} \exp\left(-S(\boldsymbol{\zeta}, t) - \frac{(x_0 - v_1 t)^2}{4 D_{11} t} \right) \right] . \tag{4.4.6}$$

In the steady state the x_1 component of the particle flux onto the boundary has magnitude $J_\mathrm{a}(x_2) = \sigma_0 P_{X_2}(x_2)$.

4.4.2 Estimates using the method of Laplace

For large $|\boldsymbol{\zeta}|$ (i.e. for large $|x_2|$) both of the integrals in equation (4.4.6) can be approximated by Laplace's method. This allows us to determine the asymptotic form of the p.d.f. of the ordinate of the absorption point, $P_{X_2}(x_2)$ and, thereby, the magnitude of the absorption flux $J_\mathrm{a}(x_2)$.

For any given values of ζ_1 and t the dominant contribution to $I(x_0, t)$ arises from a neighbourhood of the critical value ζ_2^*, at which $S(\boldsymbol{\zeta}, t)$ has a minimum with respect to x_2 and

$$I(x_0, t) \sim \exp\left[-S\left((\zeta_1, \zeta_2^*),\ t \right) \right] \int_{-\infty}^{\infty} \mathrm{d}\zeta_2 \ \exp\left[-\frac{\left(\zeta_2 - \zeta_2^*\right)^2}{2} \frac{\partial^2 S}{\partial \zeta_2^2} \left(\left(\zeta_1, \zeta_2^*\right), t \right) \right] . \tag{4.4.7}$$

Writing $\boldsymbol{\zeta}^* = \left(\zeta_1, \zeta_2^*\right)$, the critical value ζ_2^* satisfies

$$\frac{\partial S}{\partial \zeta_2}(\boldsymbol{\zeta}^*, t) = \frac{\mathrm{D}_{11}\zeta_2^* - \mathrm{D}_{12}\zeta_1 - (\mathrm{D}_{11} v_2 - \mathrm{D}_{12} v_1) t}{2 \det(\mathbf{D}) \mathrm{t}} = 0$$

so that

$$\zeta_2^* = \frac{\mathrm{D}_{12}}{\mathrm{D}_{11}} (\zeta_1 - v_1 t) + v_2 t$$

and

$$\boldsymbol{\zeta}^* - \boldsymbol{\nu} t = (\zeta_1 - v_1 t) \begin{bmatrix} 1 \\ \frac{D_{12}}{D_{11}} \end{bmatrix}$$

giving

$$S(\boldsymbol{\zeta}^*, t) = \frac{(\zeta_1 - v_1 t)^2}{4 \mathrm{D}_{11} t} \quad \text{and} \quad \frac{\partial^2 S}{\partial \zeta_2^2}(\boldsymbol{\zeta}^*, t) = \frac{\mathrm{D}_{11}}{2 \det(\mathbf{D}) t} . \tag{4.4.8}$$

and Substituting these results into equation (4.4.6) gives

$$I(x_0,t) \sim \exp\left[-\frac{(\zeta_1 - v_1 t)^2}{4\mathrm{D}_{11} t}\right] \int_{-\infty}^{\infty} \mathrm{d}\zeta_2 \exp\left[-\frac{\mathrm{D}_{11}\left(\zeta_2 - \zeta_2^*\right)^2}{4\,\det(\mathbf{D})\;t}\right]$$

and evaluating the Gaussian integral we have

$$I(x_0,t) \sim \sqrt{\frac{4\pi\,\det(\mathbf{D})\;t}{\mathrm{D}_{11}}}\;\exp\left[-\frac{(\zeta_1 - v_1 t)^2}{4\mathrm{D}_{11} t}\right]. \tag{4.4.9}$$

Equation (4.4.6) now gives

$$P_{X_2}(x_2) \sim \frac{x_0}{4\pi\sqrt{\det(\mathbf{D})}} \int_0^{\infty} \frac{\mathrm{d}t}{t^2}\left[\exp\left(-S\left(\boldsymbol{\zeta},t\right) - \frac{(x_0 - v_1 t)^2}{4\mathrm{D}_{11} t} + \frac{(\zeta_1 - v_1 t)^2}{4\mathrm{D}_{11} t}\right)\right].$$

Since $\zeta_1 = -x_0$ on the boundary the last two terms in the exponent sum to a constant value giving

$$P_{X_2}(x_2) \sim \frac{x_0}{4\pi\sqrt{\det(\mathbf{D})}} \exp\left(\frac{x_0 v_1}{\mathrm{D}_{11}}\right) \int_0^{\infty} \frac{\mathrm{d}t}{t^2} \exp\left[-S\left(\boldsymbol{\zeta},t\right)\right]. \tag{4.4.10}$$

The remaining integral may be estimated as in section (4.2.2) giving

$$\left[\boldsymbol{J}_a\left(x_2\right)\right]_1 = \sigma_0 P_{X_2}(x_2) \sim \sigma_0 A_{\mathrm{a}}(x_2) \exp\left[-\Psi_0\left(\boldsymbol{x},\boldsymbol{x}_0\right)\right] \tag{4.4.11}$$

where Ψ_0 is as given by equation (4.2.19) and

$$A_{\mathrm{a}}(x_2) = \left[\frac{x_0 \exp(x_0 v_1/\mathrm{D}_{11})}{2\sqrt{\pi\det(\mathbf{D})}}\right] \frac{\left(\boldsymbol{\nu}\cdot\mathbf{D}^{-1}\boldsymbol{\nu}\right)^{\frac{1}{4}}}{\left(\boldsymbol{\zeta}\cdot\mathbf{D}^{-1}\boldsymbol{\zeta}\right)^{\frac{3}{4}}}. \tag{4.4.12}$$

Now, on the x_2 axis far from the source $A_{\mathrm{a}}(x_2) \sim |x_2|^{-3/2}$ therefore, as $|x_2|$ increases the coefficient A_{a} and the flux onto an absorbing boundary, $J_{\mathrm{a}}(x_2)$, decay more rapidly than the corresponding flux onto a permeable boundary, J_0. However the exponent Ψ_0 in J_{a} is the same as that in J_0.

4.5 Discussion of results

4.5.1 Comparison with Monte Carlo simulation

The results derived above depend on asymptotic estimates of integrals provided by Laplace's method. It is instructive to assess their accuracy and we may do so by comparing them with the results from Monte Carlo simulations. We can generate sample particle paths, and from these simulate the particle density and boundary fluxes, using the Euler iterative scheme

$$\boldsymbol{r}_{n=0} = \boldsymbol{r}_0, \quad \boldsymbol{r}_{n+1} = \boldsymbol{r}_n + \boldsymbol{v}\delta t + \sqrt{2\,\mathbf{D}\,\delta t}\,\boldsymbol{\eta}_n, \quad n = 1, 2, 3, \cdots \tag{4.5.1}$$

where δt is a small time increment and each $\boldsymbol{\eta}_n$ is a d-dimensional vector of independent normally distributed random variables with zero mean and unit variance.

Figure (4.3) shows the results of four such simulations, corresponding to different combinations of source position, drift velocity and diffusion tensor. The location of the source $\boldsymbol{x}_0$, the drift velocity $\boldsymbol{v}$ and the diffusion tensor $\mathbf{D}$ are given in the first plot in each row, and in each row we display the same data on linear and semi-logarithmic scales, side-by-side.

The plots show the magnitudes of the steady state particle density[5] for a permeable boundary, $\rho_0(x_2)$, and the absorption flux for an absorbing boundary, $J_\mathrm{a}(x_2)$. For both the density and the absorption flux, the results obtained from the Monte Carlo simulations are compared to those obtained from the asymptotic approximations derived using the Laplace method. In addition, for the density $\rho_0(x_2)$ the value computed from the exact propagator (4.2.3) by numerical integration is also shown. Both $\rho_0(x_2)$ and $J_\mathrm{a}(x_2)$ are displayed as normalised distributions; in the case of $J_\mathrm{a}(x_2)$ this corresponds to the source intensity σ_0 being equal to unity.

In plots (a)-(f) $\boldsymbol{v} = [-1, 2]^\mathrm{T}$ and since $v_2 \neq 0$ the distributions are skewed. Plots (g) and (h) illustrate the conclusion from section (4.2.3) that our analysis remains valid even if $\mathbf{D}$ has rank one. The curves in the log-linear plots become parallel at large x_2 showing that, asymptotically, the exponential decay is the same whether or not there is an absorbing boundary.

[5] We have not plotted the flux, $J_0(x_2)$, onto a permeable boundary; this can be obtained by multiplying $\rho_0(x_2)$ by an effective drift velocity, see equation (4.2.12).

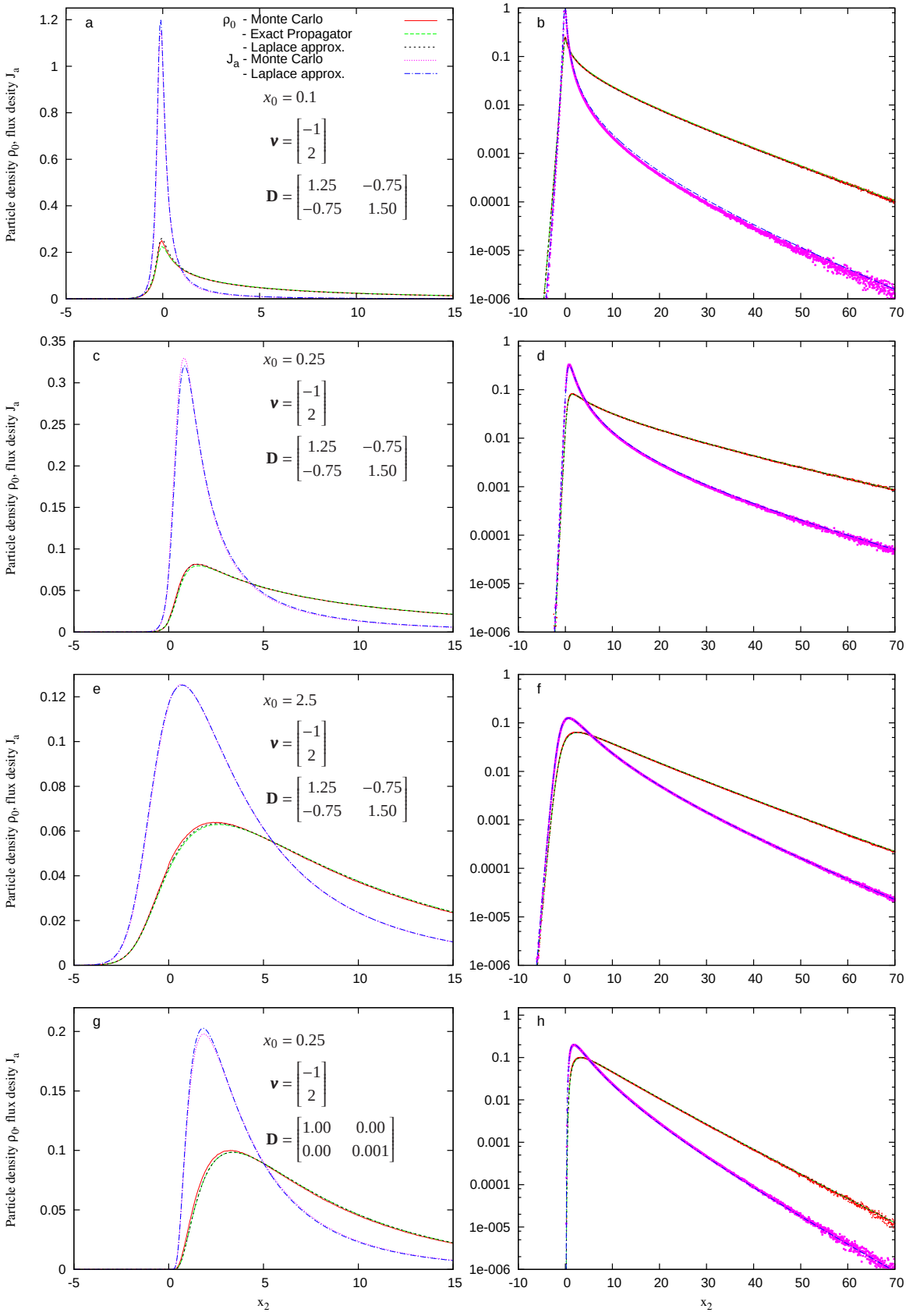

Fig. 4.3 The absorption problem: particle fluxes onto a transparent and an absorbing boundary.

In the case of the non-absorbing boundary, equation (4.2.25) is expected to serve as a precise asymptotic estimate of $\rho_0(x_2)$ as $|x_2| \to \infty$, and the plots in the figure show that this formula is indeed very accurate. In the case of the absorbing boundary, the status of equations (4.4.11) and (4.4.12) is more complicated, because there are two Laplacian integrations involved in their derivation. These equations are not precise asymptotes for $J_a(x_2)$ as $|x_2| \to \infty$ because this limit does not play a role in the estimate for the normalisation factor of the integral in the denominator of equation (4.4.3), (i.e. equation (4.4.5)). Equations (4.4.11), (4.4.12) are only precise asymptotic estimates when we take $x_0 \to \infty$ as well as $|x_2| \to \infty$. Our numerical results illustrate this: in the case of an absorbing boundary a slight deviation from the asymptotic expression (equations (4.4.11) and (4.4.12)) is visible in figure (4.3) for the smallest value of x_0 (panel (b)), while there is almost perfect agreement in the other cases.

4.5.2 Conclusion

We have investigated the flux, $J(x_2)$, onto a permeable and an absorbing boundary, as a function of the coordinate x_2 measuring the distance from the source. We found that $J(x_2)$ has the form $A(x_2)\exp[-\Psi(x_2)]$ and that the decay exponent, $\Psi(x_2) = \Psi_0(x_2)$ in both cases, where, asymptotically, $\Psi_0(x_2)$ grows linearly as $x_2 \to \infty$. Consequently, as the distance from the source increases, there is the same exponential decay in both cases. We also showed that in each case the coefficient, $A(x_2)$, has an algebraic decay, with $A(x_2) = A_a(x_2) \sim |x_2|^{-3/2}$ for the absorbing boundary, compared to $A(x_2) = A_0(x_2) \sim |x_2|^{-1/2}$ for the permeable boundary.

To check our approach we solved the one-dimensional case explicitly, showing that it gives results which agree with those from the theory of first-passage time processes, as discussed in [43, 47]. We also compared our results for two dimensions with those obtained from Monte Carlo simulations, providing further confirmation of validity.

To obtain the absorption flux, $J_a(x_2)$, we used an approach involving antiparticles. This involved the determination of the distribution, P_T, of first contact times for the boundary and the distribution, $P_{X_2|T}$, of the ordinate of first contact, X_2, conditional upon the value of the first contact time T. It is natural to ask whether the *antiparticle method* could lead to a more direct evaluation of $J_a(x_2)$ in the case where the distance of the source from the boundary, x_0, is small. In this case most of the particles emitted from the source at $\boldsymbol{x}_0 = (x_0, 0)$ will be absorbed by the boundary at a point *downstream* of the source, $\boldsymbol{x}_d = \boldsymbol{x}_0 + \boldsymbol{v}x_0/v_1$. One might

then expect that the flux at $\boldsymbol{x}$ would then be given by a *dipole approximation*:

$$J_{\mathrm{a}}(\boldsymbol{x},\boldsymbol{x}_0) \sim [J_0(\boldsymbol{x},\boldsymbol{x}_0) - J_0(\boldsymbol{x},\boldsymbol{x}_{\mathrm{d}})] \sim (\boldsymbol{x}_0 - \boldsymbol{x}_{\mathrm{d}}) \cdot \boldsymbol{\nabla}_{\boldsymbol{x}_0} J_0(\boldsymbol{x},\boldsymbol{x}_0)$$

however we were not able to produce a valid estimate of $J_{\mathrm{a}}(x_2)$ using this type of dipolar approximation.

The results obtained in this chapter are directly relevant to the study of the geometry of constellations of points sampling fractal measures [65]. Also, we note that the absorption problem is relevant to the modelling of fallout plumes, from events such as volcanic eruptions[6]. Our analysis is relevant to fallout when the diffusive dispersion is anisotropic.

[6]The study of dispersion of dust and smoke in the atmosphere has a long history, see [46, 55] and the recent review by Stockie [53]. Ermak [5] appears to have been the first author to treat settling and deposition, i.e. drift and absorption, as well as diffusive dispersion.

Chapter 5

A Matrix Contraction Process

> Many strokes, though with a little axe, hew down and fell the hardest-timber'd oak.
>
> *William Shakespeare*

In this chapter we consider a stochastic process in which i.i.d. random matrices are multiplied, and where the Lyapunov exponent of the product is positive. Whilst the Frobenius norm, $\mathcal{E}$, of the product is *less* than unity we continue to multiply the matrices, but when the norm equals or exceeds unity we reset the process to a multiple of the identity and then continue the multiplication. Our motivation for analysing this *matrix contraction process* is that it serves as a model for describing the fine-structure of strange attractors, where a dense concentration of trajectories arises from the differential of the flow being contracting in some region.

We address the problem of determining the p.d.f. of the norm, $P_{\mathcal{E}}(\varepsilon)$, and conjecture that, in the limit as $\varepsilon \to 0$, this takes the form of a *modified* power law $P_{\mathcal{E}}(\varepsilon) \sim \varepsilon^{\gamma}/[\ln(1/\varepsilon)]^{\mu}$ where γ and μ are two real parameters. Our objective is to justify this conjecture and to show how γ and μ can be determined.

We apply our analysis to a matrix-product description of the differential of the random flow in a compressible fluid. For this class of models we find that, whilst γ depends continuously on the compressibility parameter of the model, there is a phase transition with the parameter μ changing discontinously from $\mu = 0$ to $\mu = \frac{3}{2}$, as the compressibility parameter is varied.

This chapter is based on [66], 'A matrix contraction process', published in the journal of Physics A (Mathematical and Theoretical).

5.1 Contraction processes

5.1.1 The scalar case

Let $\{S_n\}_{n\geq 1}$ be a sequence of *scaling factors*, real positive i.i.d. random variables each of which has a finite probability of being less than unity and of being greater than unity, and let $0 < \varepsilon_0 < 1$ be some given real number. We define a second sequence of random variables, $\{\mathcal{E}_n\}_{n\geq 0}$, such that $\mathcal{E}_{n=0} = \varepsilon_0$ and, for $n = 1, 2, 3, \cdots$,

$$\mathcal{E}_n = \begin{cases} S_n\, \mathcal{E}_{n-1} & |S_n\, \mathcal{E}_{n-1}| < 1 \\ \varepsilon_0 & |S_n\, \mathcal{E}_{n-1}| \geq 1. \end{cases} \tag{5.1.1}$$

We can interpret the sequence $\{\mathcal{E}_n\}_{n\geq 0}$ as a sequence of values of a random variable, $\mathcal{E}$, representing the length of an interval which has initial length ε_0 and which is repeatedly scaled, by random scaling factors, or re-set to its original length whenever some maximum length, here unity, is reached. The sequence $\{\mathcal{E}_n\}_{n\geq 0}$ has one of two possible types of behaviour, depending on the distribution of the multipliers S_n, these are illustrated in figure (5.1).

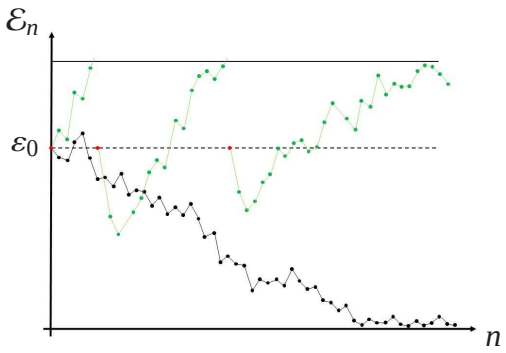

Fig. 5.1 The figure shows the two possible types of behaviour for a scalar contraction process, i.e. a sequence defined recursively by equation (5.1.1). The process either converges to zero or it contains a number of runs, or subsequences, each of which terminates when a term of the sequence reaches or exceeds the upper limit, here unity.

Either $\mathcal{E}_n \to 0$ as $n \to \infty$ or the sequence is comprised of finite subquences, or *runs*, of values which terminate when the scaling generates a length greater than unity. By re-labelling so that the iterates are indexed *within* a run the n^{th} iterate in any run can always be written as

$$\mathcal{E}_n = S_n S_{n-1} \cdots S_1 \, \varepsilon_0 = \left[\prod_{i=1}^{n} S_i \right] \varepsilon_0 \equiv M_n \, \varepsilon_0 \tag{5.1.2}$$

so that the length of the n^{th} interval is some multiple of the original length, with the multiplier being a product of n random numbers.

We are interested in the second case, where the process is repeatedly re-set, which we shall refer to as a *scalar contraction process*. This process has some similarity to an *escape problem* wherin particles in an ensemble escape from an allowable region whenever they first contact the boundary of the region.

A scalar contraction process generates a statistically stationary sequence of values of $\mathcal{E}$, with some p.d.f., $P_{\mathcal{E}}(\varepsilon)$. This p.d.f. can be most easily understood in terms of the random variable[1], $Z = -\ln \mathcal{E}$, which involves a *sum* of i.i.d. random variables, $Z_i = -\ln S_i$, each of which has a *positive* mean value.

As $\mathcal{E} \to 0$ then $Z \to \infty$. Hence, provided (as we shall assume) that the distribution of the Z_i does *not* have heavy tails, we may expect a master equation for $P_Z(z)$ to become independent of z. Therefore, since the exponential function is translationally invariant (up to a change of normalization), this *translational symmetry* can be respected by choosing a p.d.f. of the form $P_Z(z) \sim \exp(-\alpha z)$. To give a normalisable probability density the coefficient α must be positive. From this result we may deduce the form of the p.d.f. $P_{\mathcal{E}}(\varepsilon)$ by substituting $z = -\ln \varepsilon$ in right hand side of the *change of variable rule*: $P_{\mathcal{E}}(\varepsilon) = P_Z(z) \left| \dfrac{\mathrm{d}z}{\mathrm{d}\varepsilon} \right|$. We find that, for small ε, $P_{\mathcal{E}}(\varepsilon)$ is given by a power-law of the form[2].

$$P_{\mathcal{E}}(\varepsilon) \sim \varepsilon^{\gamma} \tag{5.1.3}$$

where $\gamma = \alpha - 1$.

Figure (5.2) shows log-log plots of the p.d.f. $P_{\mathcal{E}}(\varepsilon)$ for two different distributions of the scaling factors, S_i, clearly illustrating this power law behaviour. In case (a) $S_i = \exp(Z_i)$

[1] The minus sign simply ensures that the random variable is positive.

[2] The argument showing that the p.d.f. $P_{\mathcal{E}}$, has a power-law distribution for ε is presented in [15].

where the Z_i are standard normal variates and in case (b) $S_i = \exp(U_i)$ where the U_i are uniformly distributed on the interval $(-1, 1)$.

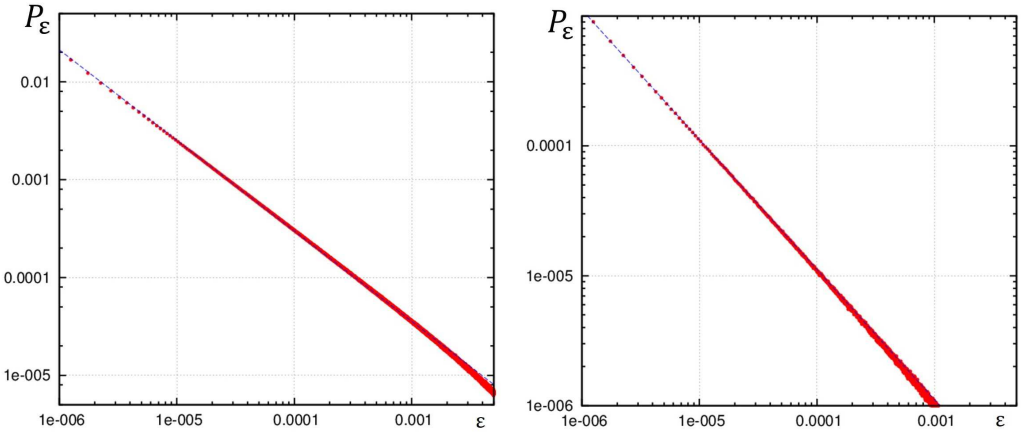

(a) $S_i = \exp(Z_i)$ with $Z_i \sim \mathcal{N}(0,1)$ (b) $S_i = \exp(U_i)$ with $U_i \sim U(-1,1)$

Fig. 5.2 The figures show the p.d.f., $P_{\mathcal{E}}(\varepsilon)$, for two different scalar contraction processes. In figure (a) the scaling factors are the exponentials of standard normal variates whilst in figure (b) they are the exponentials of variates that are uniformly distributed on $(-1, 1)$. In each case $P_{\mathcal{E}}(\varepsilon)$ is a power law.

The scalar contraction process arises naturally in dynamical systems theory, essentially as a consequence of the chain rule which allows the differential of a dynamical map to be written as a product of the differentials at each iteration. Therefore, for a system with a single degree of freedom involving a chaotic map of one variable, it is reasonable to model this differential as a product of independent random numbers, analogous to equation (5.1.2). The resetting process addresses what happens when the separation of trajectories is no longer small and the linearisation approximation fails. Since we are concerned with small separations, we ignore the dynamics while the separation becomes large and reset the process when the separation of trajectories becomes small again.

5.1.2 The matrix case

For a dynamical system with several degrees of freedom the differential of the dynamical map is described by a product of *stability matrices*, rather than a product of scalars [37]. We therefore consider the generalization of the above process to a *matrix contraction process* involving a product of square matrices of order d.

Let $\boldsymbol{L}_0$ be some given matrix, which may in general be random, and let $\{\boldsymbol{S}_n\}_{n\geq 1}$ be a sequence of real i.i.d. random matrices. We define a second sequence of random matrices, $\{\boldsymbol{L}_n\}_{n\geq 0}$ such that $\boldsymbol{L}_{n=0} = \boldsymbol{L}_0$ and, for $n = 1, 2, 3, \cdots$,

$$\boldsymbol{L}_n = \begin{cases} \boldsymbol{S}_n \boldsymbol{L}_{n-1} & \text{if} \quad \mathcal{E}(\boldsymbol{S}_{\mathrm{n}} \boldsymbol{L}_{\mathrm{n}-1}) < 1 \\ \boldsymbol{L}_0 & \text{if} \quad \mathcal{E}(\boldsymbol{S}_{\mathrm{n}} \boldsymbol{L}_{\mathrm{n}-1}) \geq 1 \end{cases} \tag{5.1.4}$$

where $\mathcal{E}(\boldsymbol{A})$ is the Frobenius norm of $\boldsymbol{A}$:

$$\mathcal{E}(\boldsymbol{A}) = \sqrt{\mathrm{tr}\left(\boldsymbol{A}^{\mathrm{T}}\boldsymbol{A}\right)}. \tag{5.1.5}$$

As in the scalar case, by re-labelling so that the iterates are indexed *within* a run, the n^{th} iterate in any run can always be written as

$$\boldsymbol{L}_n = \boldsymbol{S}_n \boldsymbol{S}_{n-1} \cdots \boldsymbol{S}_1 \boldsymbol{L}_0 = \left[\prod_{i=1}^{n} \boldsymbol{S}_n\right] \boldsymbol{L}_0 \equiv \boldsymbol{M}_n \boldsymbol{L}_0. \tag{5.1.6}$$

Writing $\mathcal{E}_n = \sqrt{\mathrm{tr}\left(\boldsymbol{L}_n^{\mathrm{T}}\boldsymbol{L}_n\right)}$, then the matrix contraction process, $\{\boldsymbol{L}_n\}_{n\geq 0}$, generates a scalar contraction process of matrix norms, $\{\mathcal{E}_n\}_{n\geq 0}$, which is characterized by a p.d.f. $P_{\mathcal{E}}$. By analogy with the scalar contraction process, we might expect that $P_{\mathcal{E}}$ is a power-law, however in section (5.2) we shall show that this is incorrect and that a more general expression, in the form of a power law modified by a logarithmic correction, is required.

The matrix contraction process arises naturally in the study of the dynamics of an evolving constellation of particles[3]. This can be seen by taking the $\boldsymbol{L}_n$ to be values of the *configuration matrix* of the constellation at times $t_n = n\delta t,\ n = 0, 1, 2, \cdots$. We define this to be the matrix whose columns are the displacement vectors of d of the vertices, or particles, relative to a reference vertex, or particle. For example, for the two dimensional system considered in subsection (3.3.1) we have $\boldsymbol{L}(t) = [\delta\boldsymbol{r}_1, \delta\boldsymbol{r}_2]$ and, from equations (2.4.1) and (3.3.1),

$$\boldsymbol{L}(t+\delta t) \approx [\boldsymbol{I} + \delta\boldsymbol{A}(t)]\,\boldsymbol{L}(t) \equiv \boldsymbol{S}(t)\,\boldsymbol{L}(t).$$

where $\delta\boldsymbol{A}(t) \equiv \sqrt{\delta t}\boldsymbol{A}(t)$, with $\boldsymbol{A}(t) = \left[\partial_j u_i\right]$ and where the velocity field $\boldsymbol{u}$ is given by equation (2.4.1). Iterating this relation at times $t_n,\ n = 0, 1, 2, \cdots$ generates a sequence of the form (5.1.6). The condition $\mathcal{E}(\boldsymbol{S}(t_n)\boldsymbol{L}(t_{n-1})) < 1$ corresponds to $\sqrt{\delta\boldsymbol{r}_1^2(t_n) + \delta\boldsymbol{r}_2^2(t_n)} < 1$ so that the process is re-set to $\boldsymbol{L}_0$ at time $t = t_n$ if either , or both, of $\delta\boldsymbol{r}_1(t_n)$ or $\delta\boldsymbol{r}_2(t_n)$ become

[3] More precisely, a *variant* of the process in which the initial value, and the values whenever the process is reset, are random matrices. We shall consider the case where $\boldsymbol{L}_0$ is random in the next chapter.

too large. We note, in passing, that since $\delta\boldsymbol{A}(t) \equiv \sqrt{\delta t}\boldsymbol{A}(t)$ with δt small, the stability matrix $\boldsymbol{S}(t) \equiv [\boldsymbol{I} + \delta\boldsymbol{A}]$ differs only slightly from the identity matrix.

In the remainder of this chapter we shall consider the two-dimensional case and we shall set $\boldsymbol{L}_0$ to be a multiple of the 2×2 identity matrix $\boldsymbol{L}_0 = \dfrac{\varepsilon_0}{\sqrt{2}}\boldsymbol{I}$, with $0 < \varepsilon_0 < 1$. Note that we then have $\mathcal{E}(\boldsymbol{L}_0) = \varepsilon_0$.

Figure (5.3) shows the evolution of a triangular constellation during a short run of the process $\{\boldsymbol{L}_n\}$.

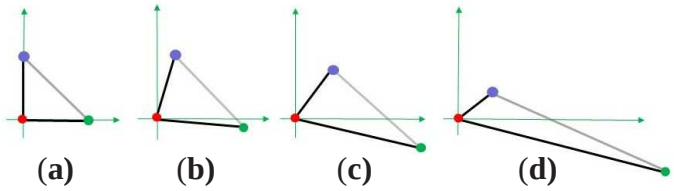

Fig. 5.3 The matrix contraction process, $\boldsymbol{L}_t$ represents the configuration of a triangular constellation of particles which initially form a small right-angled equilateral triangle (figure (a)). As the system evolves the triangle is distorted (figures (b), (c) and (d). If the sum of the squares of the lengths of the sides exceeds some upper limit (here unity) then the process is re-set to its initial value.

Initially, at $t = 0$, the constellation has the form shown in (**a**): a right-angled isosceles triangle with hypotenuse ε_0. At time $t_1 = \delta t$ the configuration matrix is $\boldsymbol{L}_1 = \boldsymbol{S}_1\boldsymbol{L}_0 = \frac{\varepsilon_0}{\sqrt{2}}\boldsymbol{S}_1\boldsymbol{I}$, and at time $t_2 = 2\delta t$ it is $\boldsymbol{L}_2 = \frac{\varepsilon_0}{\sqrt{2}}\boldsymbol{S}_2\mathbf{S}_1\boldsymbol{I}$. At some later time, shown in figure (**d**), $\delta\boldsymbol{r}_1$ has has grown sufficiently large that the process is re-set, to state $\boldsymbol{L}_0$, shown in (**a**).

5.2 Evolution of the process $\boldsymbol{L}(t)$

5.2.1 Stochastic differential equations for the singular values of $\boldsymbol{L}(t)$

To determine the p.d.f. $P_{\mathcal{E}}$ we shall make a number of assumptions about the various terms appearing in equation (5.1.6). We suppose that the $\boldsymbol{L}_n$ are values of $\boldsymbol{L}(t)$, a continuous matrix function of time, at the times $t_n = n\delta t$, where δt a small increment of time. Similarly we suppose that the $\boldsymbol{M}_n$ are the values of some continous function $\boldsymbol{M}(t)$. In the case where the $\boldsymbol{L}_n$ represent the configuration of a physical system these assumptions ensure that the evolvution of the system is continuous. We shall also assume that each of the random

multiplicative factor $\boldsymbol{S}_n$, $n = 1,2,3,\cdots$ is close to the identity[4] so that the equation can be written as

$$\boldsymbol{L}_n = \left[\prod_{i=1}^{n}(\boldsymbol{I} + \delta\boldsymbol{A}_i)\right]\boldsymbol{L}_0 \equiv \boldsymbol{M}_n\boldsymbol{L}_0, \tag{5.2.1}$$

for some matrices $\delta\boldsymbol{A}_i$. Finally, we suppose that the elements of the $\delta\boldsymbol{A}_n$ have the following statistics

$$\langle(\delta\boldsymbol{A}_n)_{ij}\rangle = 0\,, \quad \langle(\delta\boldsymbol{A}_n)_{ij}(\delta\boldsymbol{A}_m)_{kl}\rangle = 2\mathcal{D}_{ijkl}\,\delta_{nm}\delta t \tag{5.2.2}$$

so that the evolution of $\boldsymbol{L}(t)$ is characterized by a diffusive process, with diffusion coefficients $\mathcal{D}_{ijkl}$. The initial (and re-set) state is $\boldsymbol{L}_0 = \frac{\varepsilon_0}{\sqrt{2}}\boldsymbol{I}$, where $0 < \varepsilon_0 < 1$.

The analysis of the evolution of the norm, $\mathcal{E}(t) = \sqrt{\mathrm{tr}\left[\boldsymbol{L}^{\mathrm{T}}\boldsymbol{L}\right]}$, can be carried out using the singular value decomposition of the *deformation matrix* $\boldsymbol{M}(t)$. This is of the form (see [19])

$$\boldsymbol{M}(t) = \boldsymbol{R}_1\,\boldsymbol{\Lambda}\,\boldsymbol{R}_2 \tag{5.2.3}$$

where $\boldsymbol{R}_1 \equiv \boldsymbol{R}(\theta_1)$ and $\boldsymbol{R}_2 \equiv \boldsymbol{R}(\theta_2)$ are rotation matrices, of the form

$$\boldsymbol{R}(\theta) = \begin{pmatrix} \cos\theta & -\sin\theta \\ \sin\theta & \cos\theta \end{pmatrix}$$

and where

$$\boldsymbol{\Lambda} = \mathrm{diag}\,[\lambda_1, \lambda_2] = \begin{pmatrix} \lambda_1 & 0 \\ 0 & \lambda_2 \end{pmatrix}.$$

Note that the rotation angles θ_1, θ_2 and the singular values λ_1, λ_2 depend on t.

Then, from the definition of the norm $\mathcal{E}(t)$, we have[5]

$$[\mathcal{E}(t)]^2 = \mathrm{tr}\left[\boldsymbol{L}_0^{\mathrm{T}}\boldsymbol{M}^{\mathrm{T}}\boldsymbol{M}\boldsymbol{L}_0\right] = \frac{\varepsilon_0^2}{2}\mathrm{tr}\left[\boldsymbol{R}_2^{\mathrm{T}}\boldsymbol{\Lambda}^2\boldsymbol{R}_2\right] = \frac{\varepsilon_0^2}{2}\left[\lambda_1^2 + \lambda_2^2\right] \tag{5.2.4}$$

and by introducing the *scaled* singular values, $\tilde{\lambda}_i \equiv \left(\frac{\varepsilon_0}{\sqrt{2}}\right)\lambda_i$, $i = 1,2$ we can write this result as

$$[\mathcal{E}(t)]^2 = \left[\tilde{\lambda}_1^2 + \tilde{\lambda}_2^2\right]. \tag{5.2.5}$$

Note that, in terms of the scaled singular values, the re-setting condition for the matrix contraction process, that $\mathcal{E} \le 1$, assures that $\tilde{\lambda}_i \le 1$, $i = 1,2$.

[4] Practically this can be assured by taking the time increment δt sufficiently small.

[5] To aid clarity we suppress the time argument of the matrices and singular values.

Equation (5.2.4) shows that, since the initial configuration, $\boldsymbol{L}_0$, is a multiple of the identity, the value of the norm, $\mathcal{E}$, at any time does *not* depend on the rotation angles, θ_1 or θ_2 but only on ε_0 and the singular values of the deformation matrix[6]. Or, equivalently, from equation (5.2.5), we see that the value of the norm depends only on the scaled singular values. Therefore, in principle, we can determine the p.d.f. of the norm, $P_{\mathcal{E}}$, from the p.d.f. of the singular values, λ_1 and λ_2. We now consider the evolution of the singular values.

Consider the process $\boldsymbol{L}(t)$ at times $n\delta t$ and $(n+1)\delta t$. From equation (5.2.1) it follows that

$$\boldsymbol{M}_{n+1} = [\boldsymbol{I} + \delta\boldsymbol{A}_{n+1}]\,\boldsymbol{M}_n = \boldsymbol{S}_{n+1}\boldsymbol{M}_n$$

Suppose that $\boldsymbol{M}_n$ has the s.v.d. $\boldsymbol{M}_n = \boldsymbol{R}_1\boldsymbol{\Lambda}\boldsymbol{R}_2$ and let the changes in the matrices $\boldsymbol{R}_1$, $\boldsymbol{R}_2$ and $\boldsymbol{\Lambda}$ during the time interval $[n\delta t,(n+1)\,\delta t]$ be $\delta\boldsymbol{R}_1$, $\delta\boldsymbol{R}_2$, and $\delta\boldsymbol{\Lambda}$, respectively. Then the s.v.d. of $\boldsymbol{M}_{n+1}$ can be written as

$$\boldsymbol{M}_{n+1} = (\boldsymbol{R}_1 + \delta\boldsymbol{R}_1)(\boldsymbol{\Lambda} + \delta\boldsymbol{\Lambda})(\boldsymbol{R}_2 + \delta\boldsymbol{R}_2)\ .$$

Expanding this equation and comparing the two expressions for $\boldsymbol{M}_{n+1}$ gives

$$\begin{aligned}\delta\boldsymbol{A}_{n+1}\boldsymbol{M}_n = {} & \boldsymbol{R}_1\boldsymbol{\Lambda}\delta\boldsymbol{R}_2 + \boldsymbol{R}_1\delta\boldsymbol{\Lambda}\boldsymbol{R}_2 + \delta\boldsymbol{R}_1\boldsymbol{\Lambda}\boldsymbol{R}_2 + \boldsymbol{R}_1\delta\boldsymbol{\Lambda}\delta\boldsymbol{R}_2 + \delta\boldsymbol{R}_1\boldsymbol{\Lambda}\delta\boldsymbol{R}_2 \\ & + \delta\boldsymbol{R}_1\delta\boldsymbol{\Lambda}\boldsymbol{R}_2 + \delta\boldsymbol{R}_1\delta\boldsymbol{\Lambda}\delta\boldsymbol{R}_2.\end{aligned}$$

Pre-multiplying this equation by $\boldsymbol{R}_1^{-1}$ and postmultiplying it by $\boldsymbol{R}_2^{-1}\boldsymbol{\Lambda}^{-1}$ gives

$$\begin{aligned}\delta\tilde{\boldsymbol{A}}_{n+1} = {} & \boldsymbol{\Lambda}\delta\boldsymbol{R}_2\boldsymbol{R}_2^{-1}\boldsymbol{\Lambda}^{-1} + \delta\boldsymbol{\Lambda}\boldsymbol{\Lambda}^{-1} + \boldsymbol{R}_1^{-1}\delta\boldsymbol{R}_1 + \delta\boldsymbol{\Lambda}\delta\boldsymbol{R}_2\boldsymbol{R}_2^{-1}\boldsymbol{\Lambda}^{-1} \\ & + \boldsymbol{R}_1^{-1}\delta\boldsymbol{R}_1\boldsymbol{\Lambda}\delta\boldsymbol{R}_2\boldsymbol{R}_2^{-1}\boldsymbol{\Lambda}^{-1} + \boldsymbol{R}_1^{-1}\delta\boldsymbol{R}_1\delta\boldsymbol{\Lambda}\boldsymbol{\Lambda}^{-1} + \boldsymbol{R}_1^{-1}\delta\boldsymbol{R}_1\delta\boldsymbol{\Lambda}\delta\boldsymbol{R}_2\boldsymbol{R}_2^{-1}\boldsymbol{\Lambda}^{-1}\end{aligned} \tag{5.2.6}$$

where

$$\delta\tilde{\boldsymbol{A}}_{n+1} \equiv {\boldsymbol{R}_1}^{-1}\delta\boldsymbol{A}_{n+1}\boldsymbol{R}_1\ . \tag{5.2.7}$$

Now, in terms of the increments in the singular values $\delta\lambda_1, \delta\lambda_2$, we have

$$\delta\boldsymbol{\Lambda}\boldsymbol{\Lambda}^{-1} = \begin{pmatrix} \frac{\delta\lambda_1}{\lambda_1} & 0 \\ 0 & \frac{\delta\lambda_2}{\lambda_2} \end{pmatrix} = \boldsymbol{\Lambda}^{-1}\delta\boldsymbol{\Lambda} \tag{5.2.8}$$

[6] In Chapter 6 we shall see that this is no longer true if $\boldsymbol{L}_0$ is a random matrix; then the value of the norm also depends on the rotation angle θ_2 and the initial configuration.

and, to second order in $\delta\theta_i$

$$\boldsymbol{R}_i^{-1}\delta\boldsymbol{R}_i = \begin{pmatrix} -\frac{\delta\theta_i^2}{2} & -\delta\theta_i \\ \delta\theta_i & -\frac{\delta\theta_i^2}{2} \end{pmatrix} = \delta\boldsymbol{R}_i\boldsymbol{R}_i^{-1},\ i = 1,2. \tag{5.2.9}$$

Therefore, to the second order of increments, equation (5.2.6) gives

$$\delta\widetilde{\boldsymbol{A}}_{n+1} = \begin{pmatrix} \frac{\delta\lambda_1}{\lambda_1} - \frac{1}{2}\left(\delta\theta_1^2 + \delta\theta_2^2\right) - \left(\frac{\lambda_2}{\lambda_1}\right)\delta\theta_1\delta\theta_2\ , & -\left(1 + \frac{\delta\lambda_2}{\lambda_2}\right)\delta\theta_1 - \left(\frac{\lambda_1}{\lambda_2}\right)\left(1 + \frac{\delta\lambda_1}{\lambda_1}\right)\delta\theta_2 \\ \left(1 + \frac{\delta\lambda_1}{\lambda_1}\right)\delta\theta_1 + \left(\frac{\lambda_2}{\lambda_1}\right)\left(1 + \frac{\delta\lambda_2}{\lambda_2}\right)\delta\theta_2\ , & \frac{\delta\lambda_2}{\lambda_2} - \frac{1}{2}\left(\delta\theta_1^2 + \delta\theta_2^2\right) - \left(\frac{\lambda_1}{\lambda_2}\right)\delta\theta_1\delta\theta_2 \end{pmatrix} \tag{5.2.10}$$

In the limit as $\delta t \to 0$ equation (5.2.10) reduces to a system of coupled stochastic differential equations for the singular values and rotation angles[7]:

$$\frac{\mathrm{d}\lambda_1}{\lambda_1} = \mathrm{d}\tilde{\mathrm{A}}_{11} + \frac{1}{2}\left[\mathrm{d}\theta_1^2 + 2\nu\mathrm{d}\theta_1\mathrm{d}\theta_2 + \mathrm{d}\theta_2^2\right] \tag{5.2.11a}$$

$$\frac{\mathrm{d}\lambda_2}{\lambda_2} = \mathrm{d}\tilde{\mathrm{A}}_{22} + \frac{1}{2}\left[\mathrm{d}\theta_1^2 + \left(\frac{2}{\nu}\right)\mathrm{d}\theta_1\mathrm{d}\theta_2 + \mathrm{d}\theta_2^2\right] \tag{5.2.11b}$$

$$\mathrm{d}\theta_1 = \frac{\nu\left(1 + \frac{\mathrm{d}\lambda_2}{\lambda_2}\right)\mathrm{d}\tilde{\mathrm{A}}_{12} + \frac{1}{\nu}\left(1 + \frac{\mathrm{d}\lambda_1}{\lambda_1}\right)\mathrm{d}\tilde{\mathrm{A}}_{21}}{\frac{1}{\nu}\left(1 + \frac{\mathrm{d}\lambda_1}{\lambda_1}\right)^2 - \nu\left(1 + \frac{\mathrm{d}\lambda_2}{\lambda_2}\right)^2} \tag{5.2.11c}$$

$$\mathrm{d}\theta_2 = -\frac{\left(1 + \frac{\mathrm{d}\lambda_1}{\lambda_1}\right)\mathrm{d}\tilde{\mathrm{A}}_{12} + \left(1 + \frac{\mathrm{d}\lambda_2}{\lambda_2}\right)\mathrm{d}\tilde{\mathrm{A}}_{21}}{\frac{1}{\nu}\left(1 + \frac{\mathrm{d}\lambda_1}{\lambda_1}\right)^2 - \nu\left(1 + \frac{\mathrm{d}\lambda_2}{\lambda_2}\right)^2} \tag{5.2.11d}$$

where $\nu \equiv \lambda_2/\lambda_1$. Note that this system of equations is symmetric under the interchange of λ_1 and λ_2 and involves the *relative* increments $\frac{\mathrm{d}\lambda_1}{\lambda_1}$ and $\frac{\mathrm{d}\lambda_2}{\lambda_2}$ which are unaffected by any *scaling* of the singular values. We therefore introduce logarithmic variables[8]

$$Z_i = -\ln\tilde{\lambda}_i = -\ln\left(\frac{\varepsilon_0}{\sqrt{2}}\lambda_i\right), \quad i = 1,2 \tag{5.2.12}$$

then

$$\mathrm{d}Z_i = -\frac{\mathrm{d}\tilde{\lambda}_i}{\tilde{\lambda}_i} + \frac{1}{2}\left(\frac{\mathrm{d}\tilde{\lambda}_i}{\tilde{\lambda}_i}\right)^2 = -\frac{\mathrm{d}\lambda_i}{\lambda_i} + \frac{1}{2}\left(\frac{\mathrm{d}\lambda_i}{\lambda_i}\right)^2,\ i = 1,2. \tag{5.2.13}$$

[7]For clarity we suppress the time index on the $\mathrm{d}\tilde{A}_{ij}$; the remaining subscripts denote the row and column position of the matrix element.

[8]We will be dealing with scaled singular values smaller than unity; the negative sign simply ensures that the Z_i are positive.

Then, using equations (5.2.11a) - (5.2.11d) and retaining only terms upto the second order in small increments, we obtain a system of stochastic differential equations for the increments of the Z_i and θ_i in terms of the matrix elements $d\tilde{A}_{ij}$. Writing

$$\alpha \equiv \frac{\nu}{(\nu^2-1)} \tag{5.2.14}$$

we have

$$dZ_1 = -d\tilde{A}_{11} + \frac{1}{2}d\tilde{A}_{11}^2 + \frac{\alpha}{2}\left[\nu d\tilde{A}_{12}^2 + 2\nu d\tilde{A}_{12}d\tilde{A}_{21} + \left(\frac{1}{\nu}\right)d\tilde{A}_{21}^2\right] \tag{5.2.15a}$$

$$dZ_2 = -d\tilde{A}_{22} + \frac{1}{2}d\tilde{A}_{22}^2 - \frac{\alpha}{2}\left[\nu d\tilde{A}_{12}^2 + \left(\frac{2}{\nu}\right)d\tilde{A}_{12}d\tilde{A}_{21} + \left(\frac{1}{\nu}\right)d\tilde{A}_{21}^2\right] \tag{5.2.15b}$$

and

$$\begin{aligned} d\theta_1 = &-\alpha\left[\nu d\tilde{A}_{12} + \left(\frac{1}{\nu}\right)d\tilde{A}_{21}\right] - \alpha^2 d\tilde{A}_{11}\left[2d\tilde{A}_{12} + \left(\frac{\nu^2+1}{\nu^2}\right)d\tilde{A}_{21}\right] \\ &+ \alpha^2 d\tilde{A}_{22}\left[2d\tilde{A}_{21} + (\nu^2+1)d\tilde{A}_{12}\right] \end{aligned} \tag{5.2.16a}$$

$$\begin{aligned} d\theta_2 = &\alpha\left[d\tilde{A}_{12} + d\tilde{A}_{21}\right] + \left(\frac{\alpha^2}{\nu}\right)d\tilde{A}_{11}\left[2d\tilde{A}_{12} + (\nu^2+1)d\tilde{A}_{21}\right] \\ &- \alpha^2 d\tilde{A}_{22}\left[2\nu d\tilde{A}_{12} + \left(\frac{\nu^2+1}{\nu}\right)d\tilde{A}_{21}\right]. \end{aligned} \tag{5.2.16b}$$

5.2.2 The related advection-diffusion problem

Equations (5.2.15a) - (5.2.16b) can now be used to produce a F.P. equation for the joint probability density of the variables, Z_1, Z_2, θ_1 and θ_2. Since the second order terms are in fact deterministic they are necessarily equal to their expected values[9]; we can therefore simplify the equations by replacing these terms with their expected values. Further, although at this stage there is nothing to distinguish between λ_1 and λ_2, we do expect that both λ_1 and λ_2 have non-zero and distinct Lyapunov exponents. Hence, with probability unity, either $\nu \to 0$ or $\nu \to \infty$ as $t \to \infty$ and whichever case occurs is random and equiprobable. We shall assume that symmetry breaks so that $\nu \to 0$ in the long time limit. In this limit $\frac{\alpha}{\nu} \to -1$ as

[9] See section 2.3.4

$\nu \to 0$, and we obtain the following system of Langevin equations:

$$\mathrm{d}Z_1 = -\mathrm{d}\tilde{\mathrm{A}}_{11} + \frac{1}{2}\left[\langle \mathrm{d}\tilde{\mathrm{A}}_{11}^2\rangle - \langle \mathrm{d}\tilde{\mathrm{A}}_{21}^2\rangle\right] \tag{5.2.17a}$$

$$\mathrm{d}Z_2 = -\mathrm{d}\tilde{\mathrm{A}}_{22} + \frac{1}{2}\left[\langle \mathrm{d}\tilde{\mathrm{A}}_{22}^2\rangle + 2\langle \mathrm{d}\tilde{\mathrm{A}}_{12}\mathrm{d}\tilde{\mathrm{A}}_{21}\rangle + \langle \mathrm{d}\tilde{\mathrm{A}}_{21}^2\rangle\right] \tag{5.2.17b}$$

$$\mathrm{d}\theta_1 = \mathrm{d}\tilde{\mathrm{A}}_{21} - \langle \mathrm{d}\tilde{\mathrm{A}}_{11}\mathrm{d}\tilde{\mathrm{A}}_{21}\rangle \tag{5.2.17c}$$

$$\mathrm{d}\theta_2 = 0. \tag{5.2.17d}$$

Note that θ_2 freezes as $t \to \infty$. This is to be expected because the direction along which the norm is most rapidly increasing is expected to approach a limit as $t \to \infty$.

The right hand sides of equations (5.2.17a) - (5.2.17d) are independent of the variables Z_1 and Z_2. Therefore at long times these quantities have a homogeneous diffusive evolution, with advection. The components of the drift velocity $\boldsymbol{v}$ and the elements of the diffusion tensor $\boldsymbol{D}$ are given by

$$v_i = \frac{\langle dZ_i\rangle}{\mathrm{d}t}\,, \quad D_{ij} = \frac{\langle dZ_i dZ_j\rangle}{2\mathrm{d}t}. \tag{5.2.18}$$

The joint p.d.f. of Z_1 and Z_2 at time t can therefore be determined using a Green's function

$$G(\boldsymbol{z}, \boldsymbol{z}_0, t) = \frac{1}{4\pi\sqrt{\det(\boldsymbol{D})t}} \exp\left[-S(\boldsymbol{\zeta}, t)\right] \tag{5.2.19}$$

where

$$S(\boldsymbol{\zeta}, t) = \frac{1}{4t}(\boldsymbol{\zeta} - \boldsymbol{v}t)\cdot\boldsymbol{D}^{-1}(\boldsymbol{\zeta} - \boldsymbol{v}t) \tag{5.2.20}$$

and $\boldsymbol{\zeta} \equiv \boldsymbol{z} - \boldsymbol{z}_0$. Because we have assumed that $\nu \to 0$, these equations are valid provided that $Z_2 - Z_1$ is sufficiently large[10].

The diffusive evolution in the Z_1Z_2 plane is represented schematically in figure (5.4), as the motion of an *ensemble of notional* particles. Initially, at time $t = 0$, and whenever the process $\boldsymbol{L}(t)$ is re-set the scaled singular values are $\tilde{\lambda}_1 = \tilde{\lambda}_2 = \varepsilon_0/\sqrt{2}$. Therefore the particle source, **S**, is the point $\left(-\ln\left(\varepsilon_0/\sqrt{2}\right), -\ln\left(\varepsilon_0/\sqrt{2}\right)\right)$. Also, since the singular values have been ordered so that $Z_2 \geq Z_1$ the line $Z_1 = Z_2$ is a *reflecting* boundary.

The figure shows three representative particle trajectories. The blue path shows a particle which is reflected at the boundary $Z_1 = Z_2$; the black path shows is that of a particle which

[10]The treatment of the case where $Z_2 - Z_1$ is small is considered in section 5.4.3, for the random flow model.

is absorbed at **A** and the green path shows a particle representing a process whose norm has become very small.

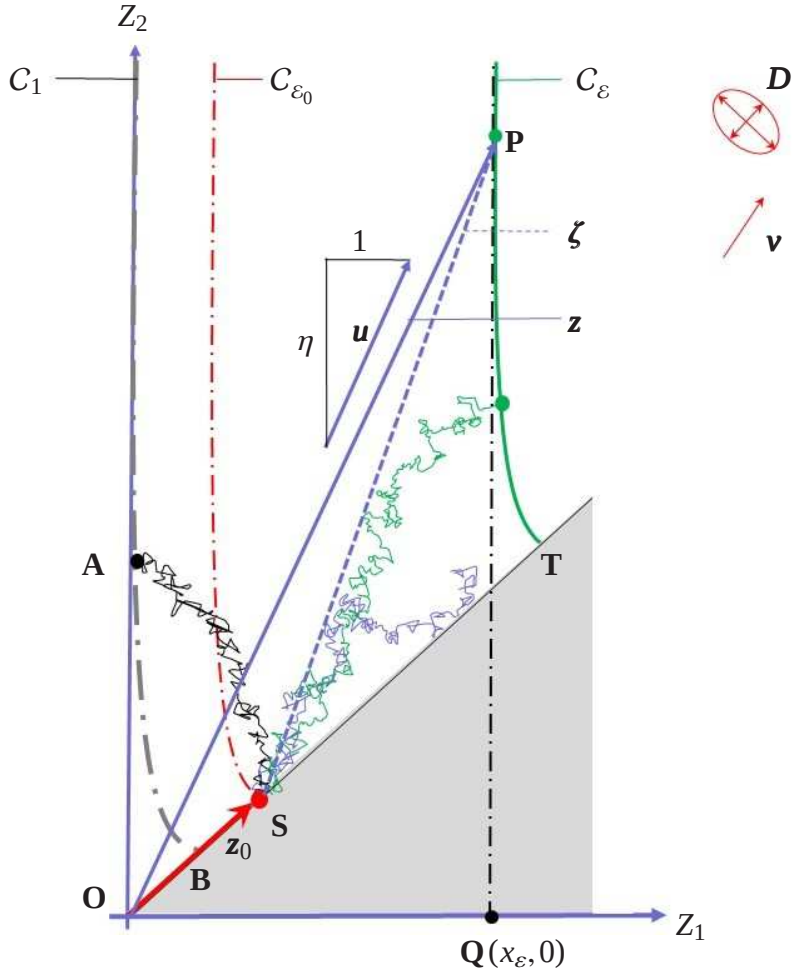

Fig. 5.4 The stochastic process $\boldsymbol{L}(t)$ is represented by an ensemble of particles undergoing advection and diffusion in a region of the Z_1Z_2 plane, with with drift velocity $\boldsymbol{v}$ and diffusion tensor $\boldsymbol{D}$. Each particle trajectory originates at the source $\boldsymbol{S}$ which has position vector $\boldsymbol{z}_0 = \left(\varepsilon_0/\sqrt{2}, \varepsilon_0/\sqrt{2}\right)$. The line $Z_1 = Z_2$ is a *reflecting* boundary. The figure shows three contours of the matrix norm $\mathcal{E}(\boldsymbol{L}) = \sqrt{\mathrm{tr}\left[\boldsymbol{L}^{\mathrm{T}}\boldsymbol{L}\right]}$. On C_1 the norm of the matrix process is unity: when a particle reaches C_1 at some point, e.g. **A**, it is absorbed and re-introduced at the source $\boldsymbol{S}$. Therefore C_1 is an *absorbing* boundary. Particles reaching the contour C_ε have norm $\mathcal{E}(\boldsymbol{L}) = \varepsilon$. The point $\boldsymbol{P}$ on C_ε has position vector $\boldsymbol{z}$; this can be written as a multiple of the direction vector $\boldsymbol{u} = [1, \eta]^{\mathrm{T}}$. If $\boldsymbol{P}$ is sufficiently far from the reflecting boundary then the vector $\overrightarrow{\boldsymbol{SP}} \equiv \boldsymbol{\zeta}$ is approximately equal to $\boldsymbol{z}$.

The curves $C_\varepsilon \equiv \left\{(z_1, z_2) : \exp(-2z_1) + \exp(-2z_2) = \varepsilon^2,\ \ z_2 \geq z_1 > 0,\ \varepsilon > 0\right\}$ are the contours of the matrix norm. On C_ε the matrix norm is $\mathcal{E}(\boldsymbol{L}) = \varepsilon$. Contour C_1 is an *absorbing* boundary: when a particle reaches C_1 at some point, e.g. **A**, the norm reaches unity and the process is reset to the value $\boldsymbol{L}_0$. In effect, the particle is removed at **A** and re-introduced at

the source, **S**. Since whenever a particle is absorbed a new particle is introduced at **S** we may take the source to have a constant, unit, strength. Note that the vertical asymptote to the contour C_ε intercepts the $\boldsymbol{Z}_1$ axis at point $\mathbf{Q}(x_\varepsilon, 0)$. This asymptote therefore has equation $Z_1 = -\ln\varepsilon \equiv x_\varepsilon$. In the physical region far from the reflecting boundary, i.e. for $Z_2 \gg Z_1$, the coordinates of any point, **P**, on the asymptote can be written in the form $(Z_1, Z_2) \approx x_\varepsilon \boldsymbol{u}$, where $\boldsymbol{u}$ is a direction vector of the form $\boldsymbol{u} = [1, \eta]^{\mathrm{T}}$, for some real parameter $\eta > 1$. We use this form for the coordinates of a point on the asymptote in the next section.

We shall refer to the wedge-like domain of the (Z_1, Z_2) plane

$$\{(z_1, z_2) \ : \ \exp(-2z_1) + \exp(-2z_2) < 1, \ z_2 > z_1 > 0\}$$

as the *physically accessible*, or physical, region. The process $\boldsymbol{L}(t)$ is therefore represented by an ensemble of notional particles which diffuse and drift in the physical region, being reflected at one edge, absorbed at the other and with the loss of particles by absorption on C_1 balanced by the injection of particles at $\boldsymbol{S}$.

5.3 Calculation of the p.d.f. $P_{\mathcal{E}}$

5.3.1 The non-degenerate case

Our objective is to understand $P_{\mathcal{E}}$, the p.d.f. of the norm $\mathcal{E}$ for the matrix contraction process when the norm is very small. In terms of the scaled singular values $\tilde{\lambda}_1, \tilde{\lambda}_2$ and the logarithmic variables Z_1, Z_2 the norm of the matrix $\boldsymbol{L}(t)$ is

$$\mathcal{E} = \sqrt{\tilde{\lambda}_1^2 + \tilde{\lambda}_2^2} = \sqrt{e^{-2Z_1} + e^{-2Z_2}} \ . \tag{5.3.1}$$

The p.d.f. of $\mathcal{E}$ may therefore be obtained from the probability of the diffusing particle to reach (z_1, z_2), i.e. from the joint p.d.f. of Z_1 and Z_2, $P_{\boldsymbol{Z}}(\boldsymbol{z}) = P_{(Z_1,Z_2)}(z_1, z_2)$.

To determine the p.d.f. $P_{\boldsymbol{Z}}(\boldsymbol{z})$ let $P(z_1, z_2, t, \tau)$ be the probability density for the point to be at (z_1, z_2) at time t after it is emitted from S *and* to be absorbed on contour C_1 at time $t + \tau$. Then $P_{\boldsymbol{Z}}(\boldsymbol{z})$ is obtained by integrating over the times:

$$P_{\boldsymbol{Z}}(\boldsymbol{z}) = \int_0^\infty \mathrm{d}t \int_0^\infty \mathrm{d}\tau \ P(z_1, z_2, t, \tau). \tag{5.3.2}$$

Because the diffusion process is Markovian we can write P as a product of two functions: $P(z_1,z_2,t,\tau) = G(z_1,z_2,t)P_{\mathrm{A}}(z_1,z_2,\tau)$ where $G(z_1,z_2,t)$ is the Green's function to reach (z_1,z_2) at time t and $P_{\mathrm{A}}(z_1,z_2,\tau)$ is the probability density for a particle released at (z_1,z_2) to be absorbed on C_1 after a time τ. From this definition of P_{A} we have

$$\int_0^\infty \mathrm{d}\tau\, P_{\mathrm{A}}(z_1,z_2,\tau) = 1 \tag{5.3.3}$$

so that

$$P_{\boldsymbol{Z}}(\boldsymbol{z}) = P_{(Z_1,Z_2)}(z_1,z_2) = \int_0^\infty \mathrm{d}t\, G(z_1,z_2,t)\,. \tag{5.3.4}$$

Strictly speaking $G(z_1,z_2,t)$ should be the Green's function for reaching (z_1,z_2) after time t by a path that does not cross the boundary C_1. However, since we are concerned with the case when $\mathcal{E}$ is very small and where $z_2 \gg z_1$ we require $P_{\boldsymbol{Z}}(\boldsymbol{z})$ for positions which are far from both the absorbing and the reflecting boundaries. We can therefore use equation (5.2.19) to approximate the Green's function $G(z_1,z_2,t)$. Also, far from the boundaries $\boldsymbol{\zeta} = \boldsymbol{z} - \boldsymbol{z}_0 \approx \boldsymbol{z}$ so that we can simply replace $\boldsymbol{\zeta}$ with $\boldsymbol{z}$.

We can use Laplace's method to approximate the value of the integral in equation (5.3.4). Using the results from Chapter 4 we find that

$$P_{\boldsymbol{Z}}(\boldsymbol{z}) \sim \frac{\exp[-\Psi(\boldsymbol{z})]}{\left(\boldsymbol{z}\cdot\boldsymbol{D}^{-1}\boldsymbol{z}\right)^{\frac{1}{4}}} \tag{5.3.5}$$

where

$$\Psi(\boldsymbol{z}) \equiv \frac{1}{2}\left[\sqrt{\boldsymbol{\nu}\cdot\boldsymbol{D}^{-1}\boldsymbol{\nu}}\sqrt{\boldsymbol{z}\cdot\boldsymbol{D}^{-1}\boldsymbol{z}} - \boldsymbol{z}\cdot\boldsymbol{D}^{-1}\boldsymbol{\nu}\right]. \tag{5.3.6}$$

The interpretation of this form of exponent, as the height of a tilted cone, was discussed in section (3.4).

Since the contour C_ε is asymptotic to the vertical line $Z_1 = -\ln\varepsilon \equiv x_\varepsilon$, then for $Z_2 \gg Z_1$ the probability density for the norm to reach the value ε can be estimated from $P_{X_\mathcal{E}}(x_\varepsilon)$, the p.d.f. for the random variable $X_\mathcal{E} = -\ln\mathcal{E}$. This can be estimated using the expression (5.3.5) on the segment of the asymptote lying in the physical region, i.e. above the line $z_1 = z_2$:

$$P_{X_\varepsilon}(x_\varepsilon) \approx \int_{z_2\approx x_\varepsilon}^\infty \mathrm{d}z_2 P_{\boldsymbol{Z}}(\boldsymbol{z}) \tag{5.3.7}$$

Now, on the asymptote to the contour C_ε we have $\boldsymbol{z} = x_\varepsilon \boldsymbol{u}$ where $\boldsymbol{u} = [1,\eta]^{\mathrm{T}}$ with $\eta \geq 1$. Therefore, on this asymptote

$$P_{\boldsymbol{Z}}(\boldsymbol{z}) = P_{\boldsymbol{Z}}(x_\varepsilon \boldsymbol{u}) \approx \frac{\exp[-x_\varepsilon \Psi(\boldsymbol{u})]}{\left[x_\varepsilon^2 \left(\boldsymbol{u}\cdot\boldsymbol{D}^{-1}\boldsymbol{u}\right)\right]^{\frac{1}{4}}} = \frac{\exp[-x_\varepsilon f(\eta)]}{\left[x_\varepsilon^2 q(\eta)\right]^{\frac{1}{4}}} \tag{5.3.8}$$

where $f(\eta) \equiv \sqrt{\boldsymbol{v}\cdot\boldsymbol{D}^{-1}\boldsymbol{v}}\,\sqrt{q(\eta)} - \ell(\eta)$, with $q(\eta) \equiv \left(\boldsymbol{u}\cdot\boldsymbol{D}^{-1}\boldsymbol{u}\right)$ and $\ell(\eta) \equiv \boldsymbol{u}\cdot\boldsymbol{D}^{-1}\boldsymbol{v}$. Note that $q(\eta)$ is a quadratic function of η and $\ell(\eta)$ is a linear function η. Hence

$$P_{X_\varepsilon}(x_\varepsilon) = \sqrt{x_\varepsilon}\int_1^\infty \mathrm{d}\eta \frac{\exp(-x_\varepsilon f(\eta))}{[q(\eta)]^{\frac{1}{4}}}. \tag{5.3.9}$$

The p.d.f. P_{X_ε} is obtained by applying Laplace's principle again. Suppose that, on the asymptote, $\Psi(\boldsymbol{z})$ has a minimum at some point $\boldsymbol{z}^*$ lying in the physical region $z_2 > z_1$. Then, since $\Psi(\boldsymbol{z})$ increases linearly along any ray from the origin, this critical point lies on the ray with direction vector $\boldsymbol{u}^* = [1,\eta^*]$, where $f\,'(\eta^*) = 0$, with $\eta^* > 1$. Since $\boldsymbol{z}^* = x_\varepsilon \boldsymbol{u}^*$, the p.d.f. of X_ε is therefore of the form

$$P_{X_\varepsilon}(x_\varepsilon) \sim \frac{\sqrt{x_\varepsilon}}{[q(\eta^*)]^{\frac{1}{4}}} \exp[-x_\varepsilon \Psi(\boldsymbol{u}^*)] \int_{-\infty}^{\infty} \mathrm{d}\eta \exp\left[-\frac{1}{2} x_\varepsilon f\,''(\eta^*)(\eta-\eta^*)^2\right]. \tag{5.3.10}$$

The Gaussian integral is equal to $\sqrt{\dfrac{2\pi}{x_\varepsilon f\,''(\eta^*)}}$, and therefore

$$P_{X_\varepsilon}(x_\varepsilon) \sim \exp[-x_\varepsilon \Psi(\boldsymbol{u}^*)] \tag{5.3.11}$$

Since $x_\varepsilon \equiv -\ln\varepsilon$ this is consistent with $P_{\mathcal{E}}(\varepsilon)$ having a power-law distribution, with exponent

$$\gamma = [\Psi(\boldsymbol{u}^*) - 1]\,. \tag{5.3.12}$$

In section (5.4) we shall estimate this exponent for the random flow model.

5.3.2 The degenerate case

In the discussion in section (5.3.1) we assumed that the critical point, $\boldsymbol{z}^*$, lies in the physical region, i.e. above the reflecting boundary line $z_1 = z_2$, so that $\eta^* > 1$. We shall refer to this case as the *non-degenerate case*. However, the minimum of $\Psi(z_1,z_2)$ along a line of constant z_1 may occur at a point outside the physical region, i.e. one for which $z_2 \leq z_1$ or, equivalently,

$\eta^* \leq 1$. In this case, which we shall refer to as the *degenerate* case, we must consider what happens in the neighbourhood of the boundary point $\boldsymbol{z} = (x_\varepsilon, x_\varepsilon)$.

Coordinate transformation

It is advantageous to work in a coordinate system in which the reflecting boundary lies along a coordinate axis. We therefore introduce the $x_1 x_2$ coordinate system defined by

$$x_1 = (z_1 + z_2) \text{ and } \mathrm{x}_2 = (\mathrm{z}_2 - \mathrm{z}_1).$$

Note that the new system is rotated through $\pi/4$ with respect to the old system and is re-scaled. This coordinate transformation is equivalent to describing the process in terms of the random variables $X_1 = Z_1 + Z_2$ and $X_2 = Z_2 - Z_1$.

From equations (5.2.2) it follows that the diffusion tensor $\boldsymbol{D}$ is represented by a symmetric 2×2 matrix. Therefore *provided* that the diagonal elements of the matrix are equal, i.e. provided that $\langle \mathrm{dA}_{11}^2 \rangle = \langle \mathrm{dA}_{22}^2 \rangle$, then in the new coordinate system the tensor will be represented by a *diagonal* matrix. This greatly simplifies the analysis and in the following arguments we assume that this condition holds; in subsection (5.4) we will see it holds for the random flow model[11].

The representation of the advection-diffusion process in the $x_1 x_2$ coordinate system, i.e. the advection-diffusion process for X_1 and X_2, is shown in figure (5.5).

In the new coordinates the particle source is located at the point $\boldsymbol{S}\left(\ln\left(2/\varepsilon_0^2\right), 0)\right)$. The x_1-axis is the reflecting barrier and the contour C_ε and the asymptote $z_1 = -\ln\varepsilon$ have equations

$$x_1 = \ln\left(\frac{2\cosh x_2}{\varepsilon^2}\right) \quad \text{and} \quad \mathrm{x}_2 = \mathrm{x}_1 + 2\ln\varepsilon$$

respectively. Contour C_ε intercepts the x_1 axis at the point $\mathbf{T}\left(\ln\left(2/\varepsilon^2\right), 0\right)$ and its asymptote intercepts the x_1 and x_2 axes at points $\mathbf{Q}'(2\ln(1/\varepsilon), 0)$ and $\mathbf{R}(0, 2\ln\varepsilon)$, respectively. The absorbing boundary, i.e. contour C_1, has equation $x_1 = \ln(2\cosh(x_2))$ and intercepts the x_1 axis at the point $\mathbf{B}(\ln 2, 0)$. The asymptote to the absorbing boundary is the line $x_2 = x_1$. A particle is absorbed at point $\boldsymbol{A}$ and the particle at point $\boldsymbol{P}$ represents a matrix whose norm has reached a very small value.

[11] However we do note that the condition does not hold in general and, consequently, that the discussion in this section is therefore specific to the class of models for which its true.

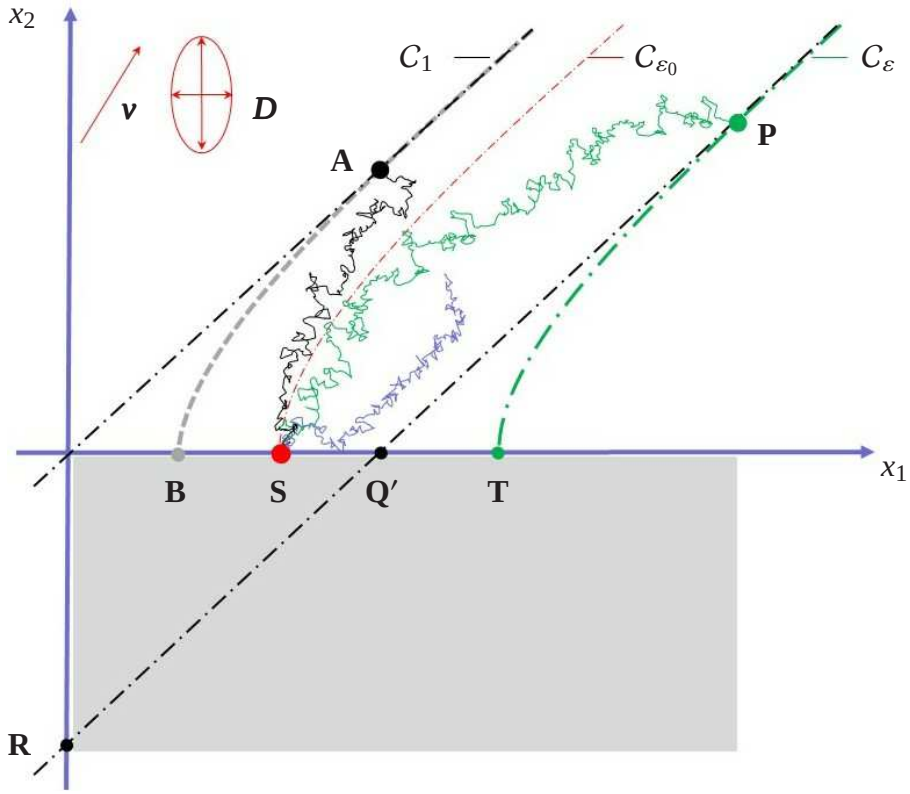

Fig. 5.5 In the x_1x_2 coordinates the stochastic process $\boldsymbol{L}(t)$ is represented by an ensemble of points undergoing advection and diffusion, with drift velocity $\boldsymbol{v}$ and diffusion tensor $\boldsymbol{D}$, where $\boldsymbol{D}$ is diagonal. The X_1-axis is a *reflecting* boundary and on the *absorbing* boundary, C_1, the norm of the matrix process is unity. C_1 is asymptotic to the line $x_2 = x_1$. [c.f. figure (5.4)]

The equations of motion, (5.2.17a), (5.2.17b) transform into

$$\mathrm{d}X_1 = -\left(\mathrm{d}\tilde{A}_{11} + \mathrm{d}\tilde{A}_{22}\right) + \frac{1}{2}\left(\langle \mathrm{d}\tilde{A}_{11}^2\rangle + 2\langle \mathrm{d}\tilde{A}_{12}\mathrm{d}\tilde{A}_{21}\rangle + \langle \mathrm{d}\tilde{A}_{22}^2\rangle\right) \tag{5.3.13a}$$

$$\begin{aligned}\mathrm{d}X_2 = &\left(\mathrm{d}\tilde{A}_{11} - \mathrm{d}\tilde{A}_{22}\right) + \frac{1}{2}\left(\langle \mathrm{d}\tilde{A}_{22}^2\rangle - \langle \mathrm{d}\tilde{A}_{11}^2\rangle\right)\\ &+\left(\frac{1}{1-\nu^2}\right)\left[\nu^2\langle \mathrm{d}\tilde{A}_{12}^2\rangle + \left(1+\nu^2\right)\langle \mathrm{d}\tilde{A}_{12}\mathrm{d}\tilde{A}_{21}\rangle + \langle \mathrm{d}\tilde{A}_{21}^2\rangle\right]\end{aligned} \tag{5.3.13b}$$

From these it follows that the drift velocity in the x_1 direction, v_1, is a constant and the drift velocity in the x_2 direction, v_2, is a function of $\nu = \exp(-x_2)$ and therefore of x_2. Also, the diffusion tensor for the fluctuations of X_1 and X_2 is diagonal, with diffusion coefficients $D_{11} \equiv D_1$, $D_{22} \equiv D_2$, which are independent of x_1 and x_2.

Therefore the dynamics in the x_1 direction is simple: diffusion with a constant drift velocity. The dynamics in the x_2 direction is more complex: diffusion with a drift velocity which is a function of x. We note that since $\nu \equiv \frac{\lambda_2}{\lambda_1} = \exp(-x_2)$ then as $x_2 \to \infty$, $\nu \to 0$ and as $x_2 \to 0$

$$v_2 \to \frac{1}{\mathrm{d}t}\left[\frac{1}{2}\left(\langle \mathrm{d}\tilde{\mathrm{A}}_{22}^2\rangle - \langle \mathrm{d}\tilde{\mathrm{A}}_{11}^2\rangle\right) + \langle \mathrm{d}\tilde{A}_{12}\mathrm{d}\tilde{A}_{21}\rangle + \langle \mathrm{d}\tilde{A}_{21}^2\rangle\right] \equiv v_0$$

where v_0 is a constant. Also, for any given value of x_1 then as $x_2 \to x_1$, $\lambda_2 \to \lambda_1$ so that $\nu \to 1$ and, therefore, $v_2 \to \infty$, corresponding to the reflection of the particle at the boundary $x_2 = x_1$.

To calculate $P_{\mathcal{E}}$ for the degenerate case we require the propagator for the representative particle to reach points on the contour C_ε, *near the reflecting boundary*[12]. Since the motions in the x_1 and x_2 directions are independent this propagator can be written as the product:

$$G(\boldsymbol{x}, t) = G(x_1, x_2, t) = P_{X_1}(x_1, t)P_{X_2}(x_2, t)\,. \tag{5.3.14}$$

where $P_{X_1}(x_1, t)$ is the p.d.f. for the motion in the x_1 direction, i.e. for the random variable X_1 to have the value x_1 at time t, and similarly for $P_{X_2}(x_2, t)$.

Since the motion in the x_1 direction is a simple advection-diffusion process, with drift velocity v_1 and diffusion coefficient D_1 we have

$$\begin{aligned} P_{X_1}(x_1, t) &= \frac{1}{\sqrt{4\pi D_1 t}}\exp\left[-\frac{(x_1 - v_1 t)^2}{4D_1 t}\right] \\ &= \frac{1}{\sqrt{4\pi D_1}}\left(\frac{1}{\sqrt{t}}\right)\exp\left[\frac{v_1 x_1}{2D_1}\right]\exp\left[-\frac{1}{4D_1}\left(\frac{x_1^2}{t} + v_1^2 t\right)\right]\,. \end{aligned} \tag{5.3.15}$$

To calculate the probability density $P_{X_2}(x_2, t)$, we must take account of the fact that $x_2 = 0$ is a reflecting barrier. The approach is outlined in the following section.

One-dimensional diffusion with reflecting boundary

Suppose that at some time, which we shall take to be $t = 0$, the particle is at some position $x_2 = x_0$, where x_0 very small. We wish to determine the distribution P_{X_2} at later times; P_{X_2}

[12] That is, to reach points on the curve $x_1 = \ln\left(\frac{2\cosh x_2}{\varepsilon^2}\right)$ in the neighbourhood of $(x_\varepsilon, x_\varepsilon)$

satisfies

$$\frac{\partial P_{X_2}}{\partial t} = D_2 \frac{\partial^2 P_{X_2}}{\partial x_2^2} - \frac{\partial}{\partial x_2}\left[v_2(x_2) P_{X_2}\right] . \tag{5.3.16}$$

This equation can be transformed to a Hermitian form by writing

$$P_X(x_2) = \psi(x_2,t)\exp\left[\chi(x_2)\right] , \tag{5.3.17}$$

where

$$\chi(x_2) = \frac{1}{2D_2}\int^{x_2} \mathrm{d}x_2'\; v_2\left(x_2'\right). \tag{5.3.18}$$

The function $\psi(x_2,t)$ satisfies a Schrödinger-like equation, with a Hermitian operator $\hat{\mathcal{H}}$:

$$\hat{\mathcal{H}}\psi \equiv -D_2\frac{\partial^2\psi}{\partial x_2^2} + V(x_2)\psi = -\frac{\partial\psi}{\partial t} \tag{5.3.19}$$

where

$$V(x_2) = \frac{1}{2}v_2'(x_2) + \frac{[v_2(x_2)]^2}{4D_2} . \tag{5.3.20}$$

Now, by introducing a nominal absorbing barrier at $x_2 = L$ we can develop the solution to equation (5.3.16) in the finite interval [0,L] as an infinite series of orthonormal eigenfunctions of the Hermitian operator $\hat{\mathcal{H}}$; we can then choose L sufficiently large that its value may be assumed to have no influence. The details of this approach may be found in section (7.1) of [30], we merely quote the result:

$$P_{X_2}(x_2,t) = \frac{2}{L}\exp\left[\frac{v_0(x_2-x_0)}{2D_1} - \frac{v_0^2 t}{4D_2}\right]\times\sum_{n=1}^{\infty}\exp\left(-\frac{n^2\pi^2 D_2 t}{L^2}\right)\sin\left(\frac{n\pi x_2}{L}\right)\sin\left(\frac{n\pi x_0}{L}\right) .$$

Approximating the sum by an integral gives

$$P_{X_2}(x_2,t) = \frac{1}{L}\exp\left[\frac{v_0(x_2-x_0)}{2D_2} - \frac{v_0^2 t}{4D_2}\right]\times\int_0^{\infty}\mathrm{d}n\;\exp\left[\frac{n^2\pi^2 D_2 t}{L^2}\right]\times \left[\cos\left(\frac{n\pi(x_2-x_0)}{L}\right) - \cos\left(\frac{n\pi(x_2+x_0)}{L}\right)\right]$$

and using the standard integral

$$\int_{-\infty}^{\infty}\mathrm{d}x\;\exp(-\alpha x^2)\cos(kx) = \sqrt{\frac{\pi}{\alpha}}\exp\left(\frac{-k^2\alpha}{4}\right)$$

we obtain the solution

$$P_{X_2}(x_2,t) = \frac{1}{\sqrt{4\pi D_2 t}} \exp\left[\frac{v_0(x_2-x_0)}{2D_2} - \frac{v_0^2 t}{4D_2}\right]\left[\exp\left(-\frac{(x_2-x_0)^2}{4D_2 t}\right) - \exp\left(-\frac{(x_2+x_0)^2}{4D_2 t}\right)\right].$$

For x_0 very small this gives

$$P_{X_2}(x_2,t) \sim \frac{x_0}{\sqrt{4\pi D_2^3}}\left(\frac{1}{t^{3/2}}\right)\left[x_2 \exp\left(\frac{v_0 x_2}{2D_2}\right)\right]\exp\left[-\left(\frac{x_2^2}{4D_2 t} + \frac{v_0^2 t}{4D_2}\right)\right]. \tag{5.3.21}$$

Implications for degenerate case

Substituting equations (5.3.15) and (5.3.21) into equation (5.3.14) gives, omitting factors which are independent of position and time[13]

$$G(\boldsymbol{x},t) \sim \frac{1}{t^2}\, f(\boldsymbol{x})\, \exp[-g(\boldsymbol{x},t)] \tag{5.3.22}$$

where

$$f(\boldsymbol{x}) \equiv x_2 \exp\left[\frac{1}{2}\boldsymbol{x}\cdot\boldsymbol{D}^{-1}\boldsymbol{v}\right] \tag{5.3.23}$$

and

$$g(\boldsymbol{x},t) \equiv \left[a(\boldsymbol{v})t + \frac{b(\boldsymbol{x})}{t}\right] \tag{5.3.24}$$

with

$$a(\boldsymbol{v}) \equiv \frac{\boldsymbol{v}\cdot\boldsymbol{D}^{-1}\boldsymbol{v}}{4} = \frac{1}{4}\left(\frac{v_1^2}{D_1} + \frac{v_0^2}{D_2}\right) \quad \text{and} \quad \mathrm{b}(\boldsymbol{x}) \equiv \frac{\boldsymbol{x}\cdot\boldsymbol{D}^{-1}\boldsymbol{x}}{4} = \frac{1}{4}\left(\frac{\mathrm{x}_1^2}{\mathrm{D}_1} + \frac{\mathrm{x}_2^2}{\mathrm{D}_2}\right). \tag{5.3.25}$$

Therefore

$$P_{\boldsymbol{X}}(\boldsymbol{x}) = \int_0^\infty \mathrm{d}t\, G(\boldsymbol{x},t) \sim f(\boldsymbol{x}) \int_0^\infty \mathrm{d}t\, \frac{1}{t^2}\, \exp[-g(\boldsymbol{x},t)] \equiv f(\boldsymbol{x})\, I(\boldsymbol{x}). \tag{5.3.26}$$

We wish to determine the behaviour of $P_{\mathcal{E}}(\varepsilon)$, for small ε, from that of $P_{\boldsymbol{X}}(\boldsymbol{x})$. When ε is small we are dealing with points far from the source and, therefore, $|\boldsymbol{x}|$ must be large. We can therefore determine the leading order behaviour of $P_{\boldsymbol{X}}(\boldsymbol{x})$ by using Laplace's method to

[13] These factors are unimportant to our argument and can, in effect, be absorbed into normalization coefficients.

evaluate the integral. This gives $I(\boldsymbol{x}) \sim (b(\boldsymbol{x}))^{-3/4}\ \exp\left[-2\sqrt{a(\boldsymbol{v})}\sqrt{b(\boldsymbol{x})}\right]$ so that

$$P_{\boldsymbol{X}}(\boldsymbol{x}) \sim \frac{f(\boldsymbol{x})}{[b(\boldsymbol{x})]^{3/4}} \times \exp\left[-2\sqrt{a(\boldsymbol{v})}\sqrt{b(\boldsymbol{x})}\right] = \frac{x_2 \exp[-\Psi(\boldsymbol{x})]}{(\boldsymbol{x}\cdot\boldsymbol{D}\boldsymbol{x})^{3/4}} \tag{5.3.27}$$

where $\Psi(\boldsymbol{x})$ is given by equation (5.3.6). Now, to determine the p.d.f. $P_{\mathcal{E}}(\varepsilon)$ from $P_{\boldsymbol{X}}(\boldsymbol{x})$ we note that, at the point $\boldsymbol{x} = (x_1, x_2)$, the norm ε is given by

$$-\ln\varepsilon = \frac{1}{2}[x_1 - \ln(2\cosh x_2)] \equiv h(x_1, x_2). \tag{5.3.28}$$

We therefore introduce the random variable $X_\varepsilon \equiv h(\boldsymbol{X}) = -\ln\mathcal{E}$, where $\boldsymbol{X} = (X_1, X_2)$ and use the p.d.f. of this variable to compute $P_{\mathcal{E}}$. To first obtain P_{X_ε} we use the standard result that, since $X_\varepsilon \equiv h(\boldsymbol{X})$ and since $\boldsymbol{X}$ has p.d.f. $P_{\boldsymbol{X}}(\boldsymbol{x})$, we have

$$P_{X_\varepsilon}(x_\varepsilon) = \langle\ \delta(X_\varepsilon - h(\boldsymbol{X}))\ \rangle\ = \int_0^\infty \mathrm{d}x_2 \int_0^\infty \mathrm{d}x_1\ \delta(x_\varepsilon - h(\boldsymbol{x}))\, P_{\boldsymbol{X}}(\boldsymbol{x}). \tag{5.3.29}$$

Hence

$$\begin{aligned} P_{X_\varepsilon}(x_\varepsilon) &= \int_0^\infty \mathrm{d}x_2 \int_0^\infty \mathrm{d}x_1\ \delta\left(x_\varepsilon - \frac{1}{2}[\ x_1 - \ln(2\cosh x_2)\ ]\right)\ P_{\boldsymbol{X}}(\boldsymbol{x}) \\ &= 2\int_0^\infty \mathrm{d}x_2 \int_0^\infty \mathrm{d}x_1\ \delta(2x_\varepsilon + \ln(2\cosh x_2) - x_1)\ P_{\boldsymbol{X}}(\boldsymbol{x})\ . \end{aligned}$$

The sifting property of the delta function selects the value $x_1 = 2x_\varepsilon + \ln(2\cosh x_2)$ in the first integral, giving

$$P_{X_\varepsilon}(x_\varepsilon) = 2\int_0^\infty \mathrm{d}x_2\ P_{\boldsymbol{X}}(\ 2x_\varepsilon + \ln(2\cosh\ x_2),\ x_2\ ) \tag{5.3.30}$$

and writing, for brevity, $\boldsymbol{w} = \boldsymbol{w}(x_\varepsilon, x_2) = (w_1, w_2) \equiv (\ 2x_\varepsilon + \ln\,(2\cosh\ x_2),\ x_2\ )$, using equation (5.3.27) we have

$$P_{X_\varepsilon}(x_\varepsilon) = 2\int_0^\infty \mathrm{d}x_2\ P_{\boldsymbol{X}}(\boldsymbol{w})\ \sim \int_0^\infty \mathrm{d}x_2\ \frac{f(\boldsymbol{w})}{[b(\boldsymbol{w})]^{3/4}} \times \exp\left[-2\sqrt{a(\boldsymbol{v})}\sqrt{b(\boldsymbol{w})}\right] \tag{5.3.31}$$

Now,

$$f(\boldsymbol{w}) = x_2 \exp\left[\frac{v_1 x_\varepsilon}{D_1}\right] \times\ \exp\left[\left(\frac{v_1}{2D_1}\right)\ln(2\cosh x_2) + \left(\frac{v_0}{2D_2}\right)x_2\right] \tag{5.3.32}$$

and

$$b(\boldsymbol{w}) = \frac{x_\varepsilon^2}{D_1}\left[1 + \frac{\ln(2\cosh\ x_2)}{x_\varepsilon} + O\left(\frac{1}{x_\varepsilon^2}\right)\right]$$

so, to leading order as $x_\varepsilon \to \infty$, we have

$$P_{X_\varepsilon}(x_\varepsilon) \sim \frac{J}{x_\varepsilon^{3/2}} \exp[-Kx_\varepsilon] \tag{5.3.33}$$

where

$$K \equiv \sqrt{\frac{v_1^2}{D_1^2} + \frac{v_0^2}{D_1 D_2}} - \frac{v_1}{D_1} \tag{5.3.34}$$

and where the integral J is given by

$$J \equiv \int_0^\infty \mathrm{d}x_2 x_2 \exp\left[-\frac{1}{2}\left(K \ln(2\cosh x_2) - \frac{v_0 x_2}{D_2}\right)\right]. \tag{5.3.35}$$

Now, since $\ln(2\cosh x_2) \approx x_2$ when x_2 is large, the integral J converges provided that

$$K - \frac{v_0}{D_2} > 0. \tag{5.3.36}$$

This convergence criterion is a *degeneracy* condition because, in the (x_1, x_2) coordinates, $\Psi(x_1, x_2)$ has the form

$$\Psi(x_1, x_2) = \frac{1}{2}\left[\sqrt{\frac{v_1^2}{D_1} + \frac{v_0^2}{D_2}}\sqrt{\frac{x_1^2}{D_1} + \frac{x_2^2}{D_2}} - \left(\frac{v_1 x_1}{D_1} + \frac{v_0 x_2}{D_2}\right)\right] \tag{5.3.37}$$

and requiring that the stationary point of $\Psi(x_1, x_2)$ on the line $x_2 = x_1 + 2\ln\varepsilon$ is degenerate, and therefore lies at a negative value of x_2, gives (5.3.36).

Therefore in the degenerate case the asymptotic behaviour of P_{X_ε} is

$$P_{X_\varepsilon}(x_\varepsilon) \sim \frac{1}{x_\varepsilon^{3/2}} \exp[-Kx_\varepsilon] \tag{5.3.38}$$

and, using the change of variable rule, we have

$$P_{\mathcal{E}}(\varepsilon) \sim \frac{\varepsilon^\gamma}{\left[\ln\left(\frac{1}{\varepsilon}\right)\right]^\mu} \tag{5.3.39}$$

with $\gamma = K - 1$ and $\mu = 3/2$.

5.4 Application to the turbulent flow model

5.4.1 Description of the model

As a specific example we consider the matrix representing the differential of the random flow, $\boldsymbol{u}$, defined by equation (2.4.1). For this flow the elements of the matrix $\delta\boldsymbol{A}$, in equations (5.2.1), (5.2.2) and (3.3.3), are random variables constructed from the second derivatives of the field potentials:

$$\delta\boldsymbol{A}(t) = \left[A_{ij}\right]\sqrt{\delta t} = \left[\frac{\partial u_i}{\partial x_j}\right]\sqrt{\delta t} = \begin{pmatrix} \beta\phi_{x_1x_1} + \psi_{x_2x_1}, & \beta\phi_{x_1x_2} + \psi_{x_2x_2} \\ \beta\phi_{x_2x_1} - \psi_{x_1x_1}, & \beta\phi_{x_2x_2} - \psi_{x_1x_2} \end{pmatrix}\sqrt{\delta t}. \tag{5.4.1}$$

The field derivatives have mean value zero and their non-zero covariances are

$$\left\langle \phi^2_{x_1x_1} \right\rangle = \left\langle \phi^2_{x_2x_2} \right\rangle = 3, \quad \left\langle \phi_{x_1x_1}\phi_{x_2x_2} \right\rangle = \left\langle \phi^2_{x_1x_2} \right\rangle = 1, \tag{5.4.2}$$

and similarly for ψ. The non-zero components of the diffusion tensor in equation (5.2.2) are

$$\mathcal{D}_{1111} = \mathcal{D}_{2222} = \frac{1}{2}\left(1 + 3\beta^2\right) \tag{5.4.3a}$$

$$\mathcal{D}_{1212} = \mathcal{D}_{2121} = \frac{1}{2}\left(3 + \beta^2\right) \tag{5.4.3b}$$

$$\mathcal{D}_{1122} = \mathcal{D}_{1221} = \frac{1}{2}\left(\beta^2 - 1\right). \tag{5.4.3c}$$

Since the model is rotationally invariant, and since the $\mathrm{d}\tilde{\boldsymbol{A}}_n$ defined by equation (5.2.7) is a rotational transformation of $\mathrm{d}\boldsymbol{A}_n$ the elements of $\mathrm{d}\tilde{\boldsymbol{A}}_n$ have the same statistics as those of $\mathrm{d}\boldsymbol{A}_n$.

Therefore, from equations (5.2.17a), (5.2.17b) and (5.2.18), it follows that, for this model the drift velocity and diffusion tensor are, respectively:

$$\boldsymbol{v} = \begin{pmatrix} \beta^2 - 1 \\ 1 + 3\beta^2 \end{pmatrix} \qquad \boldsymbol{D} = \frac{1}{2}\begin{pmatrix} 1 + 3\beta^2, & \beta^2 - 1 \\ \beta^2 - 1, & 1 + 3\beta^2 \end{pmatrix}. \tag{5.4.4}$$

Introducing

$$a = 1 + 3\beta^2, \quad b = \beta^2 - 1 \quad \text{and} \quad \mathrm{c} = \sqrt{\frac{a}{a^2 - b^2}}$$

to simplify the algebra[14], we find from equation (5.3.6) that the large deviation rate function $\Psi(z_1, z_2)$ is given by

$$\Psi(z_1, z_2) = c\sqrt{a\left(z_1^2 + z_2^2\right) - 2bz_1z_2} - z_2 \tag{5.4.5}$$

which written in full is

$$\Psi(z_1, z_2) = \frac{1}{2\beta}\sqrt{\frac{1+3\beta^2}{2(1+\beta^2)}}\sqrt{(1+3\beta^2)(z_1^2+z_2^2) - 2(\beta^2-1)z_1z_2} - z_2\ . \tag{5.4.6}$$

5.4.2 The exponent γ for the turbulent flow model

In section (5.3.1) we showed that, in the nondegenerate case, the p.d.f. $P_{\mathcal{E}}(\varepsilon)$ is given by equation (5.3.12) with $\boldsymbol{u}^* \equiv [1, \eta^*]^{\mathrm{T}}$ where $\eta^* > 1$ is a critical point of the function $f(\eta) \equiv \Psi(1, \eta)$.

For the turbulent flow model, from equation (5.4.5) we have

$$f(\eta) = c\sqrt{a(1+\eta^2) - 2b\eta} - \eta\ . \tag{5.4.7}$$

then $f'(\eta^*) = 0$ gives the quadratic $\eta^{*2} - 2\left(\frac{b}{a}\right)\eta^* + 2 - \left(\frac{a}{b}\right)^2 = 0$ and selecting the positive root, gives

$$\eta^* = 2\left(\frac{b}{a}\right) - \left(\frac{a}{b}\right) = \frac{7\beta^4 + 10\beta^2 - 1}{(1+3\beta^2)(1-\beta^2)}\ . \tag{5.4.8}$$

Then, noting that

$$(\eta^* - 1) = \frac{2(1+\beta^2)(5\beta^2-1)}{(1+3\beta^2)(1-\beta^2)} \tag{5.4.9}$$

we see that if $1 > \beta > 1/\sqrt{5}$ then $\eta^* > 1$ and the critical point is non-degenerate, but if $0 \le \beta < 1/\sqrt{5}$ then $0 < \eta^* < 1$ and the critical point is degenerate.

[14]Note that these are not the same variables as the a and b introduced in section (5.3.2).

In the non-degenerate case, we find that[15]

$$\Psi(\boldsymbol{u}^*) = f(\eta^*) = 2\frac{(1-\beta^2)}{(1+3\beta^2)}$$

so that, from equation (5.3.12),

$$\gamma = \frac{2(1-\beta^2)}{(1+3\beta^2)} - 1 = \frac{\left(1-5\beta^2\right)}{(1+3\beta^2)}\,. \tag{5.4.10}$$

In the degenerate case, setting $\eta^* = 1$ gives

$$\Psi(\boldsymbol{u}^*) = f(1) = \sqrt{(1+3\beta^2)/(2\beta^2)} - 1$$

so that

$$\gamma = \sqrt{\frac{1+3\beta^2}{2\beta^2}} - 2 \tag{5.4.11}$$

but this expression is suspect because the derivation of asymptotic expression for $P_{\mathcal{E}}$, and therefore the exponent (5.4.6) depends on the assumption that $z_1 > z_2$, which is not true at a degenerate critical point.

5.4.3 Exact equations for evolution of singular values

To understand the degenerate case in more detail, we need a more refined treatment that does not assume $Z_1 \gg Z_2$. Using the statistics for the increments $\mathrm{d}\tilde{A}_{ij}$ obtained from equations (5.4.1) and (5.4.2) the exact equations of motion in the the (x_1, x_2) coordinate system, (5.3.13a) and (5.3.13b), become:

$$\mathrm{d}X_1 = -\left(\mathrm{d}\tilde{A}_{11} + \mathrm{d}\tilde{A}_{22}\right) + 4\beta^2\mathrm{d}t \tag{5.4.12a}$$

$$\mathrm{d}X_2 = \left(\mathrm{d}\tilde{A}_{11} - \mathrm{d}\tilde{A}_{22}\right) + 2(1+\beta^2)\frac{1+\nu^2}{1-\nu^2}\mathrm{d}t \tag{5.4.12b}$$

[15] To derive this result it is useful to note that $f(\eta)$ can be written in the form

$$f(\eta) = c\sqrt{a(\eta-1)^2 + 2(a-b)\eta} - (\eta-1) - 1.$$

and the second moments of the increments are therefore

$$\langle \mathrm{d}X_1^2 \rangle = 8\beta^2 \mathrm{d}t, \quad \langle \mathrm{d}X_2^2 \rangle = 4(1+\beta^2)\mathrm{d}t, \quad \langle \mathrm{d}X_1 \mathrm{d}X_2 \rangle = 0 \; . \tag{5.4.13}$$

Since $\nu = \lambda_2/\lambda_1 = \exp(-x_2)$, from these equations we conclude that X_1 and X_2 make independent diffusive motions, with the following drift velocity and diffusion tensor:

$$\boldsymbol{v} = \begin{pmatrix} 4\beta^2 \\ 2\left(1+\beta^2\right)\coth x_2 \end{pmatrix} \quad \boldsymbol{D} = \begin{pmatrix} 4\beta^2 & 0 \\ 0 & 2(1+\beta^2) \end{pmatrix}. \tag{5.4.14}$$

This is consistent with the remarks made regarding v_1 and v_2 in the discussion of the coordinate transformation: v_1 is constant and, since $v_2(x_2) = 2\left(1+\beta^2\right)\coth x_2$, then $v_2 \to \infty$ as $x_2 \to 0$ and $v_2 \to v_0 \equiv 2(1+\beta^2)$ as $x_2 \to \infty$. We use equations (5.4.12a) and (5.4.12a) in the numerical simulations for the degenerate case, in section (5.5.2).

5.4.4 Ratio of singular values

Thus far we have considered $P_{\mathcal{E}}(\varepsilon)$, the p.d.f. of the norm, $\mathcal{E}$, of the matrix product, in the limit as $\varepsilon \to 0$, showing that it is a power-law with an additional logarithmic correction in the degenerate case. We now consider how the ratio of the singular values, $\nu = \lambda_2/\lambda_1$, is distributed for a given value of the norm, $\mathcal{E}$. Specifically, we consider the p.d.f. of the random variable $\Delta Z \equiv Z_2 - Z_1 = -\ln(\nu)$, conditional on a given value of $X_\varepsilon = -\ln \mathcal{E}$. Note that ΔZ is in fact the random variable X_2; we shall therefore denote any particular value of ΔZ by x_2 and we shall denote the conditional p.d.f. by $P_{\Delta Z|X_\varepsilon}(x_2; x_\varepsilon)$. To simplify our discussion we consider only the case where $\left|\frac{\Delta Z}{X_\varepsilon}\right| = \left|\frac{x_2}{x_\varepsilon}\right| \ll 1$, where certain simplifying assumptions can be made.

In the non-degenerate case, with $Z_2 \gg Z_1$, then the ratio ν approaches zero as $\varepsilon \to 0$. However in the degenerate case we expect the values of Z_1 and Z_2 to be comparable and, consequently, that the distribution of ΔZ is non-trivial. We therefore concentrate on the degenerate case. Our approach is to postulate that the p.d.f. $P_{\Delta Z|X_\varepsilon}(x_2; x_\varepsilon)$ for the degenerate case is a modified form of that for the non-degenerate case.

If $Z_2 \gg Z_1$ then if the norm $\mathcal{E}$ of the matrix contraction process has the value ε the diffusing particle almost lies on the asymptote to the contour C_ε. Hence $Z_1 \approx X_\varepsilon \equiv -\ln \mathcal{E}$. Therefore, if $Z_1 = x_\varepsilon$ and $\Delta Z = x_2$ then, since $Z_2 = Z_1 + \Delta Z$, we have $Z_2 = x_\varepsilon + x_2$. Therefore, the p.d.f.

that we are interest in can be written in terms of $P_{\boldsymbol{Z}}(\boldsymbol{z})$ as follows:

$$P_{\Delta Z|X_\varepsilon} = \frac{P_{\boldsymbol{Z}}(x_\varepsilon, x_\varepsilon + x_2)}{\int_0^\infty \mathrm{d}x_2'\, P_{\boldsymbol{Z}}\left(x_\varepsilon, x_\varepsilon + x_2'\right)}\,. \tag{5.4.15}$$

Also, in the non degenerate case, from equation (5.3.6) we have

$$P_{\boldsymbol{Z}}(\boldsymbol{z}) \sim (\boldsymbol{z}\cdot\boldsymbol{D}^{-1}\boldsymbol{z})^{-1/4}\exp[-\Psi(\boldsymbol{z})]$$

and provided that we can neglect the dependence of the pre-exponential factor on the value of ΔZ, i.e. on x_2, we have

$$P_{\Delta Z|X_\varepsilon}(x_2; x_\varepsilon) \sim \exp[\Psi(x_\varepsilon, x_\varepsilon) - \Psi(x_\varepsilon, x_\varepsilon + x_2)]. \tag{5.4.16}$$

We expect the result given in equation (5.4.16) to hold in the region where the Z_i undergo diffusion with a constant drift velocity, i.e. far from the reflecting boundary, so that $x_2 = z_2 - z_1 \gg 0$. But it may not hold close to the reflecting boundary where the values of Z_1 and Z_2 are comparable, and where the drift velocity is given by (5.4.14). For this case we shall *postulate that the distribution is some modified form* of (5.4.16). To find this form we consider the p.d.f. P_{X_2} for the degenerate case.

Close to the reflecting boundary, $x_2 = 0$, the governing Fokker-Planck equation for the p.d.f. $P_{X_2}(x_2)$ is

$$\frac{\partial P_{X_2}}{\partial t} = \frac{\partial^2 P_{X_2}}{\partial x_2^2} - \frac{\partial}{\partial x_2}\left(v_2(x_2)\,P_{X_2}\right) \tag{5.4.17}$$

where $v_2(x_2) = v_0 \coth x_2$, with $v_0 = D_2 = 2(1+\beta^2)$. We are interested in finding a solution which matches (5.3.21) when $x_2 \gg 1$. To eliminate the term involving the first derivative with respect to x_2 and transform the equation to a Hermitian form[16] we set $P_{X_2} = \psi(x_2, t)\,\exp(x_2)$, this gives:

$$\frac{\partial \psi}{\partial t} = D_2\frac{\partial^2 \psi}{\partial x_2^2} - V(x_2)\,\psi \tag{5.4.18}$$

where

$$V(x_2) = \frac{D_2}{4}\left(1 - \frac{1}{\sinh^2 x_2}\right).$$

[16] See page 105.

Then, to find a solution which matches (5.3.21), we set

$$\psi(x_2,t) = \phi(x_2)\ \exp\left(\frac{-v_0^2 t}{4D_2}\right)$$

and find that $\phi(x_2)$ satisfies

$$\frac{\mathrm{d}^2\phi}{\mathrm{d}x_2^2} = \frac{-\phi}{4\sinh^2(x_2)}.$$

We require a solution $\phi(x_2)$ which approaches a constant as $x_2 \to \infty$ and which approaches zero as $x_2 \to 0$. Close to $x_2 = 0$ the differential equation is approximated by

$$\frac{\mathrm{d}^2\phi}{\mathrm{d}x_2^2} = -\frac{\phi}{4x_2^2}$$

which has general solution

$$\phi(x_2) = \sqrt{x_2}\,[c_1 + c_2 \ln(x_2)]$$

where c_1 and c_2 are arbitrary constants. Since $\phi(x_2) \to 0$ as $x_2 \to 0$ we conclude that

$$\phi(x_2) \sim \sqrt{x_2} \ \text{ as } \ x_2 \to 0.$$

From equation (5.3.18) with $v_2 = D_2 \coth(x_2)$ we have $\chi(x_2) = \ln(\sqrt{\sinh(x_2)})$ and, therefore, $\exp(\chi(x_2)) \to \sqrt{x_2}$ as $x_2 \to 0$. Hence, from equations (5.3.17) and (5.4.16) we postulate that $P_{\Delta Z|X_\varepsilon}$ is of the form

$$P_{\Delta Z|X_\varepsilon}(x_2; x_\varepsilon) \sim F(x_2) \exp[\Psi(x_\varepsilon, x_\varepsilon) - \Psi(x_\varepsilon, x_\varepsilon + x_2)] \tag{5.4.19}$$

where $F(x_2) \sim x_2$ for $x_2 \ll 1$, but where $F(x_2)$ approaches a constant as $x_2 \to \infty$. We examine these predictions in the next section.

5.5 Numerical investigations

Our analysis of the matrix contraction process has led us to consider a diffusive model for the evolution of the singular values of the matrix. The predictions of this model are a consequence of the fact that the diffusion process has an unusual combination of reflecting and absorbing boundary conditions. The problem is too complex for a rigorous analysis to be practicable and we have therefore used numerical simulations to test the predictions.

5.5.1 A note on the numerical algorithms

To generate an ensemble of the random matrices, $\mathrm{d}\tilde{\boldsymbol{A}}$, it is not actually necessary to compute the velocity field. Instead, we note that the vectors $\boldsymbol{p} \equiv (\phi_{11}, \phi_{22}, \phi_{12})^{\mathrm{T}}$ and $\boldsymbol{s} \equiv (\psi_{11}, \psi_{22}, \psi_{12})^{\mathrm{T}}$ have *covariance matrix*

$$\boldsymbol{C} = \langle p_i p_j \rangle = \langle s_i s_j \rangle = \begin{pmatrix} 3 & 1 & 0 \\ 1 & 3 & 0 \\ 0 & 0 & 1 \end{pmatrix}.$$

Therefore, if $\boldsymbol{\xi} = (\xi_1, \xi_2, \xi_2)^{\mathrm{T}}$ and $\boldsymbol{\eta} = (\eta_1, \eta_2, \eta_2)^{\mathrm{T}}$ are vectors whose elements are i.i.d. Gaussian random variables with zero mean and unit variance and $\boldsymbol{K}$ is the square root of the covariance matrix:

$$\boldsymbol{C}^{1/2} = \frac{1}{\sqrt{2}} \begin{pmatrix} \sqrt{2}+1 & \sqrt{2}-1 & 0 \\ \sqrt{2}-1 & \sqrt{2}+1 & 0 \\ 0 & 0 & \sqrt{2} \end{pmatrix}$$

then the components of the random vectors $\tilde{\boldsymbol{p}} \equiv \boldsymbol{C}^{1/2}\boldsymbol{\xi}$ and $\tilde{\mathbf{s}} \equiv \boldsymbol{C}^{1/2}\boldsymbol{\eta}$ have the same statistics as the field derivatives ϕ_{ij} and ψ_{ij}.

We may therefore reproduce the required statistical behaviour of the stability matrices, $\mathrm{d}\tilde{\boldsymbol{A}}$, simply by generating a pair of Gaussian random vectors $(\boldsymbol{\xi}, \boldsymbol{\eta})$ at each timestep and, from them, generating the vectors $\tilde{\boldsymbol{p}}$ and $\tilde{\mathbf{s}}$. This approach was used for the simulations in the non degenerate case.

In the degenerate case trajectories of the notional particles were computed using the discrete version of equations (5.4.12a) and (5.4.12b) :

$$\boldsymbol{r}_{n+1} = \boldsymbol{r}_n + \boldsymbol{v}_n \delta t + \sqrt{2\boldsymbol{D}\delta t}\, \boldsymbol{\eta}_n \tag{5.5.1}$$

where $\boldsymbol{D}$ is as given in (5.4.14) and

$$\boldsymbol{r}_n = \begin{pmatrix} x_1(t_n) \\ x_2(t_n) \end{pmatrix}, \quad \boldsymbol{v}_n = \begin{pmatrix} 4\beta^2 \\ 2\left(1+\beta^2\right)\coth\left(x_2(t_n)\right) \end{pmatrix} \quad \text{and} \quad \boldsymbol{\eta}_{\mathrm{n}} = \begin{pmatrix} \eta_1 \\ \eta_2 \end{pmatrix} \tag{5.5.2}$$

with $t_n = n\delta t$, where δt a small time step, and where the *noise* term, $\boldsymbol{\eta}_n$, is a random vector whose two components are independent Gaussian random variables, with mean zero and unit variance.

5.5.2 The p.d.f. $P_{\mathcal{E}}$

The results from simulations of the matrix contraction process, discussed in section (5.4), are shown in figure (5.6). The numerically determined p.d.f.s are shown in red and the theoretical distributions, given by equations (5.3.39), (5.4.10) and (5.4.11), are shown in blue.

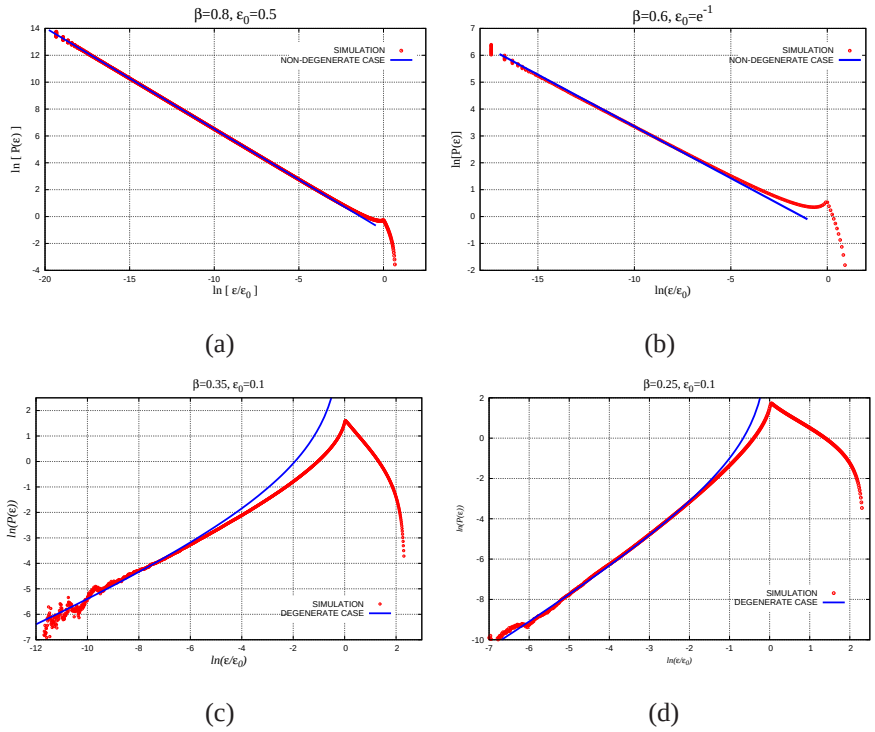

Fig. 5.6 The p.d.f. of the matrix norm, $P_{\mathcal{E}}$ for different values of the compressibility parameter β. Each plot shows a comparison between the theoretical p.d.f. of the matrix norm (shown in blue) and the numerically determined p.d.f. of the matrix norm (shown in red). For $1 > \beta > \frac{1}{\sqrt{5}}$ the predicted form of the p.d.f. is a power law whilst for $\frac{1}{\sqrt{5}} > \beta > 0$ the predicted form is a modified power law, with logarithmic correction factors. In each case the numerical simulations give results which are in excellent agreement with the theoretical predictions.

Plots (**a**) and (**b**) show results for the non-degenerate case, with $\beta = 0.8$, and $\beta = 0.6$, respectively. In both cases the distribution is a simple power-law. Equation (5.4.10) predicts the correct values of γ: $\gamma = -0.753$ and $\gamma = -0.385$ respectively. Plots (**c**) and (**d**) show results for the degenerate case, with $\beta = 0.35$ and $\beta = 0.25$ respectively. Equation (5.4.11) correctly predicts that $\gamma = 0.363$ and $\gamma = 1.082$ respectively. In each case, the p.d.f. of $\mathcal{E}$ has a factor $[\ln(1/\varepsilon)]^{-3/2}$. These results demonstrate the validity of our predictions for the form

of $P_{\mathcal{E}}$ and for the value of γ, for both the non-degenerate case with $1/\sqrt{5} < \beta < 1$, and the degenerate case with $0 < \beta < 1/\sqrt{5}$.

5.5.3 The p.d.f. $P_{\Delta Z|X_{\mathcal{E}}}$

Figure (5.7) shows the p.d.f. $P_{\Delta Z|X_\varepsilon}(x_2; x_\varepsilon)$, where $\Delta Z = X_2 = Z_2 - Z_1$ and $X_\varepsilon = -\ln \mathcal{E}$, for a simulation of the degenerate case where $\beta = 0.3$, $\varepsilon_0 = 0.01$ and $X_\varepsilon = -10$. Note that the distribution peaks at $\Delta Z \approx 1.5$ for which $\nu = \lambda_2/\lambda_1 \approx \exp(-1.5) \approx 0.2$.

The plot also shows segments of two fitted curves: the straight line $P_{\Delta Z|X_\varepsilon}(x_2; x_\varepsilon) = c_1 x_2$ and the exponential tail $P_{\Delta Z|X}(x_2; x_\varepsilon) = c_2 \exp[\Psi(x_\varepsilon, x_\varepsilon) - \Psi(x_\varepsilon, x_\varepsilon - x_2)]$, where c_1 and, c_2 are constants. These are shown in black and blue respectively.

The results demonstrate that the form of $P_{\Delta Z|X_\varepsilon}(x_2; x_\varepsilon)$ is consistent with equation (5.4.19): for $|x_2/x_\varepsilon| \ll 1$ we have $P_{\Delta Z|X_\varepsilon}(x_2; x_\varepsilon) \sim x_2$ and for $|x_2/x_\varepsilon| \gg 1$ the p.d.f. has an exponential tail.

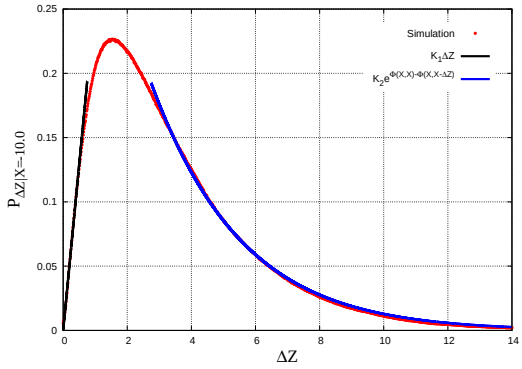

Fig. 5.7 The plot shows the numerically determined conditional p.d..f. $P_{\Delta Z|X_\varepsilon}$ for $\beta = 0.3$, together with the theoretically predicted forms for the density at small and large values of ΔZ. Since $\Delta Z = -\ln \nu = -\ln \frac{\lambda_2}{\lambda_1}$ the plot illustrates the distribution of the ratio of singular values for a given value of the norm, $\mathcal{E}$. The p.d.f. has an exponential tail and when ΔZ is small the p.d.f. is approximately linear, consistent with the predictions made in section 5.4.4.

5.6 Conclusion

In this chapter we have investigated a stochastic process whose state is given by the product of random matrices. Each factor in the matrix product is close to the identity and the factors have diffusive fluctuations. Such processes occur naturally when examining the evolving configuration of small constellations of particles in a chaotic dynamical system, or constellations of points in the phase space of the system. The linear approximation to the differential of the dynamical flow can be written as a product of stability matrices which, in the case of a chaotic dynamical system, are random. The (Frobenius) norm, $\mathcal{E}$, of the matrix product is a measure of the size of a constellation, and our objective here was to understand the distribution of this norm, when the constellations are small.

For the scalar version of this problem the distribution of the norm, $\mathcal{E}$, is always a power-law. However for the matrix version of the process we showed that the distribution is a modified power law of the form

$$P_{\mathcal{E}}(\varepsilon) \sim \frac{\varepsilon^{\gamma}}{\left[\ln\left(\frac{1}{\varepsilon}\right)\right]^{\mu}} \quad \text{as} \quad \varepsilon \to 0 \tag{5.6.1}$$

where μ is either 0 or $\frac{3}{2}$. The value of μ that applies depends on the location of the stationary point of a large deviation rate function, Ψ, with μ changing discontinuously as the stationary point passes from the interior to the exterior of a physically accessible region. For the random advective flow model we were able to derive an expression for γ in terms of the compressibility parameter of the flow, β, and we showed that the discontinuous transition in the exponent μ occurs at the critical value $\beta_c = \frac{1}{\sqrt{5}}$.

During the evolution of a chaotic dynamical system the particles, or phase points, repeatedly separate and accumulate. As the particles separate the linear approximations to the dynamics eventually break down and when they accumulate they do so in a manner unrelated to any earlier configuration. To reflect this behaviour the stochastic process studied here includes a resetting mechanism, in which the state of the process is re-set to a multiple of the identity whenever the norm exceeds an upper limit.

In a more realistic model of the dynamics of a chaotic system we would re-initialize the matrix contraction process to a *random* matrix value. This is considered in the next chapter, where, for a particular dynamical system, we relate the distribution of the norm to a fractal dimension of the attractor of the dynamical system.

Chapter 6

The Rényi dimension D_3 and $P_{\mathcal{E}}$

.... the true logic for this world is the calculus of probabilities.

James Clerk Maxwell

The structure of a strange attractor of a chaotic dynamical system can be understood as the result of the stretching, squeezing and folding of volume elements of phase space during the evolution of the system [37]. These dynamical processes can bring trajectories into close proximity and can give an attractor a Cantor-set-like structure. We expect the size and shape statistics of triangular constellations to be related to the resultant clustering of trajectories. In particular, recalling from section (2.2.3) that D_3, the Rényi dimension of order 3, can be expressed in terms of the 3-point correlation sum, $C_3(N,\varepsilon)$, it follows that D_3 is related to the clustering of *triples* of points or, equivalently, to the probability of finding pairs of points in an ε-ball *centred on a reference point*. We therefore expect D_3 to be related to the distribution of the *size*, ε, of triangular constellations. In this chapter we examine this relationship. We use a modified version of the matrix contraction process, considered in Chapter 5, to model the dynamical processes giving rise to an attractor. This chapter is based on the manuscript [67].

6.1 A random matrix model for constellation dynamics

6.1.1 Squeezing, stretching and folding

Figure (6.1) shows plots of a small area of the fractal shown in the introduction, in figure (1.1), at some times t_0, $t_1 = t_0 + \delta t$, $t_2 = t_0 + 2\delta t$, $\cdots$ t_5, where δt is a small time interval. As the particles, shown in red, are advected along their individual trajectories by the random flow, the lines and filaments, formed by clusters of particles, are squeezed, stretched and folded. Each plot also shows the same reference particle, $\mathbf{P}_0$, and the same two, randomly chosen, companion particles, $\mathbf{P}_1$ and $\mathbf{P}_2$, in black green and blue respectively. The three particles can be considered to be at the vertices of a small triangular constellation, and as the system evolves the triangle is deformed.

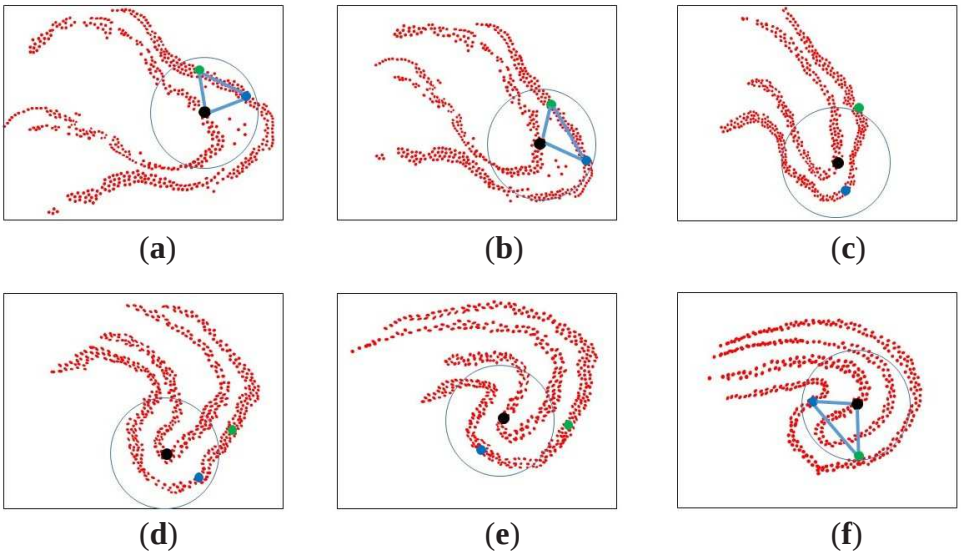

Fig. 6.1 The plots in this figure show a small region of the fractal distribution of particles in figure (1.1) of chapter 1, at successive times $t_0, t_0 + \delta t, t_0 + 2\delta t, \cdots$, where δt is a small time increment. The filaments formed by the particles are stretched, squeezed and folded as the system evolves. The plots also show the evolution of a small triangular constellation of particles. The particle shown in black is the *reference* particle for the triangle and the circle centred on it shows the region within which we may treat the dynamics of the constellation by using a linearized approximation to the flow. In plot (c) the linear approximation breaks down. In plot (f) the particles return to proximity, in a configuation which is uncorrelated with that in plot (c).

At any time t the size and shape of the constellation is defined by a *configuration matrix*, $\boldsymbol{L} \equiv [\delta \boldsymbol{r}_1, \delta \boldsymbol{r}_2]$, whose columns are the relative displacements of the vertices $\mathbf{P}_1$ and $\mathbf{P}_2$,

with respect to the reference particle, $\mathbf{P}_0$. Whilst the two companion particles lie within a small disk centred on $\mathbf{P}_0$ their relative displacements, with respect to $\mathbf{P}_0$, can be described adequately by a linearized equation of motion, but this linear approximation does not hold for particles lying outside the small disk. Therefore, if the vertices remain inside the disk between times t and $t+\delta t$ we have $\boldsymbol{L}(t+\delta t) \approx \boldsymbol{S}(t)\boldsymbol{L}(t)$ where $\boldsymbol{S}(t)$ is some *stability matrix* for the system. Hence, if the three particles were inside the disk at some initial time, $t = 0$ say, and *remained* in the disk until some later time t, then iterating this relation at the times $t_r = r\delta t,\ r = 1,2,3,\cdots,n$ where $n = \mathrm{int}(t/\delta t)$, we have

$$\boldsymbol{L}(t) \approx \left[\prod_{r=1}^{n} \boldsymbol{S}(t_r)\right] \boldsymbol{L}_0 \equiv \boldsymbol{M}(t)\,\boldsymbol{L}_0 \tag{6.1.1}$$

where $\boldsymbol{L}_0$ is the initial configuration, at $t = 0$. Note that the matrix $\boldsymbol{M}(t)$, which is a product of stability matrices, corresponds to the *deformation* matrix, introduced in section (2.1.3)

In the case of a chaotic dynamical system the separations of particles eventually grows exponentially fast and, after a finite time, the linearization approximation breaks down. This occurs in plot (**c**) of the figure, and persists for the two following timesteps. At a later time the dynamics brings the particles into proximity again (see plot (**f**)), and when this occurs the configuration of the constellation is uncorrelated with that at the time the linearization approximation failed.

6.1.2 The matrix model of the dynamics

We are interested in the structure of dense accumulations of phase points, for which equation (6.1.1) provides an adequate description of the dynamics. To understand these we shall adopt a random matrix model of the dynamics, proceeding as follows. We choose an initial configuration matrix $\boldsymbol{L}_0$ from some ensemble and then calculate the configuration matrix, $\boldsymbol{L}(t)$, by multiplying $\boldsymbol{L}_0$ by a deformation matrix $\boldsymbol{M}(t)$. The deformation matrix is generated from a product of random stability matrices whose statistics are specific to the dynamical system at hand. We then evaluate the Frobenius norm of $\boldsymbol{L}(t)$

$$\mathcal{E}[\boldsymbol{L}(t)] = \sqrt{\mathrm{tr}\left[\boldsymbol{L}^{\mathrm{T}}(t)\,\boldsymbol{L}(t)\right]} = \sqrt{\delta\boldsymbol{r}_1^2 + \delta\boldsymbol{r}_2^2}. \tag{6.1.2}$$

If this norm exceeds some predetermined value, $\varepsilon_{\max}$, we interpret this as the breakdown of the linear approximation and reset the iteration by replacing $\boldsymbol{L}(t)$ with a new, randomly chosen, $\boldsymbol{L}_0$.

This model is variant of the matrix contraction process, examined in Chapter 5. In this case the initial configuration, and the configuration when reset, is a *random* matrix instead of a multiple of the identity (see section (5.1.2)). This randomness is important for two reasons. First, it is a more accurate model of the dynamics. It reflects the fact that, for a randomly chosen pair of points in an ε-ball centred on a reference point, the initial configuration matrix is random. Also whenever the process is re-set the configuration matrix, being uncorrelated with its value prior to re-setting, is again random. Second, this randomness can generate triangular constellations which are very nearly degenerate *and* whose axis is aligned with a direction along which contraction is taking place. We will see that, under certain circumstances, this mechanism, i.e. alignment of nearly degenerate triangles along a direction of contraction, is an important mechanism for generating very small triangular constellations. The randomness of the initial and configuration and the configuration when re-set is an essential feature of any reasonable model of a random dynamical system. It will soon be apparent that it creates considerable complications.

6.2 Deformation of triangular constellations

6.2.1 The geometry of constellations

Figure (6.2), repeated here from Chapter 3 for convenience, shows the configuration of a typical constellation at some time t:

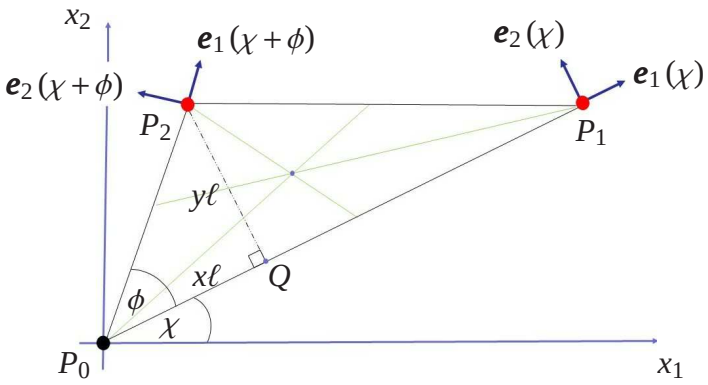

Fig. 6.2 The configuration of a triangular constellation can be specified using the lengths, angles and unit basis vectors shown in the figure (c.f. figure (3.3)).

The corresponding 2×2 configuration matrix is :

$$\mathbf{L} = [\delta\boldsymbol{r}_1, \delta\boldsymbol{r}_2] = \begin{pmatrix} \delta x_1 & \delta x_2 \\ \delta y_1 & \delta y_2 \end{pmatrix}. \tag{6.2.1}$$

This can be factored into a form which emphasizes the size, orientation and shape of the triangle:

$$\mathbf{L} = \ell\, \boldsymbol{R}(\chi) \begin{pmatrix} 1 & x \\ 0 & y \end{pmatrix} \equiv \ell\, \boldsymbol{R}(\chi)\, \boldsymbol{H} \tag{6.2.2}$$

where ℓ is the length of the base, $\mathbf{P}_0\mathbf{P}_1$, and where x and y are, respectively, the *ratios* of the lengths $\mathbf{P}_0\mathbf{Q}$ and $\mathbf{Q}\mathbf{P}_2$ to that of the base. We shall refer to x as the *base ratio* and to y as the altitude ratio and since the matrix $\boldsymbol{H}$ essentially defines the shape of the triangle we shall refer to it as the *shape matrix* of the constellation. $\boldsymbol{R}(\chi)$ is the rotation matrix

$$\boldsymbol{R}(\chi) = \begin{pmatrix} \cos\chi & -\sin\chi \\ \sin\chi & \cos\chi \end{pmatrix}. \tag{6.2.3}$$

Note that in a chaotic dynamical system ℓ, x and y and χ are time-dependent random variables and, therefore, $\boldsymbol{H}$ and $\boldsymbol{R}$ are time-dependent random matrices.

The size and shape of the triangle are independent of the orientation angle, χ, and they are invariant under rotation. Therefore, any size and shape *parameters* which we use to describe the triangle must depend only on the rotational invariants of the configuration matrix. These are the determinant, $\det[\boldsymbol{L}]$, the scalar product of the displacement vectors, $\delta\boldsymbol{r}_1 \cdot \delta\boldsymbol{r}_2$ and the trace of the the symmetric matrix $\boldsymbol{L}^{\mathrm{T}}\boldsymbol{L}$. The size of a constellation is given by the Frobenius

norm of $\boldsymbol{L}$:

$$\mathcal{E}(\boldsymbol{L}) = \sqrt{\mathrm{tr}(\boldsymbol{L}^{\mathrm{T}}\boldsymbol{L})} \tag{6.2.4}$$

In terms of the length of the base ℓ, and the ratios x and y, then at time t the size parameter, $\mathcal{E}$, is

$$\mathcal{E} = \ell\ \sqrt{1+x^2+y^2}. \tag{6.2.5}$$

Initially, and whenever re-set, the configuration of the constellation is given by a configuration matrix of the form

$$\mathbf{L}_0 = \ell_0\ \boldsymbol{R}\left(\chi_0\right)\begin{pmatrix} 1 & x_0 \\ 0 & y_0 \end{pmatrix} \equiv \ell_0\ \boldsymbol{R}\left(\chi_0\right)\boldsymbol{H}_0 \tag{6.2.6}$$

for some random rotation angle, χ_0, and random variables, ℓ_0, x_0 and y_0. The values of χ_0, ℓ_0, x_0 and y_0 are different each time the process is re-set and, each time, the corresponding initial values of the size parameter is[1]

$$\varepsilon_0 = \ell_0\ \sqrt{1+x_0^2+y_0^2}. \tag{6.2.7}$$

Note that the matrix contraction process considered in Chapter 5 is reproduced by setting $\ell_0 = \varepsilon_0/\sqrt{2}$, $\chi_0 = 0$, so that $\boldsymbol{R}\left(\chi_0\right) = \boldsymbol{I}_{2\times 2}$, and $x_0 = 0$, $y_0 = 1$, so that $\boldsymbol{H}\left(\chi_0\right) = \boldsymbol{I}_{2\times 2}$ and by setting the maximum permissible value of the norm, $\varepsilon_{\max}$, to unity. Henceforth in this chapter we shall assume that $\ell_0 = \varepsilon_0/\sqrt{2}$ and that $\varepsilon_{\max} = 1$, but χ_0, x_0 and y_0 will remain random.

Our objective is to understand the p.d.f. of the parameter $\mathcal{E}$ and, for constellations in the strange attractor of a dynamical system, to relate this to the fractal dimension, D_3, of the attractor.

6.2.2 Singular value decomposition of linearised map

To determine the distribution of $\mathcal{E}$ we must consider how it is transformed by the dynamics of the system.

The linearised approximation given by equation (6.1.1) is valid only when the separation of trajectories is sufficiently small. Whilst it holds the configuration of the system is given in

[1]Note that here we have an unfortunate abuse of standard notation. The length ratios x and y and their initial values x_0 and y_0 are *random* variables, as is the size parameter $\mathcal{E}$ and its initial value, $\mathcal{E}_0$.

terms of an initial state and a deformation matrix, $\boldsymbol{M}(t)$, which captures the dynamics of the system. Following the approach taken in earlier chapters, we shall express these dynamics using the s.v.d. of the deformation matrix. This is

$$\mathbf{M}(t) = \mathbf{R}(\theta_1)\boldsymbol{\Lambda}\mathbf{R}(\theta_2) \equiv \mathbf{R}_1\boldsymbol{\Lambda}\mathbf{R}_2 \tag{6.2.8}$$

where $\boldsymbol{\Lambda} = \mathrm{diag}(\lambda_1, \lambda_2)$ and $\boldsymbol{R}_1$ and $\boldsymbol{R}_2$ are rotation matrices, with rotation angles θ_1, θ_2 respectively. For a chaotic dynamical system, the singular values λ_1, λ_2 and the rotation angles θ_1, θ_2 are real, time-dependent random variables.

Whenever the displacement matrix is re-set to a random value the dynamics resumes, according to the *same* equations of motion. We therefore regard the deformation matrices, $\mathbf{M}(t)$, as being drawn from a *stationary* ensemble.

6.2.3 Transformation of the size parameter

The initial configuration, or state, of the constellation is defined by the length, ε_0, an orientation angle, χ_0, and a shape matrix, $\boldsymbol{H}_0$. The angle and the matrix are each chosen from statistical ensembles. In effect, the deformation matrix $\boldsymbol{M}(t)$ *transforms* this initial state into a *current* state, given by equation (6.2.2). Using the s.v.d. of $\boldsymbol{M}(t)$ the current state, $\boldsymbol{L}(t)$, can be written as

$$\boldsymbol{L}(t) = \frac{\varepsilon_0}{\sqrt{2}}\,\boldsymbol{R}_1\boldsymbol{\Lambda}\boldsymbol{R}\boldsymbol{H}_0 \tag{6.2.9}$$

where the rotation matrix, $\boldsymbol{R}$, with no subscript, is

$$\boldsymbol{R} \equiv \begin{pmatrix} \cos\left(\theta_2+\chi_0\right) & -\sin\left(\theta_2+\chi_0\right) \\ \sin\left(\theta_2+\chi_0\right) & \cos\left(\theta_2+\chi_0\right) \end{pmatrix} \equiv \begin{pmatrix} c & -s \\ s & c \end{pmatrix}$$

with $c \equiv \cos\left(\theta_2+\chi_0\right)$ and $s \equiv \sin\left(\theta_2+\chi_0\right)$. Note that, via the angles θ_2 and χ_0 respectively, $\boldsymbol{R}$ depends on both the dynamics and the initial state of the system.

Introducing *scaled* singular values[2] $\tilde{\lambda}_i = \left(\varepsilon_0/\sqrt{2}\right)\lambda_i$, $i = 1,2$, and the random variables $c_1 \equiv \cos(\theta_1)$, $s_1 \equiv \sin(\theta_1)$, $p \equiv x_0 c - y_0 s$ and $q \equiv x_0 s + y_0 c$, then equation (6.2.9) can be written as

$$\boldsymbol{L}(t) \equiv \begin{pmatrix} \tilde{\lambda}_1 c_1 c - \tilde{\lambda}_2 s_1 s & \tilde{\lambda}_1 c_1 p - \tilde{\lambda}_2 s_1 q \\ \tilde{\lambda}_1 s_1 c + \tilde{\lambda}_2 s_1 s & \tilde{\lambda}_1 s_1 p + \tilde{\lambda}_2 c_1 q \end{pmatrix}. \tag{6.2.10}$$

[2] c.f. Section (5.2)

Therefore, $\det[\boldsymbol{L}] = \tilde{\lambda}_1\tilde{\lambda}_2(cp - sq) = \tilde{\lambda}_1\tilde{\lambda}_2 y_0$, and the relative displacements of particles $\mathbf{P_1}$ and $\mathbf{P_2}$ from the reference particle $\mathbf{P_0}$ are, respectively,

$$\delta\boldsymbol{r}_1(t) = \begin{pmatrix} \tilde{\lambda}_1 c_1 c - \tilde{\lambda}_2 s_1 s \\ \tilde{\lambda}_1 s_1 c + \tilde{\lambda}_2 s_1 s \end{pmatrix} \quad \text{and} \quad \delta\boldsymbol{r}_2(t) = \begin{pmatrix} \tilde{\lambda}_1 c_1 p - \tilde{\lambda}_2 s_1 q \\ \tilde{\lambda}_1 s_1 p + \tilde{\lambda}_2 c_1 q \end{pmatrix}.$$

Hence, from equation (6.2.4), the norm is

$$\mathcal{E}(t) = \sqrt{\tilde{\lambda}_1^2[c^2 + p^2] + \tilde{\lambda}_2^2[s^2 + q^2]}, \tag{6.2.11}$$

Introducing the random variables $\mathrm{U}_1^2 \equiv c^2 + p^2$ and $\mathrm{U}_2^2 \equiv s^2 + q^2$ then the expression for the norm can be written as

$$\mathcal{E}(t) = \sqrt{\tilde{\lambda}_1^2\mathrm{U}_1^2 + \tilde{\lambda}_2^2\mathrm{U}_2^2}. \tag{6.2.12}$$

The U_i depend on the initial conditions and the rotation angle θ_2, but are independent of the singular values. We also note that if the initial shape matrix, $\boldsymbol{H}_0$, is the identity matrix then $x_0 = 0$ and $y_0 = 1$ and

$$\mathrm{U}_1^2 = c^2 + p^2 = \cos^2(\theta_2 + \chi_0) + [x_0\cos(\theta_2 + \chi_0) - y_0\sin(\theta_2 + \chi_0)]^2 = 1$$

and, similarly, $U_2 = 1$, so that the U_i are not random, in this case.

From equation (6.2.12) we can see that in contrast to the situation in Chapter 5, now, via the random variables U_1 and U_2, the norm depends on the initial shape and orientation of the constellation, and on the rotation angle θ_2. The initial shape and orientation parameters are fixed during any particular *run* or cycle of the process, but θ_2 varies with time. Therefore, to achieve our objective of determining the p.d.f. of $\mathcal{E}$, we shall need some knowledge of the joint p.d.f. of the U_i and the λ_i. Fortunately, in section (6.3), we shall see that some simplification is possible.

6.2.4 Making small triangles

We are interested in the form of the p.d.f. of the norm, $\mathcal{E}$, when the norm is very small. It is therefore informative to consider the mechanisms which can give rise to very small triangles.

During the evolution of the system we expect that $\nu \equiv \lambda_2/\lambda_1 = \tilde{\lambda}_2/\tilde{\lambda}_1 \ll 1$ therefore, from equation (6.2.12), we see that if $\tilde{\lambda}_1 \ll 1$ (and $\tilde{\lambda}_2 \ll 1$) then the norm is small[3]. This case arises when the differential of the dynamical map is contracting in the region of the phase space containing the triangle. The triangle is then squeezed in two directions, given by the eigenvectors of the deformation matrix; this is the *usual* mechanism for creating small triangles.

From equation (6.2.12) we can also see that even if λ_1 is not particularly small then $\mathcal{E}$ can be small *provided that* U_1 is small. This requires the coincidence of two special circumstances. First, that *initially* the triangle is nearly *degenerate*, so that the vertices are nearly aligned along some axis. In this case y_0 is very small and $U_1 \approx x_0 \cos(\theta_2 + \chi_0)$. The second condition is that the triangle remains very flat until a time when θ_2 takes a value for which $\cos(\theta_2 + \chi_0) \approx 0$. The interpretation of this condition is that the triangle remains near-degenerate and becomes aligned with the principal direction of contraction. This direction is orthogonal to the left eigenvector associated with the largest singular value, λ_1. Although this double coincidence is a rare event it allows the production of a small triangle even when largest singular value, $\tilde{\lambda}_1$ is not very small. In some cases this mechanism, of squeezing a nearly degenerate triangle along its axis, may be the most probable route to making a very small triangle.

We expect the properties of the configuration matrix, $\boldsymbol{L}(t)$, to be largely determined by the dynamics of the system, and therefore insensitive to most aspects of the ensemble from which the initial state, $\boldsymbol{L}_0$, is drawn. However, because the second mechanism for making small triangles depends upon starting with a flat triangle, with a very small value of y_0, the distribution of the *altitude* ratio, y_0, is likely to be important. A reasonable model for probability density of y_0 is that it is uniform in the vicinity of $y_0 = 0$.

6.3 Application to the random flow model

It is not possible to examine the relationship between D_3, the Rényi dimension of order 3, and the p.d.f., $P_{\mathcal{E}}$, of the *norm* of the matrix process $\boldsymbol{L}(t)$ (i.e. the size of triangular constellations) for a general random dynamical system. We will therefore examine this relationship for the random flow model introduced in section (2.4).

[3]Note that since we are assuming that the base of the triangle is the longest side, we have $\sqrt{x_0^2 + y_0^2} \leq 1$ therefore U_1^2 and U_2^2 are bounded above by $1 + \sqrt{x_0^2 + y_0^2} \leq 2$, and therefore $U_i \leq \sqrt{2}$

6.3.1 The p.d.f. $P_{\boldsymbol{Z}}$

From equation (6.2.12) we see that the norm, $\mathcal{E}(t)$, depends on the singular values, λ_i, of the deformation matrix, $\boldsymbol{M}(t)$, and the random variables U_1, U_2 (which depend on the variables x_0, y_0 and χ_0 in the shape matrix $\boldsymbol{H}_0$). Therefore, to determine $P_{\mathcal{E}}$, the p.d.f. of the norm, we will require the p.d.f.s of these variables.

From sections (5.2.1) and (5.2.2) of Chapter 5 we know that the logarithmic variables

$$Z_1 = -\ln \tilde{\lambda}_1 \quad \text{and} \quad Z_2 = -\ln \tilde{\lambda}_2 \tag{6.3.1}$$

undergo an advection-diffusion process, with drift velocity and diffusion tensor given, respectively, by

$$\boldsymbol{v} = \begin{pmatrix} \beta^2 - 1 \\ (1+3\beta^2) \end{pmatrix}, \quad \boldsymbol{D} = \frac{1}{2}\begin{pmatrix} (1+3\beta^2), & (\beta^2-1) \\ (\beta^2-1), & (1+3\beta^2) \end{pmatrix}. \tag{6.3.2}$$

The joint p.d.f.[4], $P_{\boldsymbol{Z}}(\boldsymbol{z})$, for reaching the point $\boldsymbol{z} \equiv (z_1, z_2)$ can be expressed in the large-deviation form:

$$P_{\boldsymbol{Z}}(\boldsymbol{z}) \sim g(\boldsymbol{z}) \exp[-\Psi(\boldsymbol{z})] \tag{6.3.3}$$

where the rate function, or entropy function, $\Psi(\boldsymbol{z})$, is given by

$$\Psi_{\boldsymbol{Z}}(\boldsymbol{z}) = \frac{1}{2}\left[\sqrt{\boldsymbol{z} \cdot \boldsymbol{D}^{-1}\boldsymbol{z}}\, \sqrt{\boldsymbol{v} \cdot \boldsymbol{D}^{-1}\boldsymbol{v}} - \boldsymbol{z} \cdot \mathbf{D}^{-1}\boldsymbol{v} \right] \tag{6.3.4}$$

and the pre-exponential factor is

$$g(\boldsymbol{z}) = \frac{1}{\left[\boldsymbol{z} \cdot \boldsymbol{D}^{-1}\boldsymbol{z}\right]^{1/4}} \,. \tag{6.3.5}$$

For the drift velocity and diffusion tensor given in equation (6.3.2) we have

$$\Psi(z_1, z_2) = c\sqrt{a\left(z_1^2 + z_2^2\right) - 2bz_1z_2} - z_2 \tag{6.3.6}$$

where

$$a = 1 + 3\beta^2, \quad b = \beta^2 - 1 \quad \text{and} \quad \mathrm{c} = \sqrt{\frac{a}{a^2 - b^2}}.$$

[4]Note that this is *not* the p.d.f. of the flatness parameter, which is denoted by $P_{\mathcal{Z}}$

In principle we can use the p.d.f. $P_{\boldsymbol{Z}}(\boldsymbol{z})$ to determine the p.d.f. $P_{\mathcal{E}}$ for the random flow model. However the randomness of the initial configuration must also be taken into account. We consider this in the next section.

6.3.2 The p.d.f. $P_{\mathcal{E}}$

As in section (5.3.1) of Chapter 5, we shall use the p.d.f. of the random variable $X_\varepsilon \equiv -\ln\mathcal{E}$ to calculate the p.d.f. of $\mathcal{E}$. In terms of the logarithmic variables, Z_i, from equation (6.2.12), we have

$$\mathcal{E}^2(t) = e^{-2Z_1}\mathrm{U}_1^2 + e^{-2Z_2}\mathrm{U}_2^2. \tag{6.3.7}$$

Now, let $\boldsymbol{W} = (W_1, W_2)$, where $W_1 \equiv -\ln U_1$ and $W_2 \equiv -\ln U_1$, then

$$\mathcal{E}^2(t) = e^{-\,2(Z_1+W_1)}\left[1 + e^{-\,2(Z_2-Z_1)} \times e^{-\,2(W_2-W_1)}\right]$$

so that the random variable X_ε is given by

$$X_\varepsilon \equiv h(\boldsymbol{Z},\boldsymbol{W}) = Z_1 + W_1 - \frac{1}{2}\times\ln\left[1 + e^{-2(Z_2-Z_1)}\; e^{-2(W_2-W_1)}\right]. \tag{6.3.8}$$

The p.d.f. of X_ε can be defined by

$$P_{X_\varepsilon}(x_\varepsilon) = \langle \delta[X_\varepsilon - h(\boldsymbol{Z},\boldsymbol{W})]\rangle .$$

To calculate this expectation value we require the joint p.d.f. of $\boldsymbol{Z}$ and $\boldsymbol{W}$. Since the λ_i and the U_i are independent random variables, $\boldsymbol{Z}$ and $\boldsymbol{W}$ are also independent random variables and their joint p.d.f. factorizes. We therefore have

$$P_{X_\varepsilon}(x_\varepsilon) = \int_{z_2=z_1}^{\infty}\int_{z_1=0}^{\infty}\int_{w_2=\omega}^{\infty}\int_{w_1=\omega}^{\infty} \mathrm{d}z_2\mathrm{d}z_1\mathrm{d}w_2\mathrm{d}w_1\; \delta[x_\varepsilon - h(\boldsymbol{z},\boldsymbol{w})]\; P_{\boldsymbol{Z}}(\boldsymbol{z})\; P_{\boldsymbol{W}}(\boldsymbol{w})\;.$$

Note that since the maximum value of U_1 and U_2 is $\sqrt{2}$ the lower limit on the integrals with respect to w_1 and w_2 is $\omega \equiv -\ln\sqrt{2}$.

Now, since $Z_2 \geq Z_1$, we expect the last term in equation (6.3.8) to be small, and if we have $\exp[-2(Z_2 - Z_1)] \times \exp[-2(W_2 - W_1)] \ll 1$ then we can neglect this term, giving

$$P_{X_\varepsilon}(x_\varepsilon) \approx \int_{z_2=z_1}^{\infty}\int_{z_1=0}^{\infty}\int_{w_2=\omega}^{\infty}\int_{w_1=\omega}^{\infty} \mathrm{d}z_2\mathrm{d}z_1\mathrm{d}w_2\mathrm{d}w_1\; \delta[x_\varepsilon - w_1 - z_1]\; P_{\boldsymbol{Z}}(\boldsymbol{z})\; P_{\boldsymbol{W}}(\boldsymbol{w}).$$

The sifting property of the delta function selects the value $z_1 = x_\varepsilon - w_1$ in the integral with respect to z_1. Also, since w_2 appears in the integrand only in the joint p.d.f. $P_{\boldsymbol{W}}(w_1, w_2)$, we may integrate out the w_2 dependence leaving the marginal density $P_{W_1}(w_1)$. Hence

$$P_{X_\varepsilon}(x_\varepsilon) \approx \int_\omega^\infty \int_{z_2 = x_\varepsilon - w_1}^\infty \mathrm{d}w_1 \mathrm{d}z_2 \; P_{\boldsymbol{Z}}(x_\varepsilon - w_1, z_2) \; P_{W_1}(w_1) \tag{6.3.9}$$

Since we have $P_{\boldsymbol{Z}}(\boldsymbol{z})$ in the large deviation form given in equation (6.3.3) then, in principle, if we can determine $P_{W_1}(w_1)$ in an exponential form we may apply Laplace's method to give an approximate asymptotic expression for $P_{X_\varepsilon}(x_\varepsilon)$.

The p.d.f. of W_1, P_{W_1}

We know that the form of a p.d.f. determined by Laplace's method depends on the location of the stationary point of the exponent in the integrand. From equation (6.3.9), we can see that *if* the integrand has a maximum at $w_1 = 0$ *and* we can approximate the p.d.f. of W_1 by a delta function, $P_{W_1}(w_1) = \delta(w_1)$, then P_{X_ε} reduces, precisely, to the form considered in Chapter 5. Such an approximation is plausible because the distribution of the singular values can be expected to be much broader than that of the other random variables and, for the matrix contraction process considered in Chapter 5, W_1 is not random, but vanishes identically. However in the more general case, where the integrand in (6.3.9) has a maximum for a non-zero value of w_1, we need to determine the form of $P_{W_1}(w_1)$ in order to produce an approximation for P_{X_ε}. We can do this using the following geometrical argument which is illustrated in figure (6.3).

By definition $U_1^2 = c^2 + p^2$, where $p = [x_0 c - y_0 s]$ with $c = \cos\left(\theta_2 + \chi_0\right)$ and $s = \sin\left(\theta_2 + \chi_0\right)$. We can write $p = k \sin\left(\theta_2 + \chi_0 - \alpha\right)$, where $k \equiv \sqrt{x_0^2 + y_0^2}$ and $\tan\alpha = x_0/y_0$, and since we have $x_0^2 + y_0^2 \leq 1$ it follows that $k \leq 1$. We can therefore interpret U_1 as being the distance from the origin to a point on an ellipse, with Cartesian coordinates (c, p) (see for example plots (**b**), (**c**) or (**d**)). The ellipse lies in the square $\mathcal{S} \equiv \{(c, p) : -1 \leq c \leq 1, \; -1 \leq p \leq 1\}$ in the (c, p) plane.

During any particular run of the advection-diffusion process, the variables x_0, y_0 and χ_0 are fixed by the shape matrix, i.e. by the initial shape and orientation of the triangular constellation. These, in turn, fix the orientation and eccentricity of the ellipse and the starting position of the point (c, p), for that run of the process. The point then moves on the ellipse

as the angle θ_2 varies in time. Consequently the value of the length of the radius vector, i.e. the distance U_1, fluctuates with time, due to the fluctuations in the angle θ_2.

This situation is illustrated in plots (**a**)-(**e**); these show the ellipse $U_1^2 = c^2 + p^2$, for five different runs of the process. In each case the ellipse lies in the square $\mathcal{S}$ in the (c, p) plane, Plot (**f**) shows the ensemble of ellipses superimposed.

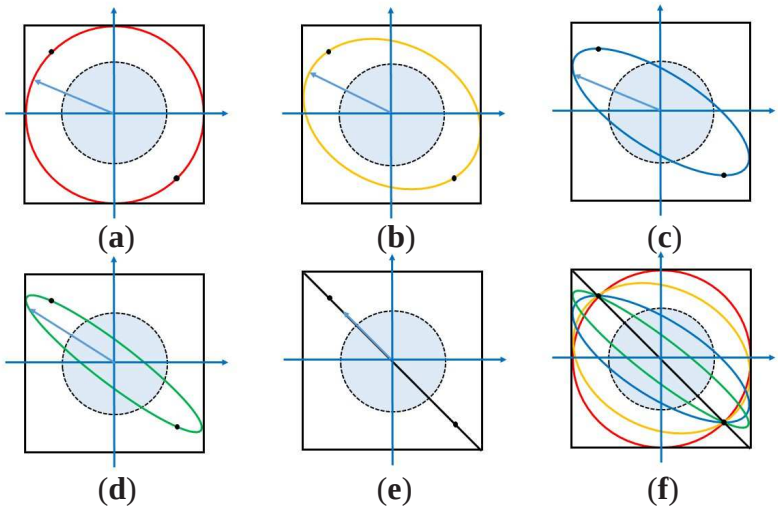

Fig. 6.3 The random variable U_1 can be interpreted as the length of the position vector of a variable point which lies on an ellipse, which sits inside the square $[-1,1]\times[-1,1]$. The orientation and eccentricity of the ellipse are determined by the initial configuration of the triangular constellation. The variable point moves at random on the ellipse as the system evolves. The initial position of the variable point is determined by the initial orientation of the constellation and subsequent positions depend on the value of the second singular value decomposition rotation angle, θ_2. In a large number of runs of the process an ensemble of ellipses cover the unit disc uniformly, so that for any disc of radius $u < 1$, such as that shown in blue, the probability that the representative point lies in the interior of this disk is proportional to the area of the disc, i.e. to u^2. Hence, for $u < 1$ the cumulative distribution function $F_{U_1}(u) \sim u^2$ from which we deduce that, for $u < 1$, the p.d.f. $P_{U_1}(u) \sim u$.

In plot (**a**) $x_0 = 0$ and $y_0 = 1$, corresponding to the inital shape matrix $\boldsymbol{H}_0 = \boldsymbol{I}$. In this case $U_1 = 1$ for all θ_2, and the ellipse is a circle. In plot (**b**) $x_0 = 0.25$ and $y_0 = 0.75$, in plot (**c**) $x_0 = 0.5$ and $y_0 = 0.5$ and in plot (**d**) $x_0 = 0.75$ and $y_0 = 0.25$. In plot (**e**) $x_0 = 1.0$ and $y_0 = 0.0$ and the ellipse is degenerate, i.e. a straight line.

Each radius vector in plots (**a**) - (**e**) shows the position of the point (c, p) at some arbitrary time during the particular run of the process; the length of this vector is equal to U_1. The (blue) disk shown in each plot has some radius $u_1 < 1$. Where points on an ellipse lie in the interior of the disk we have $U_1 < u_1$. Plot (**f**) shows the ensemble of ellipses, corresponding

to all five runs of the process; note that a number of ellipses contain points interior to the disk. In a large number of runs of the process the ensemble of ellipses will cover the unit disk uniformly, because of the randomness of the initial conditions. Therefore, for any given $u_1 < 1$ we expect that the probability that a point (c, p) lies inside a disk of radius u_1 to be proportional to the area of the disk, i.e. to u_1^2. Hence, the cumulative probability distribution of U_1 is of the form $F_{U_1}(u_1) \sim u_1^2$, for $u_1 < 1$. We therefore conclude that, for $u_1 < 1$, the p.d.f. of U_1 is given by

$$P_{U_1}(u_1) = F'_{U_1}(u_1) \sim u_1 \tag{6.3.10}$$

and, from the change of variable rule, the p.d.f. of $W_1 = -\ln U_1$ is given by

$$P_{W_1}(w_1) = \left[P_{U_1}(u_1) \left| \frac{\mathrm{du}_1}{\mathrm{dw}_1} \right| \right]_{u_1 = e^{-w_1}} \sim e^{-2w_1}. \tag{6.3.11}$$

When $1 < U_1 \leq \sqrt{2}$ the point (c, p) lies outside the unit disk (i.e. the point lies outside the red circle in plot (**f**), but inside the square). In this case there is no simple geometrical argument that we can use to determine the form of the p.d.f. of U_1. However, from the above discussion, it seems plausible to assume that the behaviour of the system is dominated by cases for which $U_1 \leq 1$. We shall therefore make this assumption and, correspondingly, in equation (6.3.9) we shall set $\omega = 0$.

Continuing with the calculation of P_{X_ε}, substituting (6.3.3) and (6.3.11) into (6.3.9) gives

$$P_{X_\varepsilon}(x_\varepsilon) \sim \int_{w_1=0}^{\infty} \int_{z_2=x_\varepsilon - w_1}^{\infty} \mathrm{d}w_1 \mathrm{d}z_2 \; g(x_\varepsilon - w_1, z_2) \times \exp\left[-\Phi(x_\varepsilon - w_1, z_2, w_1) \right] \tag{6.3.12}$$

where

$$\Phi(z_1, z_2, w_1) \equiv \Psi(z_1, z_2) + 2w_1 \tag{6.3.13}$$

and the pre-exponential factor is given by equation (6.3.5). Now applying Laplace's method to estimate the integral gives an estimate for $P_{X_\varepsilon}(x_\varepsilon)$ of the form

$$P_{X_\varepsilon}(x_\varepsilon) \sim \Gamma(x_\varepsilon) g^*(x_\varepsilon) \times \exp\left[-\Phi^*(x_\varepsilon) \right] \tag{6.3.14}$$

where $\Gamma(x_\varepsilon)$ is a Gaussian integral and the exponent, $\Phi^*(x_\varepsilon)$, is the solution of the *constrained* minimization problem:

$$\Phi^*(x_\varepsilon) \equiv \min \{ \Phi(z_1, z_2, w_1) \; : w_1 \geq 0, \; z_1 \geq 0, \; z_2 \geq z_1, \; z_1 + w_1 = x_\varepsilon \}. \tag{6.3.15}$$

The pre-exponential factor $g^*(x_\varepsilon)$ is the value of the function g, defined by equation (6.3.5), at the constrained stationary point of Φ. To leading order in x_ε, we can write

$$\Gamma(x_\varepsilon) g^*(x_\varepsilon) \sim x_\varepsilon^{-\mu} \tag{6.3.16}$$

for some parameter μ whose value depends on the position of the stationary point.

The minima $\Phi^*(x_\varepsilon)$

Typically, the critical points of a constrained optimization problem occur on the boundary defined by the constraints, and we shall assume that is the case here[5]. On inspection of the constraints we see that a stationary point on the boundary satisfies either: **(i)** $w_1 > 0$, $z_2 = x_\varepsilon$, $z_1 = x_\varepsilon - w_1$ or **(ii)** $w_1 = 0$, $z_2 = x_\varepsilon$, $z_1 = x_\varepsilon - w_1$, or **(iii)** $w_1 = 0$, $z_2 > x_\varepsilon$, $z_1 = x_\varepsilon - w_1$. We shall discuss each case in turn and, for each, we shall consider the corresponding form of the pre-exponential factor and the p.d.f. $P_{X_\varepsilon}(\varepsilon)$.

In **case (i)** the function $\Phi(z_1, z_2.w_1)$ can be written as

$$\Phi(z_1, z_2, w_1) = \Psi(z_1, x_\varepsilon) + 2(x_\varepsilon - z_1) = x_\varepsilon [f(\zeta) - \zeta + 1] \equiv x_\varepsilon \ell(\zeta) \tag{6.3.17}$$

where $\zeta \equiv z_1 / x_\varepsilon$ and $f(\zeta) = c\sqrt{a(1+\zeta^2) - 2b\zeta} - \zeta$ with a, b and c as given in section (6.3.1). Therefore

$$\Phi^*(x_\varepsilon) = \ell(\zeta^*) x_\varepsilon \tag{6.3.18}$$

where $\ell'(\zeta^*) = 0$, where ζ^* is the positive root of the quadratic equation

$$(\zeta^*)^2 - 2\left(\frac{b}{a}\right)\zeta^* - \left(\frac{a\left(4a^2 - 5b^2\right)}{4b^2 - 3a^2}\right) = 0.$$

We find $\zeta^* = b/a + 2\left(a^2 - b^2\right)/(ar)$ where $r \equiv \sqrt{4b^2 - 3a^2} = \sqrt{1 - 26\beta^2 - 23\beta^4}$, provided the square root is real, and writing $\zeta^* = p + q$, where $p = b/a$ and $q = 2\left(a^2 - b^2\right)/(ar)$ we find

$$\ell(\zeta^*) = c\sqrt{a(1 + p^2 + q^2) + 2q(ap - b) - 2bp} - 2(p + q) + 1 = \frac{a - 2b + r}{a}$$

which, in terms of β is

$$\ell(\zeta^*) = \frac{3 + \beta^2 + \sqrt{1 - 26\beta^2 - 23\beta^4}}{1 + 3\beta^2}. \tag{6.3.19}$$

[5]This assumption is indeed confirmed by a simple linear search computer program.

The pre-exponential factor, $g^*(x_\varepsilon)$, has the asymptotic form $1/\sqrt{x_\varepsilon}$ as $x_\varepsilon \to \infty$ and, on the boundary $z_1 = x_\varepsilon$, we find $\partial^2\Phi/\partial w_1^2 \sim (x_\varepsilon)^{-1}$, so that the Gaussian integral with respect to w_1 gives a factor asymptotic to $\sqrt{x_\varepsilon}$. The asymptotic x_ε-dependence of these factors cancel, so that $\mu = 0$.

So, when the minimum of $\Phi(z_1, z_2, w_1)$ occurs at a point $(z_1, z_2, w_1) = \left(x_\varepsilon - w_1^*, x_\varepsilon, w_1^*\right)$, with $w_1^* > 0$, then $\Phi^* = x_\varepsilon \ell(\zeta^*)$, with $\ell(\zeta^*)$ given by equation (6.3.17) and since $z_2 > z_1$ at the stationary point, $P_{\mathcal{E}}$ is a simple power law:

$$P_{\mathcal{E}}(\varepsilon) \sim \varepsilon^{\ell(\zeta^*)-1}. \tag{6.3.20}$$

This case applies if $0 < \beta < 1/\sqrt{29}$.

In **cases (ii) and (iii)**, at the minimum $w_1 = 0$, so that these are in fact the cases treated in Chapter 5. In both cases we have

$$\Phi(z_1, z_2, w_1) = \Phi(x_\varepsilon, z_2, 0) = \Psi(x_\varepsilon, z_2) = x_\varepsilon \Psi(1, \eta) \equiv x_\varepsilon f(\eta)$$

where $\eta \equiv z_2/x_\varepsilon$ and the function f is as given above in case (i). Therefore in each case we have

$$\Phi^*(x_\varepsilon) = f(\eta^*)\, x_\varepsilon \tag{6.3.21}$$

where η^* is the value of η at which f has a minimum. Equations (6.3.14) and (6.3.16) shows that the p.d.f. of X_ε is of the form

$$P_{X_\varepsilon}(x_\varepsilon) \sim x_\varepsilon^{-\mu} \times \exp[-\, f(\eta^*) x_\varepsilon],$$

so that the p.d.f. of $\mathcal{E}$ is of the form

$$P_{\mathcal{E}}(\varepsilon) \sim \frac{\varepsilon^\gamma}{[\ln(1/\varepsilon)]^\mu} \tag{6.3.22}$$

for some parameters γ and μ. The exponent γ is given by $\gamma \equiv f(\eta^*) - 1$ and the exponent of the logarithmic term, μ, depends on the nature of the minimum. In a *non-degenerate* case, where $z_2 > z_1$ at the minimum, then $\mu = 0$ and in a *degenerate* case, where $z_2 = z_1$ at the minimum, $\mu = 3/2$. These values apply here since the minimum of $\Phi(z_1, z_2, w_1)$ occurs at a point where the fluctuations of W_1 can be neglected, that is at $W_1 = 0$.[6]

[6]Note that this corresponds to the condition $U_1 = 1$, which holds if the initial shape matrix of the triangle is $\boldsymbol{H}_0 = \boldsymbol{I}$.

In **case (ii)** $z_2 = z_1 = x_\varepsilon$ at the minimum, so that this case is degenerate. We find

$$f(\eta^*) = \sqrt{\frac{1+3\beta^2}{2\beta^2}} - 1 \tag{6.3.23}$$

and $P_\mathcal{E}$ is a modified power law of the form (6.3.22) with $\gamma = f(\eta^*) - 1$ and $\mu = 3/2$. This degenerate case applies for $1/\sqrt{29} < \beta < 1/\sqrt{5}$.

In **case (iii)** $z_2 > z_1$ at the minimum, so that this case is non degenerate. We find

$$f(\eta^*) = \frac{2(1-\beta^2)}{1+3\beta^2} \tag{6.3.24}$$

and $P_\mathcal{E}$ is a simple power law, of the form (6.3.22) with $\gamma = f(\eta^*) - 1$ and $\mu = 0$. This non-degenerate case applies for $1/\sqrt{5} < \beta < 1$.

6.3.3 The Rényi dimension D_3

The distribution of small triangles is related to D_3, the Rényi dimension of order 3. This fractal dimension can be defined in terms of the mean square number of particles $\langle \mathcal{N}^2(\varepsilon)\rangle$ in an ε disc, centred on a reference particle. From equation (2.2.8) we have

$$2D_3 = \lim_{\varepsilon\to 0}\left[\frac{\ln\langle \mathcal{N}^2(\varepsilon)\rangle}{\ln\varepsilon}\right] \tag{6.3.25}$$

Now, $\langle \mathcal{N}^2(\varepsilon)\rangle$ is proportional to the cumulative probability for *three* points to be found inside an ε disc, and is therefore proportional to the *cumulative distribution function* of $\mathcal{E}$. Therefore in non-degenerate cases, where $\mu = 0$ and the leading asymptotic behaviour of $P_\mathcal{E}$ is a simple power-law, equations (6.3.22) and (6.3.25) imply that $2D_3 = f(\eta^*) = \gamma + 1$ so that

$$P_\mathcal{E}(\varepsilon) \sim \varepsilon^{2D_3 - 1} \tag{6.3.26}$$

In the degenerate case, where $P_{\mathcal{E}}(\varepsilon) \sim \dfrac{\varepsilon^{\gamma}}{[\ln(1/\varepsilon)]^{3/2}}$, we have[7]

$$\begin{aligned}\langle \mathcal{N}^2(\varepsilon)\rangle &\sim \int_0^{\varepsilon} \mathrm{d}r\, P_{\mathcal{E}}(r) \\ &\sim \frac{2}{\sqrt{\ln(1/\varepsilon)}}\left[\varepsilon^{\gamma+1} - \sqrt{\pi(\gamma+1)\ln(1/\varepsilon)}\left\{1-\mathrm{erf}\left(\sqrt{(\gamma+1)\ln(1/\varepsilon)}\right)\right\}\right] \\ &\to \frac{\varepsilon^{\gamma+1}}{(\gamma+1)[\ln(1/\varepsilon)]^{3/2}}, \text{ as } \varepsilon \to 0, \end{aligned} \tag{6.3.27}$$

which is the same result as would be obtained simply by treating the logarithmic factor as a constant. Therefore in the degenerate case from (6.3.25) and (6.3.27) it follows that $2D_3 = f(\eta^*) = \gamma + 1$. Hence, for the turbulent flow model we find that the third Renyi dimension, D_3, as a function of the compressibility parameter, β, is

$$D_3 = \begin{cases} \dfrac{3+\beta^2+\sqrt{1-26\beta^2-23\beta^4}}{2(1+3\beta^2)} & 0 \le \beta \le \dfrac{1}{\sqrt{29}} \\ \dfrac{1}{2}\left(\sqrt{\dfrac{1+3\beta^2}{2\beta^2}}-1\right) & \dfrac{1}{\sqrt{29}} \le \beta \le \dfrac{1}{\sqrt{5}} \\ \dfrac{1-\beta^2}{1+3\beta^2} & \dfrac{1}{\sqrt{5}} \le \beta \le 1 \end{cases} \tag{6.3.28}$$

These results are equivalent to those given in [2].

6.3.4 Numerical investigation of $P_{\mathcal{E}}$

Figure (6.4) shows log-log plots of the numerically determined p.d.f., $P_{\mathcal{E}}$, for the three different non-trivial asymptotic regimes discussed in section (6.3), together with the corresponding theoretical distributions. The numerical results have been determined using the random matrix model of section (6.1.2).

[7] The integral and the limiting value given in equation (6.3.27) were obtained using the Maple® computer algebra system.

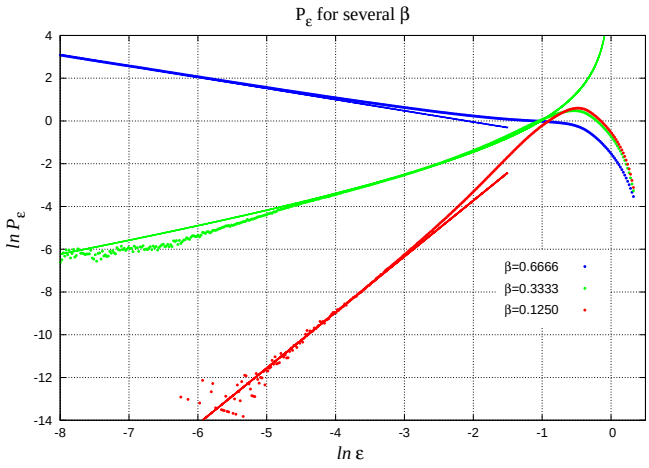

Fig. 6.4 The plot shows the theoretical and numerically determined p.d.f.s of the matrix norm, $P_{\mathcal{E}}$, for $\beta = \frac{1}{8}$, $\frac{1}{3}$ and $\frac{2}{3}$. In each case the numerical simulations give results which are in good agreement with the theoretical predictions. Note that, in contrast to the corresponding results shown in figure (5.6), here the plots obtained from the numerical simulations do not have a cusp, because of the variability in the initial conditions.

Note that, in contrast to the plots of $P_{\mathcal{E}}$ given in Chapter 5, the curves here do not have a cusp because here the process is reset to a random matrix. For $\beta = 1/8$ the predicted asymptotic form of $P_{\mathcal{E}}$ is a simple power-law, shown by the solid red straight line. The exponent, predicted by (6.3.20), is $f(\eta^*) - 1 = 2.613$ (to 3 dec. pl.). For $\beta = 1/3$ the predicted asymptotic form of $P_{\mathcal{E}}$ contains a logarithmic correction to a power-law, and is shown by the solid green curve. The exponent, predicted by (6.3.23) is $f(\eta^*) - 1 = 0.449$ (to 3 dec. pl.). For $\beta = \frac{2}{3}$ the predicted fom of $P_{\mathcal{E}}$ is once again a simple power-law, shown by a solid blue line. Equation (6.3.24) gives the exponent $f(\eta^*) - 1 = -0.524$ (to 3 dec. pl.). These results are clearly in excellent agreement with the analysis carried out in section (6.3).

Chapter 7

Conclusions

> "No book can ever be finished. While working on it we learn just enough to find it immature the moment we turn away from it.
>
> *Karl Popper*

7.1 Review and critique of the main results

The broad aim of the research undertaken for this thesis has been to examine the possibility of characterizing the local structure of fractal sets by using 'statistical geometry' - the statistics of the size and shape of small constellations of points sampling the fractal. A second aim was to develop the techniques that such an approach, if feasible, would entail. We have focused on the two-dimensional case and have characterized the geometry of triangular constellations using the scaled radius of gyration, R, and a flatness parameter, $Z \sim \mathcal{A}/R^2$, where $\mathcal{A}$ is the area of the triangle. We have given an interpretation of Z in terms of a *shape space*, the Kendall sphere.

In our early numerical simulations of $P_Z(z)$, the p.d.f. of the flatness parameter Z (defined in equation (3.1.5)), for constellations in fractal sets arising from a compressible chaotic flow, we found that $P_Z(z)$ undergoes a phase transition as the compressibility parameter of the flow is varied through a critical value β_c. This result is, to our knowledge, the first significant finding in this field. We found that below β_c the p.d.f. of Z is approximately independent of the compressibility and above β_c the p.d.f. of Z has the power-law form

$P_Z(z) \sim z^{\alpha}$, with an exponent which takes one of two different values, α_1 or α_2, depending upon how small z is. By modelling the evolution of the geometry of a constellation using an advection-diffusion process, we determined β_c analytically for the model flow and we gave a qualitative explanation of the existence of the two values of the exponent.

In the random flow we found that the logarithms of the angles and lengths defining a triangular constellation satisfy stochastic equations of motion. Correspondingly, their joint probability density satisfies an advection-diffusion equation. In principle these observations are generalizable to other chaotic dynamical systems and to higher dimensional fractal clusters. This led us to consider the homogeneous advection-diffusion equation, with an absorbing boundary. For the two dimensional case we investigated the flux of particles onto the x_2-axis due to a steady point source. To model the absorption we treated the boundary as a source of 'antiparticles'. We showed that, far from the source, the flux onto the boundary has the form $J(x_2) \sim A(x_2)\exp[-\Psi(x_2)]$, where as $x_2 \to \infty$, $A(x_2) \sim x_2^{-p}$, with $p = \frac{1}{2}$ for a completely transparent 'boundary' , and $p = \frac{3}{2}$ for an absorbing boundary. We also found that the exponent $\Psi(x_2)$ is the same for both non-absorbing and absorbing boundaries and grows linearly as $x_2 \to \infty$. Our numerical investigations demonstrate the validity and quality of these asymptotic approximations.

The configuration of a constellation can be described naturally by a matrix of relative displacement vectors. The size of the constellation is then given by the Frobenius norm, $\mathcal{E}$, of the matrix. Consequently, to model the evolution of a constellations in a random flow we introduced a stochastic matrix process whose state is given by the product of random matrices. The factors in the matrix product are stability matrices which are close to the identity matrix and which have diffusive fluctuations.

We showed that the p.d.f. of $\mathcal{E}$ takes the form $P_{\mathcal{E}}(\varepsilon) = \varepsilon^{\gamma}/[\ln(1/\varepsilon)]^{\mu}$. The value of μ depends on the location of the stationary point of a large deviation rate function, Ψ, and μ changes discontinuously from 0 to $3/2$ as the stationary point passes from the interior to the exterior of a physically accessible region. Consequently under certain conditions $P_{\mathcal{E}}$ has the form of a modified power law. For the random advective flow model we derived an expression for γ in terms of , β, the compressibility parameter of the flow and we showed that the discontinuous transition in the exponent μ occurs at the critical value $\beta_c = \frac{1}{\sqrt{5}}$.

By generalizing the original matrix contraction process, so that the initial configuration of a constellation is random, we applied the techniques from our earlier work to derive an expression for the Renyi dimension, D_3, in terms of the exponent in the probability density

$P_{\mathcal{E}}(\varepsilon)$. This was found to be in agreement with the results obtained by other authors, using different methods, thereby demonstrating the general validity of the our approach.

7.2 Conclusion and next steps

We have certainly shown that it is possible to characterize the local structure of fractal sets using the shape statistics of small constellations, at least in the case of triangular constellations in two-dimensional fractals generated by a random flow. However the approach needs further development, and further validation. In particular, it needs to be applied to other models of chaotic dynamics in two dimensions, for example inertial particles in a random flow, and extended to three dimensional systems. Also, whilst the techniques applied here can be applied, quite naturally, to more complicated dynamics, and to three dimensional fractals, the resulting mathematics quickly becomes extremely, and perhaps prohibitively, complex. It would therefore be of interest to study a range of different dynamical systems with the objective of developing more general analytical techniques and, possibly, identifying more 'universal' results.

There are a number of immediate opportunities for continued research. For example in the p.d.f. of the flatness parameter, $P_Z(z)$, a quantitative treatment of the exponents α_1, α_2, when $\beta > \beta_c$, will require a more sophisticated model for the propagator of the advection diffusion process, taking account the behaviour near and on the non-absorbing boundary $x_2 = 0$. Also, it would be of interest to know the form of the p.d.f. of $\mathcal{E}$ for higher dimensional models and for other dynamical systems, for example inertial particles in a random flow. Similarly, it would be of interest to understand the distribution of the norm of more general stochastic matrix processes.

More ambitiously, it would be very interesting to examine if and how statistical geometry can offer insight into the physical implications of local geometrical structures in fractal clusters of real particles. For example, how do these structures affect the scattering of light, or sound, or electrical conductivity, and can the characteristics of these phenomena be related to the p.d.f.s of the shape statistics? This avenue of research would offer opportunities for very interesting theoretical and experimental work.

References

[1] Beč, J. (2003). Fractal clustering of inertial particles in random flows. *Phys. Fluids*, 15(11):L81–84.

[2] Beč, J., Gawedzki, K., and Horvai, P. (2004). Multifractal clustering in compressible flows. *Phys. Rev. Lett.*, 92:224501.

[3] Castiglione, P. and Pumir, A. (2001). Evolution of triangles in a two dimensional turbulent flow. *Phys. Rev. E.*, 64.5:056303.

[4] Coffey, W. T., Kalmykov, Y. P., and Waldron, J. (2004). *The Langevin Equation*. World Scientific, Singapore, second edition.

[5] Ermak, D. L. (1977). An analytical model for air pollutant transport and deposition from a point source. *Atmos. Environ.*, 11:231–37.

[6] Falconer, K. (1990). *Fractal Geometry: mathematical foundations and applications*. Wiley, New York.

[7] Falkovich, G., Fouxon, A., and Stepanov, M. (2002). Acceleration of rain initiation by cloud turbulence. *Nature*, 419:151.

[8] Falkovich, G., Gawedzki, K., and Vergassola, M. (2000). Particles and fields in turbulence. *Rev. Mod. Phys.*, 73:913–975.

[9] Femia, N., Niemeyer, L. L., and Tucci, V. (1993). Fractal characteristics of electrical discharges: experiments and simulation. *Jour. Phys. D: Applied Physics*, 26:619–627.

[10] Fredrickson, P., Kaplan, J., Yorke, E., and Yorke, J. (1983). The Liapunov Dimensions of Strange Attractors. *J. Diff. Eq.*, 49:185–207.

[11] Graebel, W. P. (2007). *Advanced Fluid Mechanics*. Academic Press, Burlington MA USA, first edition.

[12] Graham, C. and Talay, D. (2013). *Stochastic Simulation and Monte Carlo Methods*. Springer, New York, 1 edition.

[13] Grant, J. and Wilkinson, M. (2015). Advection diffusion equation with absorbing boundary. *J. Stat. Phys.*, 160:622–635.

[14] Grassberger, P. and Procaccia, I. (1983). Measuring the strangeness of strange attractors. *Physica D: Nonlinear Phenomena*, 9:189–208.

[15] Guichardaz, R., Pumir, A., and Wilkinson, M. (2016). Non-thermal einstein relations. *Europhys. Lett.*, 115:10009–.

[16] Halsey, T. C., Jensen, M. H., Kadanoff, L. P., Procaccia, I., and Shraiman, B. I. (1986). Fractal measures and their singularities: The characterization of strange sets. *Phys. Rev. A*, 33:1141.

[17] Hassler, U. (2016). *Stochastic Processes and Calculus*. Springer, New York, 1 edition.

[18] Hirsch, M. W., Smale, S., and Devaney, R. L. (2004). *Differential equations, dynamical systems, and an introduction to chaos*, volume 60 of *Pure and Applied Mathematics*. Elsevier Academic Press, San Diego CA, second edition.

[19] Horn, R. A. and Johnson, C. R. (2013). *Matrix Analysis, 2nd. edn.* Cambridge University Press, New York.

[20] J A Yorke, K. T. A. and Sauer, T. D. (2000). *Chaos an Introduction to Dynamical Systems*. Springer, New York, 1 edition.

[21] Kaplan, J. and Yorke, J. (1979). Chaotic behviour of multidimensional difference equations. In Walther, H. O., editor, *Functional Differential Equations and the Approximation of Fixed points*, pages 204–207. Springer.

[22] Keener, R. W. (2010). *Theoretical Statistics*. Springer, New York, first edition.

[23] Kendall, D. (1977). The diffusion of shape. *Adv. Appl. Prob.*, 9:428–430.

[24] Kendall, D. (1984). Shape manifolds, procrustean metrics, and complex projective spaces. *Bull. London Math. Soc.*, 16:81–121.

[25] Kinsner, W. (2007). A unified approach to fractal dimensions. *Int. Journal of Cognitive Informatics and Natural Intelligence*, 1:26–45.

[26] Kraichnan, R. H. (1991). Stochastic Modelling of Isotropic Turbulence. In Sirovich, L., editor, *New Perspectives in Turbulence*, pages 1–54. Springer.

[27] Langevin, P. (1908). Sur la théorie du mouvement brownien. *Comptes Rendus Acad. Sci.(Paris)*, 146:530–533.

[28] Lesieur, M. (2008). *Turbulence in Fluids*. Springer, Dortrecht, Netherlands, fourth edition.

[29] Liu, J. Z., Zhang, L. D., and Yue, G. H. (2003). Fractal dimension in human cerebellum measured by magnetic resonance imaging. *J. Biophys.*, 85(6):4041–4046.

[30] Mahnke, R., Kaupužs, J., and Lubashevsky, I. (2009). *Physics of Stochastic Processes*. Wiley-VCH, Weinheim, second edition.

[31] Mandelbrot, B. B. (1982). *The Fractal Geometry of Nature*. Freeman, San Fancisco, first edition.

[32] Martin-Garin, B., Lathuiliére, B., Verrecchia, E. P., and Geister, J. (2007). Use of fractal dimensions to quantify coral shape. *Coral Reefs*, 26:541–550.

[33] Maxey, M. R. and Riley, J. (1983). Equation of motion of a small rigid sphere in a nonuniform flow. *Phys. Fluids*, 26:883–890.

[34] Nayfeh, A. H. and Balachandran, B. (1995). *Applied Nonlinear Dynamics*. Wiley, second edition.

[35] Niemeyer, L. L., Pietronero, L., and Weismann, H. J. (1984). Fractal dimension of dielectric breakdown. *Physical review Letters*, 53:1033–1036.

[36] Oseledets, V. I. (1968). A multiplicative ergodic theorem; characteristic Lyapunov exponents of dynamical systems. *Trans. Moscow Math. soc.*, 19:179–210.

[37] Ott, E. (2002). *Chaos in Dynamical Systems*. Cambridge University Press, second edition.

[38] Panchev, S. (1971). *Random Functions and Turbulence*. Pergamon Press, 1 edition.

[39] Pietronero, L. (1987). The fractal structure of the universe - correlations of galaxies and clusters and the average mass density. *Physica A*, 144:257–.

[40] Poincaré, H. (1890). Sur le problème des trois corps et les équations de la dynamique. *Acta Mathematica*, 13:1–270.

[41] Pumir, A., Shraiman, B., and Chertkov, M. (2000). Geometry of lagrangian dispersion in turbulence. *Phys. Rev. Lett.*, 85:5324.

[42] Pumir, A. and Wilkinson, M. (2013). A model for the shapes of advected triangles. *J. Stat. Phys.*, 152:934–53.

[43] Redner, S. (2001). *A Guide to First Passage Processes*. Cambridge University Press.

[44] Rényi, A. (1970). *Probability Theory*. North-Holland, Amsterdam.

[45] Risken, H. (1984). *The Fokker-Planck Equation. Methods of Solution and Applications*. Springer, Berlin.

[46] Roberts, O. F. T. (1924). The theoretical scattering of smoke in a turbulent atmosphere. *Phil. Trans. Roy. Soc. Lond. A*, 104:640–54.

[47] Schuss, Z. (2010). *Theory and Applications of Stochastic Processes: An Analytical Approach*, volume Applied Mathematical Sciences vol. 170. Springer.

[48] Sinha, S. K. (1989). Scattering from fractal structures. *Physica D*, 38:310–314.

[49] Small, C. G. (1996). *The Statistical Theory of Shape*. Springer, New York, first edition.

[50] Sommerer, J. and Ott, E. (1993). Particles floating on a random flow: a dynamically comprehensible physical fractal. *Science*, 359:334–.

[51] Sorensen, C. M. (2001). Light scattering by fractal aggregates: A review. *Aerosol Science and Technology*, 35:648–687.

[52] Sprott, J. C. and Rowlands, G. (2001). Improved correlation dimension calculation. *Int. J. of Bifurcation and Chaos*, 11:1865–1880.

[53] Stockie, J. M. (2011). The mathematics of atmospheric dispersion modelling. *SIAM Rev.*, 53:349–72.

[54] Strogatz, S. H. (1994). *Nonlinear Dynamics and Chaos: with applications to physics, biology, chemistry, and engineering*. Perseus Books, Reading MA, first edition.

[55] Sutton, O. G. (1932). A theory of eddy diffusion in the atmosphere. *Proc. Roy. Soc. Lond. A*, 135:143–65.

[56] Szymczak, P. and Ladd, A. (2003). Boundary conditions for stochastic solutions of the convection-diffusion equation. *Phys. Rev. E*, 68:036704–12.

[57] Theiler, J. (1990). Estimating fractal dimension. *J. Optical Society of America, A*, 7:1055–1073.

[58] Touchette, H. (2009). The large deviation approach to statistical mechanics. *Phys. Rep.*, 478:1–69.

[59] Tritton, D. J. (1988). *Physical Fluid Dynamics*. Oxford University Press, Oxford, U.K., second edition.

[60] Tsinober, A. (2009). *An Informal and Conceptual Introduction to Turbulence*. Springer, New York, second edition.

[61] Tsonis, A. A. and Eisner, J. B. (1986). Fractal characterization and simulation of lightening. *Beitr. Phys. Atmosph.*, 60:187–192.

[62] Uhlenbeck, G. E. and Ornstein, L. S. (1930). On the theory of Brownian motion. *Phys. Rev.*, 36:823–841.

[63] van Kampen, N. G. (1981). *Stochastic Processes in Physics and Chemistry*. North-Holland, Amsterdam, second edition.

[64] Viana, M. (2014). *Lectures on Lyapunov Exponents*. Cambridge University Press, first edition.

[65] Wilkinson, M. and Grant, J. (2014). Triangular constellations in fractal measures. *Europhysics Letters*, 107(5):50006.

[66] Wilkinson, M. and Grant, J. (2018). A matrix contraction process. *J. Phys. A*, 51:105002.

[67] Wilkinson, M. and Grant, J. (2019). Statistics of contracted constellations of a dynamical system. *Unpublished manuscript*. .

[68] Wilkinson, M., Kennard, H. R., and Morgan, M. A. (2012a). Spectal dimension of fractal sets. *J. Phys. A*, 45:415102.

[69] Wilkinson, M., Mehlig, B., and Gustavsson, K. (2010). Correlation dimension of inertial particles in random flows. *Europhys. Lett.*, 89(5):50002.

[70] Wilkinson, M., Mehlig, B., Gustavsson, K., and Werner, E. (2012b). Clustering of exponentially separating trajectories. *Eur. Phys. J. B*, 85:18.

[71] Wilkinson, M., Yang, F., Austin, E. J., and O'Donnell, K. P. (1992). A statistical topographical model for exciton luminescence. *J. Phys. Condens. Matter*, 4:8863–8878.

[72] Witten, T. A. and Sander, L. M. (1983). Diffusion-limited aggregation in three dimensions. *Phys. Rev. B, Condensed matter*, 27(9):5686–5697.

[73] Xu, H., Ouellette, N. T., and Bodenschatz, E. (2008). Evolution of geometric structures in intense turbulence. *New Journal of Physics*, 10(1):013012.